1. Karageorgiou V, Kaplan D. Porosity of 3D biomaterial scaffolds and osteogenesis. Biomaterials. 2005;26(27):5474–91.

2. Olivares-Navarrete R, Hyzy SL, Slosar PJ et al. Implant materials generate different peri-implant inflammatory factors: poly-ether-ether-ketone promotes fibrosis and microtextured titanium promotes osteogenic factors. Spine. 2015;40(6):399–404.

3. Olivares-Navarrete R, Hyzy SL, Gittens RA, et al. Rough titanium alloys regulate osteoblast production of angiogenic factors. Spine J. 2013;13(11):1563–70.

4. Ponader S, von Wilmowsky C, Widenmayer M, et al. In vivo performance of selective electron beam-melted ti-6al-4v structures. J Biomed Mater Res A 2010;92A:56–62

5. Li JP, Habibovic P, et al.: Bone ingrowth in porous titanium implants produced by 3D fiber deposition. Biomaterials 28:2810, 2007.

6. Data on file at Nexxt Spine, LLC.

7. Kienle A, Graf N, Wilke HJ. Does impaction of titanium-coated interbody fusion cages into the disc space cause wear debris or delamination? The Spine Journal 16 (2016) 235–242.

Available online at www.sciencedirect.com
SCIENCE DIRECT®
Biomaterials 26 (2005) 5474–5491
Biomaterials
www.elsevier.com/locate/biomaterials

Review

Porosity of 3D biomaterial scaffolds and osteogenesis

Vassilis Karageorgiou, David Kaplan*

Departments of Chemical and Biological Engineering and Biomedical Engineering, Tufts University, 4 Colby Street, Medford, MA 02155, USA

Received 27 August 2004; accepted 8 February 2005
Available online 7 April 2005

Abstract

Porosity and pore size of biomaterial scaffolds play a critical role in bone formation in vitro and in vivo. This review explores the state of knowledge regarding the relationship between porosity and pore size of biomaterials used for bone regeneration. The effect of these morphological features on osteogenesis in vitro and in vivo, as well as relationships to mechanical properties of the scaffolds, are addressed. In vitro, lower porosity stimulates osteogenesis by suppressing cell proliferation and forcing cell aggregation. In contrast, in vivo, higher porosity and pore size result in greater bone ingrowth, a conclusion that is supported by the absence of reports that show enhanced osteogenic outcomes for scaffolds with low void volumes. However, this trend results in diminished mechanical properties, thereby setting an upper functional limit for pore size and porosity. Thus, a balance must be reached depending on the repair, rate of remodeling and rate of degradation of the scaffold material. Based on early studies, the minimum requirement for pore size is considered to be $\sim$100 μm due to cell size, migration requirements and transport. However, pore sizes $>$300 μm are recommended, due to enhanced new bone formation and the formation of capillaries. Because of vascularization, pore size has been shown to affect the progression of osteogenesis. Small pores favored hypoxic conditions and induced osteochondral formation before osteogenesis, while large pores, that are well-vascularized, lead to direct osteogenesis (without preceding cartilage formation). Gradients in pore sizes are recommended for future studies focused on the formation of multiple tissues and tissue interfaces. New fabrication techniques, such as solid-free form fabrication, can potentially be used to generate scaffolds with morphological and mechanical properties more selectively designed to meet the specificity of bone-repair needs.

Keywords: Porosity; Scaffolds; Bone; Osteogenesis; Tissue engineering; Polymeric biomaterials

Contents

*Corresponding author. Tel.: +1 617 627 3251; fax: +1 617 627 3231.
E-mail address: david.kaplan@tufts.edu (D. Kaplan).

0142-9612/$ - see front matter © 2005 Elsevier Ltd. All rights reserved.
doi:10.1016/j.biomaterials.2005.02.002

1. Introduction

A key component in tissue engineering for bone regeneration is the scaffold that serves as a template for cell interactions and the formation of bone-extracellular matrix to provide structural support to the newly formed tissue. Scaffolds for bone regeneration should meet certain criteria to serve this function, including mechanical properties similar to those of the bone repair site, biocompatibility and biodegradability at a rate commensurate with remodeling. Scaffolds serve primarily as osteoconductive moieties, since new bone is deposited by creeping substitution from adjacent living bone [1]. In addition to osteoconductivity, scaffolds can serve as delivery vehicles for cytokines such as bone morphogenetic proteins (BMPs), insulin-like growth factors (IGFs) and transforming growth factors (TGFs) that transform recruited precursor cells from the host into bone matrix producing cells [1], thus providing osteoinduction. Finally, osteogenesis occurs by seeding the scaffolds before implantation with cells that will establish new centers for bone formation [1], such as osteoblasts and mesenchymal cells that have the potential to commit to an osteoblastic lineage. Genetically transduced cells that express osteoinductive factors can also be used. Combining scaffolds, cytokines and cells to generate ex vivo tissue-engineered constructs is hypothesized to provide more effective bone regeneration in vivo in comparison to biomaterial matrices alone. In addition, improved bone-like tissue growth in vitro offers new options to study disease progression.

Scaffolds for osteogenesis should mimic bone morphology, structure and function in order to optimize integration into surrounding tissue. Bone is a structure composed of hydroxyapatite ($Ca_{10}(PO_4)_6(OH)_2$) crystals deposited within an organic matrix (~95% is type I collagen) [2]. The morphology is composed of trabecular bone which creates a porous environment with 50–90% porosity (typical apparent density values for femoral cortical bone $1.85 \pm 0.06\,g/cm^3$) [3] (for relation between porosity and apparent density refer to *Methods to measure porosity and pore size* section) and pore sizes at the order of 1 mm in diameter [4], with cortical bone surrounding it. Cortical bone has a solid structure with a series of voids, for example haversian canals, with a cross-sectional area of 2500–12,000 μm^2 that results in 3–12% porosity [5] (typical apparent density values for proximal tibial trabecular bone $0.30 \pm 0.10\,g/cm^3$ [3]). The degree of mineralization varies within different bone tissues: for example, in trabecular bone from the calcaneus was measured at $1.135 \pm 0.147\,g/cm^3$, while in trabecular bone from the iliac crest it was measured $1.098 \pm 0.077\,g/cm^3$ [6]. Four cell types are present in bone tissue: osteoblasts, osteoclasts, osteocytes and bone lining cells [2]. Bone is at a constant state of remodeling with osteoblasts producing and mineralizing new bone matrix, osteocytes maintaining the matrix and ostoclasts resorbing the matrix [2]. Bone lining cells are inactive cells that are believed to be precursors for osteoblasts [2]. Various hormones, such as parathyroid hormone (PTH) and 1α, $25(OH)_2$ vitamin D_3, and cytokines, such as IGFs, platelet-derived growth factor (PDGF), fibroblast growth factors (FGFs), vascular endothelial growth factors (VEGFs), TGFs and BMPs are sequestered in bone matrix and regulate bone metabolism, function and regeneration [7].

Mechanical properties of bone depend on age; 3, 5, and 35-year-old femoral specimens had modulus of elasticity values of 7.0, 12.8, 16.7 GPa, respectively [8]. It is generally reported that, after maturation, the tensile strength and modulus of elasticity of femoral cortical bone decline by approximately 2% per decade [3]. Mean values for bone modulus of elasticity and ultimate strength are presented in Table 1. The complexity of architecture and the variability of properties of bone tissue (e.g. porosity, pore size, mechanical properties, mineralization or mineral density, cell type and cytokines gradient features), as well as differences in age, nutritional state, activity (mechanical loading) and disease status of individuals establish a major challenge in fabricating scaffolds and engineering bone tissues that will meet the needs of specific repair sites in specific patients.

Scaffold properties, depend primarily on the nature of the biomaterial and the fabrication process. The nature of the biomaterial has been the subject of extensive studies including different materials such as metals, ceramics, glass, chemically synthesized polymers, natural polymers and combinations of these materials to form composites. Properties and requirements for scaffolds in bone tissue engineering have been extensively reviewed and recent examples include aspects of degradation

Table 1
Mean values for bone modulus of elasticity and ultimate strength

Type of bone	Direction and type of load	Ultimate strengh (MPa)	Modulus of elasticity (GPa)	Reference
Cortical (midfemoral)	Longitudinal tension	133	17	[125]
	Longitudinal compression	193	17	[125]
	Longitudinal shear	68	3	[125]
	Transverse tension	51	11.5	[125]
	Transverse compression	33	11.5	[125]
Trabecular (proximal tibia)		5.3	0.445	[126]
Trabecular (proximal femoral)	Axial	6.8	0.441	[127]

[9–12], mechanical properties [9,13–17], cytokine delivery [18–25] and combinations of scaffolds and cells [23,26–30].

Porosity is defined as the percentage of void space in a solid [31] and it is a morphological property independent of the material. Pores are necessary for bone tissue formation because they allow migration and proliferation of osteoblasts and mesenchymal cells, as well as vascularization [32]. In addition, a porous surface improves mechanical interlocking between the implant biomaterial and the surrounding natural bone, providing greater mechanical stability at this critical interface [33]. The most common techniques used to create porosity in a biomaterial are salt leaching, gas foaming, phase separation, freeze-drying and sintering depending on the material used to fabricate the scaffold. The minimum pore size required to regenerate mineralized bone is generally considered to be ~100 μm after the study of Hulbert et al., where calcium aluminate cylindrical pellets with 46% porosity were implanted in dog femorals [34]. Large pores (100–150 and 150–200 μm) showed substantial bone ingrowth. Smaller pores (75–100 μm) resulted in ingrowth of unmineralized osteoid tissue. Smaller pores (10–44 and 44–75 μm) were penetrated only by fibrous tissue [34]. These results were correlated with normal haversian systems that reach an approximate diamter of 100–200 μm [34]. However, using laser perforation techniques and titanium plates, four different pore sizes (50, 75, 100 and 125 μm) were tested in rabbit femoral defects under non-load-bearing conditions [35]. Bone ingrowth was similar in all the pore sizes suggesting that 100 μm may not be the critical pore size for non-load-bearing conditions [35].

In the present review pore size and porosity for different biomaterials are reviewed in the context of mechanical properties and extent and type of bone formation in vitro and in vivo. Based on this assessment conclusions are drawn regarding the relationship between these morphological and functional features to provide guidance regarding design choices for scaffolds related to bone repair.

2. Necessity for porosity

The necessity for porosity in bone regeneration has been shown by Kuboki et al. using a rat ectopic model and solid and porous particles of hydroxyapatite for BMP-2 delivery: no new bone formed on the solid particles, while in the porous scaffolds direct osteogenesis occurred [32]. Further support comes from studies with metal porous-coated implants compared to the non-coated material. Treatment of titanium alloy implant surfaces with sintered titanium beads (Porocoat®) created a porous coating that enhanced cortical shear strength of the implants recovered from sheep tibiae, while further coating with beads with hydroxyapatite did not result in significant improvement [36]. Titanium fiber-metal porous coatings (45% porosity and 350 μm average pore size) maximized bone ingrowth and increased the potential for stress-related bone resorption of femoral stems in a canine total hip arthroplasty model [37]. A similar result was observed for plasma spray-coated titanium implants with 56–60% porosity, although bone ingrowth was maximized for an open-pore titanium fiber mesh (60% porosity and 170 μm average pore size) coated with polyvinyl alcohol hydrogel [38]. D'Lima et al. showed that surface roughness was more important for osseointegration of titanium implants in rabbit femors, since an acid-etched coating (highest surface roughness) showed a higher overall osseintegration when compared with grit-blasted and fiber mesh (average pore size 400 μm) coatings [39]. The presence of a thicker (600–1000 nm) porous (13–24% porosity, pores less than 8 μm) oxide film on the surface of titanium screws resulted in more bone formation when implanted in tibia defects in rabbits compared to controls with a nonporous oxide layer of 17–200 nm in thickness [40,41]. Lower porosity of the oxide layer (19% versus 24%) resulted in decreased surface roughness (0.97 versus 1.02 μm) as measured by confocal laser scanning profilometry [42]. Coating titanium alloy implants with a 50 μm layer of porous hydroxyapatite did not increase the percentage of osseointegrated surface in the mandible of dogs,

although bone extended into the micropores of hydroxyapatite resulting in an osseous micro-interlocking [43]. However, in the maxillae there was more bone apposing the coated implants suggesting a beneficial effect for areas of poorer bone quality [43].

Although macroporosity (pore size $>50\,\mu m$) has a strong impact on osteogenic outcomes, microporosity (pore size $<10\,\mu m$) and pore wall roughness play an important role as well: hydroxyapatite ceramic rods with average pore size of 200 μm and smooth and dense pore walls failed to induce ectopic bone formation in dogs, in contrast to rods made from the same material with average pore size 400 μm but with rough and porous pore walls [44]. Microporosity results in larger surface area that is believed to contribute to higher bone-inducing protein adsorption as well as to ion exchange and bone-like apatite formation by dissolution and re-precipitation [44]. Surface roughness enhances attachment, proliferation and differentiation of anchorage-dependent bone forming cells [44]. The solid freeform fabrication technique allowed the fabrication of poly(desaminotyrosyl-tyrosine ethyl ester carbonate) (a tyrosine derived pseudo-polyamino acid) scaffolds with four axial and four radial channels and fixed 500 μm pores separated by 500 μm solid walls or 80% porous walls [45]. Scaffolds from the same material with random pore distributions served as controls. Although there was no statistical difference in the bone formed in cranial defects in rabbits, bone ingrowth followed the architecture of the scaffolds: a continuous ingrowth from the outer periphery was observed in the random pore size scaffolds, while scaffolds with same sized pores and solid walls promoted discontinuous ingrowth with bone islands throughout the whole scaffold; scaffolds with same sized pores and porous walls resulted in both types of bone ingrowth [45]. It was hypothesized that discontinuous bone ingrowth may result in faster healing, since bone will be forming not only from the margins but also throughout the whole space of the defect [45]. These studies demonstrate the enhanced osteogenesis of porous versus solid implants, both at the macroscopic as well as the microscopic level.

3. Methods to measure porosity and pore sizes

Different methods are used to measure porosity and pore sizes in scaffolds. Total porosity (Π) is measured by gravimetry [46–48] according to the equation [46,47]

$$\Pi = 1 - \rho_{\text{scaffold}}/\rho_{\text{material}}, \tag{1}$$

where ρ_{material} is the density of the material of which the scaffold is fabricated and ρ_{scaffold} is the apparent density of the scaffold measured by dividing the weight by the volume of the scaffold.

Mercury intrusion porosimetry is a method used to measure both porosity [46,47,49–54] and pore sizes [6,47,50,53–55]. The scaffolds are placed in a penetrometer and infused with mercury under increasing pressure. As the pressure (P) increases, the radius of pores (r) that can be filled decreases according to the Washburn equation [47]

$$P = 2\sigma \cos\theta/r, \tag{2}$$

where σ is the surface tension of mercury and θ is the contact angle. The open porosity (π) (porosity accessible to mercury intrusion) is given as [47]

$$\pi = V_{\text{intrusion}}/V_{\text{scaffold}}, \tag{3}$$

where $V_{\text{intrusion}}$ is the total intrusion volume of mercury and V_{scaffold} is the volume of the scaffold. Finally, the closed porosity (ϖ), porosity not accessible to mercury, can be determined as [47]

$$\varpi = \Pi - \pi. \tag{4}$$

The open porosity can be calculated by the liquid displacement method as well [56–58]. The scaffold is submerged in a known volume (V_1) of liquid that is not a solvent for the scaffold and a series of brief evacuation–repressurization cycles is conducted to force the liquid into the pores of the scaffold. After these cycles the volume of the liquid and liquid-impregnated scaffold is V_2. When the liquid-impregnated scaffold is removed, the remaining liquid volume is V_3 and open porosity is given as [56,57]

$$\pi = (V_1 - V_3)/(V_2 - V_3). \tag{5}$$

Applied pressures for mercury intrusion porosimeters range between slightly higher than 0.5 to 60,000 psi [31]. Biomaterials that may compress or collapse at high pressures should be analyzed at relatively low pressures or a correction for compressibility should be included in the interpretation of experimental measurements [31].

Scanning electron microscopy (SEM) images are analyzed with various computer software to measure porosity [53,59–61] and, particularly, pore sizes [48,49,52,55,56,59–65]. For statistical analysis, different sample sizes are used, for example, ranging from measures from 10 to 40 pores [56,61] to a minimum of 100 [66]. Finally, microcomputed tomography (micro-CT) imaging and analysis have been used to determine porosity and pore sizes in 3D biomaterial scaffolds used in bone tissue engineering [67,68]. Briefly, isotropic slice data are obtained and reconstructed into 2D images, which are compiled and analyzed to generate 3D images and obtain quantitative morphological detail [68]. This technique is particularly appealing, since it is non-invasive and can be used to image and quantify bone repair.

4. Porosity of biomaterial scaffolds for bone tissue engineering

4.1. Ceramics

4.1.1. Crystalline ceramics

Ceramic implants for osteogenesis are based mainly on hydroxyapatite, since this is the inorganic component of bone. The usual fabrication technique for ceramic implants is sintering of the ceramic powder at high temperatures. For example, hydroxyapatite powder has been sintered to generate blocks with fully interconnected pores (500 μm), 77% porosity, compressive and three-point bending strength of 17.4 and 7.2 MPa, respectively, and elastic modulus of 0.12 GPa [49]. These scaffolds induced ectopic bone formation when implanted subcutaneously in mice [49]. Cylindrical synthetic porous hydroxyapatite implants with pore sizes of 400–600 μm and 80% porosity healed femoral defects in rats [62]. Porous particles of hydroxyapatite (average pore size 150 μm, porosity 70%) and porous coral-replicated hydroxyapatite (exoskeletal microstructures of calcium carbonate of corals converted into hydroxyapatite by hydrothermal chemical exchange) blocks (average pore size 230 μm, porosity 66%) were used for delivery of BMP-2 in a rat ectopic model and induced direct osteogenesis (without preceding cartilage formation) [32]. Other types of ceramics used in bone repair include porous calcium metaphosphate ($[Ca(PO_3)_2]_n$) blocks (pore size 200 μm) that were used for culturing rat marrow stromal cells ex vivo and for ectopic bone formation in athymic mice [69] and natural coral scaffolds molded into the shape of a human mandibular condyle with pore sizes 150–220 μm and 36% porosity that were seeded with rabbit marrow mesenchymal cells and induced ectopic bone formation in nude mice [70]. Combinations of ceramics also have been explored: porous biphasic ceramic (hydroxyapatite—tricalcium phosphate) with 50% porosity and 100–150 μm pore sizes have been shown to heal femoral defects in dogs [71]. Porosities and pore sizes for ceramics are summarized in Table 2. In general, ceramic biomaterials are able to form bone apatite-like material or carbonate hydroxyapatite on their surfaces, enhancing their osseointegration. These materials are also able to bind and concentrate cytokines, as is the case of natural bone [72]. Brittleness and slow degradation rates are disadvantages associated with their use.

4.1.2. Amorphous glasses and glass-ceramics

Ceramics include glasses and glass-ceramics. Gong et al. fabricated glass implants with 5% porosity and pores that ranged from 100–200 μm to the <10 μm range, and also glass-ceramic implants with macropores (100–200 μm) and micropores (<5 μm) [63]. Glassy carbon pellets with 40% porosity induced bone ingrowth in tibia defects in rabbits [73]. Bioglass (materials with different compositions of SiO_2,CaO, Na_2O, and P_2O_5 [74,75]) scaffolds have an interconnected network, 10–500 μm, and framework (2–50 nm) [75] and have been shown to support culture of human primary osteoblasts [74]. In other studies Bioglass implants with pores ranging from 100 to 600 μm induced ectopic bone formation in dogs [65]. Silica/calcium phosphate scaffolds with different porosities (51%, 47% and 43% generated by decreasing the silica content) and a broad distribution of pore sizes (10–300 μm) helped to regenerate bone in femoral defects in rabbits [53]. Upon retrieval, the silica-rich scaffolds were almost filled with new bone and showed higher resorbability than scaffolds with lower silica content [53]. This stronger osteogenic outcome was attributed to the chemical composition (high content of pyrophosphate) and not to differences in porosity [53]. Properties of amorphous glass and glass-ceramic scaffolds are summarized in Table 3.

4.2. Metals

Stainless steel and titanium or titanium alloys (i.e. Ti-6Al-4V) are the materials that usually comprise the basis of metal implants for bone regeneration. The bulk phase of the implants consists of solid metal, while titanium particle coatings create a porous surface (thickness ranging from a few nanometers to the hundreds of micrometers depending on the fabrication technique [33,37,40–42,76]. Different techniques have been used to manufacture the porous coatings (Table 4), including plasma-spraying in the case of implants with 50–60% porosity and 200–400 μm pore size coatings for healing femoral defects in dogs [60], or sintering in the case of implants with 35% porosity and 50–200 μm pore size coatings [77]. Other techniques include machining, shot-blasting and acid-etching, but result in pore sizes of less than 10 μm [77]. Examples of completely porous metal scaffolds are titanium fiber meshes with 86% porosity and a 250 μm average pore size that have been used for the ex vivo culture of rat bone marrow stromal cells under static conditions [78] or in a flow perfusion bioreactor [79] and subsequent implantation in cranial defects in rats [78,79]. These scaffolds have also found application as delivery systems for transforming growth factor $\beta-1$ (TGF-β1) and have been used to repair rabbit cranial defects [80]. The main advantage of metal implants is their excellent mechanical properties, which makes them the most widely applied implant material used in bone surgical repairs. However, the lack of tissue adherence [34] and the low rate of degradation results either in a second surgery to remove the implant or in permanent implantation in the body with the related risks of toxicity due to accumulation of metal ions due to corrosion [81].

Table 2
Porosities and pore sizes of crystalline ceramic scaffolds for bone regeneration (pores are denoted either as range or as average pore size)

Crystalline ceramic	Fabrication technique	Shape	Pore size (μm)	Porosity (%)	Application	References
Hydroxyapatite	Sintering	Scaffolds with honeycomb pores	90–120 and 350		BMP-2 delivery and ectopic bone formation in rats	[107,112,113]
	Sintering	Scaffolds with honeycomb pores	100–200		BMP-2 delivery and ectopic bone formation in rats	[112]
	Sintering	Scaffolds	366 and 444	38 and 44	Mandible defects	[103]
	Sintering	Scaffolds	400 and 800	60 and 70	Goat bone marrow stromal cells ex vivo and ectopic bone formation in goats	[104]
	Sintering	Blocks	500	77	Ectopic bone formation in mice	[49]
	Sintering	Cylinders	400–600	80	Femoral defects in rats	[62]
	Sintering	Blocks	100–200		BMP-2 delivery and ectopic bone formation in rats	[112]
	Sintering	Blocks	106–212, 212–300, 300–400, 400–500, and 500–600		Ectopic bone formation in rats	[107,108]
	Sintering	Particles	150	70	Ectopic bone formation in rats	[32]
	Sintering	Particles	230	66	Ectopic bone formation in rats	[32]
	Sintering	Rods	200 and 400		Ectopic bone formation in dogs	[44]
Tricalcium phosphate cement	Salt-leaching	Pellets	0.2 and 8.7	31 and 62		[115]
Calcium metaphosphate	Sintering	Blocks	200		Rat bone marrow stromal cells ex vivo and ectopic bone formation in mice	[69]
Natural coral	Sintering	Human mandibular condyle	150–200	36	Rabbit marrow mesenchymal cells ex vivo and ectopic bone formation in mice	[70]
Hydroxyapatite/ tricalcium phosphate	Sintering	Blocks	100–150	36	Femoral defect in dogs	[71]

Table 3
Porosities and pore sizes of amorphous glass and glass-ceramic scaffolds for bone regeneration (pores are denoted either as range or as average pore size)

Material	Fabrication technique	Pore size (μm)	Porosity (%)	Application	References
Glasses	Sintering	100–200	5		[63]
			40	Tibia defects in rabbits	[73]
Bioglass	Foaming	10–500		Primary human osteoblasts in vitro	[74,75]
	Sintering	100–600		Ectopic bone formation in dogs	[65]
Glass-ceramics	Sintering	100–200			[63]
	Phase transformation	10–300	51, 47 and 43	Femoral defects in rabbits	[53]

Table 4
Porosities and pore sizes of metal scaffolds for bone regeneration (pores are denoted either as range or as average pore size)

Porous surface technique	Pore size (μm)	Porosity (%)	Application	References
N/A (sintered titanium fiber meshes)	250	86	Rat bone marrow stromal cells ex vivo and cranial defects in rats	[78,79]
N/A (sintered titanium fiber meshes)	250	86	TGF-β1 delivery in cranial defects in rabbits	[80]
N/A (self-propagating high temperature synthesized nitinol implants)	259 and 505	66 and 47	Femoral defects in rats	[105]
	353, 218 and 179	43, 54 and 51	Cranial defects in rabbits	[111]
N/A (laser perforated titanium implants)	50, 75, 100, 125		Femoral defects in rabbits	[35]
Sintering	50–200	35		[77]
Plasma-spraying	200–400	50–60	Femoral defects in dogs	[60]
		56–60	Femoral condyles in dogs	[38]
Diffusion	350	45	Hip arthroplasty in dogs	[37]
Laser-texture	100, 200 and 300		Femoral defect in rabbits	[109]
Electrochemical oxidation	<8	13–24	Tibia defects in rabbits	[40–42]
Machining	Submicron to 10			[77]
Shot-blasting	<10			[77]
		44 and 48	Mandible and femoral defects in dogs	[33]
Acid-etching	Submicron to 1			[77]
			Femoral defects in rabbits	[39]
Deposition through polystyrene latex beads	0.4, 13 and 40		Human bone derived cells in vitro	[76]

4.3. Natural polymers

Many polymers from Nature have the advantage of biocompatibility and biodegradability, since they compose the structural materials of tissues (i.e. collagen and glycosaminoglycans). A benzyl ester derivative of hyaluronic acid with 80–90% porosity and pores ranging from 100 to 600 μm was used for delivery of BMP-2 in vitro and osteogenic differentiation of the murine pluripotent cell line C3H10T1/2 [59]. Collagen matrices with pores ranging from 11 to 105 μm and 14 to 134 μm healed tibia defects in rats [64]. Porous collagen/hyaluronic acid scaffolds were produced by freeze-drying at −196, −70 and −20 °C resulting in 40, 90 and 230 μm average pore size, respectively, and 58%, 59% and 56% porosities, respectively; cross-linking with 1-ethyl-3-(3-dimethyl aminopropyl) carbodiimide (EDC) and re-freeze-drying at −20 °C generally increased pore size (84, 186 and 190, respectively) and porosity (62%, 62% and 64%, respectively) (Table 5) [61]. Nevertheless, the low mechanical strength and high rates of degradation of natural polymers often result in their use in composites or in chemical modification by cross-linking to improve properties and reduce degradation rates. However, these changes may cause cytotoxic effects and reduce biocompatibility [82].

To overcome these issues we have focused on fabricating silk-based biomaterials, due to the biocompatibility [83–85], excellent mechanical properties [86], and long-standing use of silk as suture material. Silk fibroin, extracted from silkworm cocoons, has been processed into porous scaffolds (Table 5). Freeze-drying and the addition of porogens (salt leaching and gas foaming) were used as fabrication methods. The porogens improved control of average pore size (202 and 155 μm, respectively) and mechanical properties (compressive stress up to 250 and 280 KPa, respectively, and compressive modulus up to 790 and 1000 KPa, respectively) [56]. Porosity depended on the porogen used and ranged from 84% to 98% for scaffolds prepared by salt leaching and from 87% to 97% for scaffolds prepared by gas foaming [56]. Recently, when salt-leached scaffolds were used to differentiate human bone marrow stromal cells in vitro under static culture conditions, the deposited mineral was hydroxyapatite that formed trabecular-like geometries [87].

4.4. Synthetic polymers

The versatility of chemically synthesized polymers enables the fabrication of scaffolds with different features (forms, porosities and pore sizes, rates of degradation, mechanical properties) to match tissue specific applications. Hu et al. studied the effect of fabrication parameters on poly(α-hydroxy acid) (poly(D,L-lactide) and poly(lactide-*co*-glycolide)) scaffold properties [46]. Lowering the solution freezing temperature resulted in smaller pores, but did not affect the porosity. Increasing

Table 5
Porosities and pore sizes of scaffolds for bone regeneration made from natural polymers (pores are denoted either as range or as average pore size)

Natural polymer	Fabrication technique	Pore size (μm)	Porosity (%)	Application	References
Hyaluronic acid	Salt-leaching	100–600	80–90	BMP-2 delivery and C3H10T1/2 cells in vitro	[59]
Collagen	Freeze-drying	11–105 and 14–134		Tibia defects in rats	[64]
Collagen/hyaluronate	Cross-linking	45.7 and 35.4		Cranial defects in rats	[110]
Collagen/hyaluronic acid (cross-linked with EDC)	Freeze-drying	84 (−196 °C)	62 (−196 °C)		[61]
		186 (−70 °C)	62 (−70 °C)		
		190 (−20 °C)	64 (−20 °C)		
Silk fibroin	Freeze-drying	50 (−20 °C) 15 (−80 °C)	99		[56]
	Salt-leaching	202	84–98	Human bone marrow stromal cells in vitro	[56,87]
	Gas foaming	155	87–97		[56]

the water co-solvent content in dioxane above 3% (v/v) led to interconnected circular pores, but dioxane contents higher than 7% lead to fibrous polymers with poor handling qualities. Increasing polymer solution concentration diminished pore size and porosity. Higher polymer molecular weight increased median pore size and porosity. Two types of theses scaffolds, poly(D,L-lactide) (118 μm average pore size and 92% porosity) and poly(lactide-*co*-glycolide) (78 μm average pore size and 90% porosity), were tested in vitro and supported proliferation and differentiation of osteoprecursor cells [46]. Hollow poly(lactide-*co*-glycolide) microcarriers (500–860 μm) were sintered into porous scaffolds with median pore size of 187 μm and 31% porosity [50]. Poly(lactide-*co*-glycolide) has also been used for culturing human osteoprogenitor cells in scaffolds with 200 μm mean pore size [88] and for fabricating tooth implants with 65% porosity and a mean pore size of 100 μm [47]. A promising technique to fabricate highly porous scaffolds is electrospinning: electrospun nanofibrous structures of poly(lactide-*co*-glycolide) had 92% porosity; the pore size distribution was broad (2–465 μm) [89]. Another polymer that has found application in bone regeneration is poly(propylene fumarate) used as scaffolds with 70% porosity and 300–500 μm pore sizes for TGF-β1 delivery and implantation in cranial defects in rabbits [90]. Scaffolds in the form of coat formulations that developed pores in vivo (51% porosity and a wide range of pore distribution with a median pore size of 70 μm and at least 30% of pores >200 μm) due to the effervescent reaction (CO_2 production from the reaction of carbonate salts with acids) were prepared from poly(propylene fumarate), as well [55]. These scaffolds were used in tibia defects in rats with and without autograft material and the addition of autograft material resulted in more bone formation, although the percentage of autograft material content (75% and 25%) did not affect bone ingrowth [55].

Combining solid freeform fabrication with phase separation, emulsion-solvent diffusion and porogen leaching, Taboas et al. created a variety of pure and composite scaffolds while controlling porosity, pore size, pore geometry, pore branching, pore connectivity and pore orientation [91]. They successfully prepared poly(lactide) scaffolds with 600 μm channels (global pores) and 50–100 μm porous walls (local pores), discrete composites of poly(lactide) and poly(glycolide) with 800 μm global pores or poly(lactide) and hydroxyapatite with 600 and 500 μm global pores, respectively, and poly(lactide) scaffolds with complex architecture that mimicked human trabecular bone [91]. Other types of polymer combinations include polymeric foams from blends of poly(lactide-*co*-glycolide) and poly(ethylene glycol) with 85% porosity and 300–500 μm pores which supported proliferation and mineralization of periosteal cells in vitro [92], and poly(lactide-*co*-glycolide)/polyvinyl alcohol scaffolds with 200–300 μm pore sizes and 90% porosity (both independent from the polyvinyl alcohol content) [52]. The addition of polyvinyl alcohol resulted in more bone formation, when plain poly(lactide-*co*-glycolide) scaffolds and scaffolds with 5 wt% polyvinyl alcohol were implanted in rabbit skulls [52]. Finally, poly(propylene glycol-*co*-fumaric acid) scaffolds that developed pores ranging from 100–500 μm in vivo due to the effervescent reaction healed cortical defects in rats [93]. Values for pore sizes and porosities for different polymers are given in Table 6. A constraint with some of these polymers is that they have low mechanical properties even in the form of solid screws and rods, and they have therefore been applied in areas of low mechanical stress in vivo [94].

Table 6
Porosities and pore sizes of scaffolds for bone regeneration made from chemically synthesized polymers (pores are denoted either as range or as average pore size)

Polymer	Fabrication technique	Pore size (μm)	Porosity (%)	Application	References
Poly(lactide)	Salt-leaching	600			[91]
Poly(lactide)/poly(glycolide)	Molding	800			[91]
Poly(L-lactide-*co*-D,L-lactide)	Porogen melting		58 and 80		[68]
Poly(lactide-*co*-glycolide)	Sintering	72, 164, 101 and 210	>30		[116]
	Consolidation by pressure drop	100	65	Teeth implants	[47]
	Sintering	187	31		[50]
	Gas foaming	200		Human mesenchymal cells in vitro	[88]
	Electrospinning	2–465	92		[89]
Poly(lactide-*co*-glycolide)/ poly(ethylene glycol)	Porogen dissolving	300–500	85	Periosteal cells in vivo	[92]
Poly(lactide-*co*-glycolide)/ polyvinyl alcohol	Salt-leaching	200–300	90	Cranial defects in rabbits	[52]
Poly(multifunctional lactic acid based oligomer)	Salt-leaching	45–150 and 300–600	80		[117,118]
Poly(propylene fumarate)	Gas foaming with effervescent reaction (in vivo)	70	51	Tibia defects in rats	[55]
	Salt-leaching	300–500	70	TGF-β1 delivery in cranial defects in rabbits	[90]
	Salt-leaching		80		[119]
	Salt-leaching	300–500 and 600–800	57–75	Cranial defects in rabbits	[106]
Polyethylene terephthalate	Melt-blowing		93–97	Rat mesenchymal stem cells in vitro	[101]
Polymeric foams	Emulsion polymerization	40 and 100		Rat osteoblasts in vitro	[99]
Poly(propylene glycol-*co*-fumaric acid)	Gas foaming with effervescent reaction (in vivo)	100–500		Cortical defects in rats	[93]
Poly(desaminotyrosyl-tyrosine ethyl ester carbonate)	Salt-leaching	500	80 to 87.5 (gradient)	Cranial defects in rabbits	[45]

4.5. Composites

Although each individual material has advantages for osteogenic applications, each also has drawbacks associated in certain properties (i.e. brittleness of ceramics) that can be overcome by combining different materials. Coating hydroxyapatite scaffolds (87% porosity and 150–200 μm pore size) with a hydroxyapatite/poly(ε-caprolactone) composite improved the mechanical properties: higher amounts of the composite coating (more polymer) increased compressive strength (maximum 0.45 versus to 0.16 MPa for no coating) and elastic modulus (maximum 1.43 versus 0.79 for no coating) [48]. In hydroxyapatite/chitosan-gelatin composites (with most pores between 300 and 500 μm) porosity can be increased by decreasing the chitosan-gelatin concentration and increasing the chitosan-gelatin/hydroxyapatite ratio [58]. These scaffolds supported the proliferation and mineralization of rat calvarial osteoblasts in vitro [58]. Another example of composites are ceramic coatings to increase the osseointegration of other biomaterials. Collagen scaffolds have been coated with hydroxyapatite (pores 30–100 μm, porosity 85%), since osseintegration is enhanced by the surface formation of a bioactive apatite layer, and supported attachment and proliferation of rabbit periosteal cells [95]. Coating porous-surfaced titanium implants (35% porosity and 50–200 μm pore size) with calcium phosphate resulted in earlier and greater bone ingrowth and enhanced mechanical properties for implants retrieved from rabbit femorals [96]. Similarly, biomimetic nano-apatite coatings of porous titanium scaffolds resulted in enhanced human osteoblast culture as well as greater bone formation in a canine bone-ingrowth chamber [54]. Calcium phosphate coated titanium meshes with 86% porosity and 250 μm average pore size were loaded with rat bone marrow cells and induced ectopic bone formation in rats [97].

Table 7
Porosities and pore sizes of composite scaffolds (pores are denoted either as range or as average pore size)

Composite	Fabrication technique	Pore size (μm)	Porosity (%)	Application	References
Hydroxyapatite/poly(ε-caprolactone)	Sintering	150–200	87		[48]
Hydroxyapatite/chitosan-gelatin	Freeze-drying	300–500		Rat calvarial osteoblasts in vitro	[58]
Hydroxyapatite/β-tricalcium phosphate/chitosan	Sintering	300–600			[114]
Collagen/hydroxyapatite	Freeze-drying	30–100	85	Rabbit periosteal cells in vitro	[95]
	Freeze-drying	50–300	49, 73 and 79	MC3T3-E1 osteoblasts in vitro	[100]
Titanium/calcium phosphate	Sintering	50–200 (surface coating)	35 (surface coating)	Femoral defects in rabbits	[96]
	Sintering	250 (porous meshes)	86 (porous meshes)	Ectopic bone formation in rats	[97]
	Soaking			Human osteoblasts in vitro	[54]
				Canine bone-ingrowth chamber	[54]
Titanium/polyvinyl alcohol	Sintering	170	60	Femoral condyles in dogs	[38]
Titanium/boron	Self-propagating high temperature synthesis		15–55	Cranial defects in rats	[98]
Poly(L-lactide-*co*-D,L-lactide)/β-tricalcium phosphate	Salt-leaching	125–150	80–87.5 (gradient)	Cranial defects in rabbits	[10]
Poly(propylene fumarate)/β-tricalcium phosphate	Salt-leaching	150–300	69 and 74		[120]
Poly(L-lactide)/bioglass	Phase separation	50–200			[122]
Silica/ceramic	Sintering	10–300	51, 47 and 43	Femoral defects in rabbits	[53]
Poly(lactide-*co*-glycolide)/collagen/apatite	Salt-leaching	355–425	87		[51]

Self-propagated high-temperature synthesis allows manufacturing of porous titanium-boron (Ti-TiB_x) composites with porosities ranging from 15% to 55% [98]. Bone ingrowth occurred when samples were implanted in calvarial defects in rats [98].

Combining three materials used in bone tissue engineering Chen et al. fabricated poly(lactide-*co*-glycolide) scaffolds with 91% porosity and 355–425 μm pores, with a collagen infused microsponge slightly decreasing porosity [51]. Apatite particulates were deposited on the collagen microsponges further reducing the porosity to 87% [51]. Different combinations of materials used to form composite implants are presented in Table 7.

5. Effect of porosity and pore size on osteogenesis

5.1. Effect of porosity and pore size in vitro

The effect of different porosities and pores sizes on the extent of osteogenesis in vitro has been demonstrated both with osteoblasts and undifferentiated cells. The high internal phase emulsion polymerization route of styrene yields porous polymeric foams, with pore sizes that increases with higher emulsion processing temperatures [99]. When primary rat osteoblasts were seeded into scaffolds with different pore sizes, more cells were found in the small pore (40 μm) scaffolds [99]. Cells migrated faster inside the larger pore (100 μm) scaffolds; however, pore size did not affect cell penetration depth or mineralization extent [99]. Similarly, smaller pores (0.4 and 13 μm) in TiO_2 films on titanium surfaces enhanced the proliferation of human cells trypsinized from bone in contrast to larger pores (49 μm) [76]. In composites of apatite and collagen with pores ranging from 50 to 300 μm, higher apatite contents (90, 70, and 0 wt%) decreased the porosity (49%, 73%, and 79%, respectively), but no significant differences were observed in MC3T3-E1 osteoblast proliferation [100]. Rat mesenchymal stem cells were studied on non-woven fabrics prepared from polyethylene terephthalate fibers with different diameters (2–42 μm) and porosities (93–97%). Smaller diameter fibers resulted in lower cell attachment and more spherical cells, because the size of the cells was comparable or even larger than the fiber

diameter [101]. A similar trend was noticed for cell proliferation and this was attributed to the smaller pore space of scaffolds made from thinner fibers [101]. Fiber diameters of 9 and 12 μm stimulated alkaline phosphatase activity and osteocalcin expression more than any other diameter [101]. Higher porosity did not affect cell attachment, but resulted in increased cell proliferation, since pore space increased with porosity and facilitated transport of oxygen and nutrients [101]. In contrast, cells cultured on scaffolds with lower porosity showed higher alkaline phosphatase activity and expressed more osteocalcin; the authors attributed this effect to suppressed proliferation and to cell aggregation that was observed on fabrics made out of the thicker fibers [101]. In summary, osteogenesis in vitro is not affected by pore size, but is enhanced by lower porosity. It should be noted, however, that the dimensions of pores studied are one order of magnitude lower that the minimum requirement for osteogenesis in vivo and that in an environment where osteogenesis depends on other processes, such as vascularization, the effect of porosity would be opposite, as will be discussed in the following section.

5.2. Effect of porosity in vivo

Bone regeneration in a scaffold in vivo involves recruitment and penetration of cells from the surrounding bone tissue, as well as vascularization. Higher porosity is expected to enhance osteogenesis and numerous studies have verified this hypothesis. Using a solid freeform fabrication technique a porosity gradient from 80% to 88% was created in scaffolds of poly(L-lactide-*co*-D,L-lactide) containing 20 wt% β-tricalcium phosphate (pore size 125–150 μm) [10]. More tissue ingrowth and new bone formation occurred in areas with higher porosity after implantation in rabbit craniums [10]. Scaffolds formed with four axial and four radial macroscopic channels enhanced further osteogenesis [10]. In order to create porosity during bone healing, poly(propylene fumarate) was combined with soluble calcium filler salts; after implantation in rat tibias, scaffolds with a higher percentage of salts (and subsequently higher porosity formed in vivo) showed greater and deeper bone ingrowth [102]. Dental implants were coated with cancellous structured titanium with 44% and 48% porosity and implanted in canine mandibles and femorals; there was more bone ingrowth for the higher porosity coatings at all timepoints (14 weeks) in the femorals and at the initial timepoints (2 and 4 weeks) in the mandibles [33]. Hydroxyapatite scaffolds with 30 MPa compressive strength and 1.4 GPa compressive modulus were tested in mandibular defects with two channel geometries: orthogonal and radial (channel size 444 and 366 μm, respectively, and porosity 44% and 38%, respectively) [103]. Although there were no significant differences in percent bone ingrowth, the shape of the newly formed bone was affected by channel architecture; the orthogonal architecture gave rise to an interpenetrating matrix of hydroxyapatite and newly formed bone, while the radial architecture resulted in bone as a solid piece at the center of the implant [103]. Kruyt et al. compared hydroxyapatite scaffolds with different porosities (70% porosity and 800 μm average pore size (70/800) versus 60% porosity and 400 μm average pore size (60/400)). More goat bone marrow stromal cells (gMSC) proliferated during a 6-day ex vivo culture in the 60/400 scaffolds [104]. However, when scaffolds seeded with gMSC were implanted in bilateral paraspinal muscles in goats more bone formed in the 70/800 scaffolds [104]. This result was likely due to the larger surface area that resulted in higher ion exchange and bone-inducing factor adsorption [104].

There are a limited number of reports in the literature that show no effect of porosity on the amount of apposited bone. For example, nickel–titanium alloy (nitinol) implants with 66% porosity had higher, although not statistically significant, bone-implant contact than implants with 47% porosity in rat femoral defects [105]. Similarly, in poly(propylene fumarate) scaffolds with different porosities (57–75%) that were implanted subcutaneously in cranial defects in rabbits, no statistical difference could be detected in bone formation [106]. The absence of any reports on the beneficial effects of lower porosity scaffolds in vivo solidifies the requirement of highly porous implants for bone regeneration.

5.3. Effect of pore sizes in vivo

Apart from the initial work from Hulbert et al. [34], where the minimum requirement of pore size was first defined as 100 μm, many researchers have explored pore sizes above 100 μm in order to define optima for bone-related outcomes. Porous blocks of hydroxyapatite with different pore sizes (106–212, 212–300, 300–400, 400–500, 500–600 μm) were compared when implanted subcutaneously in rats [107,108]. Alkaline phosphatase activity, osteocalcin content and new bone formation were higher for the 300–400 μm pore size and this was the critical size above which capillaries could be observed [107,108]. Onset of bone remodeling was delayed in surface laser-textured titanium alloy (Ti6Al4V) with 100 μm pores versus implants with 200 and 300 μm pores that were implanted in distal femoral cortex of rabbits [109]. Although the 300 μm pore implants had the highest percentage of lamellar bone, their osseointegration was slower than the 200 μm pore size implants based on the lower percentages of total (within-pore and surface bone-implant) contact [109]. Even where pore sizes lower that the accepted minimum were compared, increasing pore size from 35.4 to

45.7 μm by decreasing the initial percentage of hyaluronate polymer (10% versus 66%) in collagen/hyaluronate scaffolds resulted in more new bone formation in rat calvarial defects [110].

An example of a comparative study for pore sizes where no difference in osteogenesis was observed, is the that by Ayers et al. [111]. No difference was found in both ingrowth in nitinol implants placed in cranial defects in rabbits with different pore sizes (353, 218 and 179 μm average pore sizes with respective porosities of 43%, 54% and 51%) [111]. Nevertheless, since the implant thickness was of the same order of magnitude as the pore size, the authors hypothesized that there should be a minimum thickness to pore size ratio to observe the effect of different pore sizes on bone ingrowth [111]. When poly(propylene fumarate) scaffolds with different porosities (57–75%) and pore sizes (300–500 and 600–800 μm) were implanted subcutaneously or in cranial defects in rabbits, no statistical difference could be detected in bone formation or in the inflammatory response [106]. Finally, no statistical difference in bone-implant contact, but more fibrosis was observed, with nitinol implants with 505 μm average pore size compared 209 μm average pore size when implanted in rat femoral defects [105].

A very interesting aspect of the effect of pore size on bone regeneration is the impact on the progression toward osteogenesis. Honey-combed-shaped hydroxyapatite scaffolds with small (90–120 μm) and large tunnel (350 μm) diameters were used for BMP-2 delivery and were implanted subcutaneously in rats [107,112,113]. In small diameter tunnels chondrogenesis occurred before osteogenesis; in contrast, in tunnels with large diameter bone was formed directly [107,112,113]. The enhanced vascularization that was observed in tunnels with the larger diameters resulted in higher oxygen tension and supply of nutrients, conditions that favored direct osteogenesis [107,112,113]. A similar effect on the type of bone formation has been found to depend on the type of BMP-2 loaded porous hydroxyapatite scaffold. When scaffolds with similar average pore sizes (100–200 μm) were implanted subcutaneously in rats, in both particle and block forms, direct bone formation took place. However, in honey-combed-shaped hydroxyapatite, osteochondral ossification occurred [112]. The geometry of the scaffold allowed enhanced vascularization for blocks and particles favoring direct bone formation; in contrast, low oxygen conditions in the honey-combed-shaped hydroxyapatite induced an initial chondrogenesis phase [112]. Direct bone formation was also affected by pore geometry: longer and curved pores in the blocks hindered penetration of mesenchymal cells and capillaries resulting in bone formation only on the outer surface of the material as opposed to the particle systems where bone was found deeper in the material [112].

6. Effect of porosity on mechanical properties

Although increased porosity and pore size facilitate bone ingrowth, the result is a reduction in mechanical properties, since this compromises the structural integrity of the scaffold. Chitosan sponges with 100 μm pores were formed inside hydroxyapatite/β-tricalcium phosphate scaffolds with macropores (300–600 μm) and both compressive modulus and yield stress increased about four times [114]. By increasing the weight ratio of sodium phosphate solution ice flakes to tricalcium phosphate cement (no ice to 1:3) higher porosities (31–62%) were achieved [115]. The increased porosity resulted in a higher median pore size (0.2–8.7 μm) and lower percentage of nanopores (<100 nm) [115]. At the same time, lower compressive strength (37000–430 kPa), compressive (2900–37 MPa) and Weibull (4.2–2.0) modulus, was the result [115] (Weibull modulus is a dimensionless number used to characterize the variability in measured strength of components made from brittle materials which arises from the presence of flaws having a distribution in size and orientation).

Porous foams were fabricated by sintering poly(lactide-*co*-glycolide) microspheres; increasing the microsphere diameter from 212–250 to 600–710 μm resulted in larger median pore size (from 72 to 164 μm for 2 h of heating and from 101 to 210 μm for 4 h of heating) and a wider pore distribution (38–110 μm difference in size, respectively), but had no effect on total porosity (>30%) [116]. The compressive modulus was decreased from 297 to 232 MPa [116]. Similarly, higher porosity (80% as opposed to 58%) decreased mechanical properties of porous poly(L-lactide-*co*-D,L-lactide) scaffolds: compressive strength decreased from 11.0 to 2.7 MPa and modulus from 168.3 to 43.5 MPa [68]. Increasing the pore size from 45–150 to 300–600 μm increased the elastic modulus (3.1–7.8 MPa) but did not affect yield strength in scaffolds produced by photopolymerization of a multifunctional lactic acid-based oligomer created by grafting 10 lactic acid units on each side of a di(ethylene glycol) core [117]. The porosity of these scaffolds was ~80%, since lower porosity resulted in less interconnected pores [118] and higher porosity to scaffolds with low mechanical properties [117]. Eighty percent porosity was the critical point between interconnectivity and mechanical properties of scaffolds made by photocross-linking of poly(propylene fumarate) as well; the toughest scaffolds with fully interconnected pores fabricated by this technique had an elastic modulus of 2.3 MPa and a compressive strength of 0.11 MPa [119]. Although higher molecular weight (1.45 kDa) poly(propylene fumarate) increased the fracture toughness (0.376 MPa $m^{1/2}$ as opposed to 0.134 MPa $m^{1/2}$ for the 0.86 kDa) of scaffolds coated with β-tricalcium phosphate with pore sizes 150–300 μm, it reduced the porosity (69% compared to 74%) [120].

Porter et al. studied the effects of porogen and β-tricalcium phosphate concentration on the mechanical properties of poly(propylene fumarate) scaffolds [121]. Increasing the porogen content (20–40 wt% NaCl) decreased bending (16.9–9.2 MPa for 0.5 g of β-tricalcium phosphate/g of poly(propylene fumarate) and 9.1–4.4 MPa for 0.25 g of β-tricalcium phosphate/g of poly(propylene fumarate)) and compressive (70.9–25.6 MPa for 0.5 g of β-tricalcium phosphate/g of poly(propylene fumarate) and 37.7–16.7 MPa for 0.25 g of β-tricalcium phosphate/g of poly(propylene fumarate)) strength, but did not affect bending and compressive elastic modulus [121]. Increasing the amount of β-tricalcium phosphate from 0.25 to 0.5 g of β-tricalcium phosphate/g of poly(propylene fumarate) enhanced all mechanical properties: bending (9.1–16.9 MPa for 20 wt% NaCl and 4.4–9.2 MPa for 40 wt% NaCl) and compressive (37.7–70.9 MPa for 20 wt% NaCl and 16.7–25.6 MPa for 40 wt% NaCl) strength and bending (625.1–1274.7 MPa for 20 wt% NaCl and 619.3–1151.1 MPa for 40 wt% NaCl) and compressive (622.6–1024.2 MPa for 20 wt% NaCl and 354.1–638.1 MPa for 40 wt% NaCl) elastic modulus [121]. Higher porosity (48% versus 44%) of cancellous structured titanium surface coating of dental implants resulted in lower tensile strength (16.1 versus 31.7 MPa) [33]. In general, the compromise in mechanical properties of the scaffold with increasing porosity sets an upper limit in terms of how much porosity and the pore size that can be tolerated.

Zhang et al. discussed a computational model to predict the effect of porosity on the mechanical properties of poly(L-lactide)/bioactive glass composites with pores between 50 and 200 μm present in a network of smaller interconnected pores (<10 μm) [122]. The elastic modulus, E, of the porous composite is given by [122]

$$E = E_0[1 - (P + V_{GP})]^n, \quad (6)$$

where E_0 is the elastic modulus of the solid composite, P the pore fraction, V_{GP} the glass fraction incorporated in

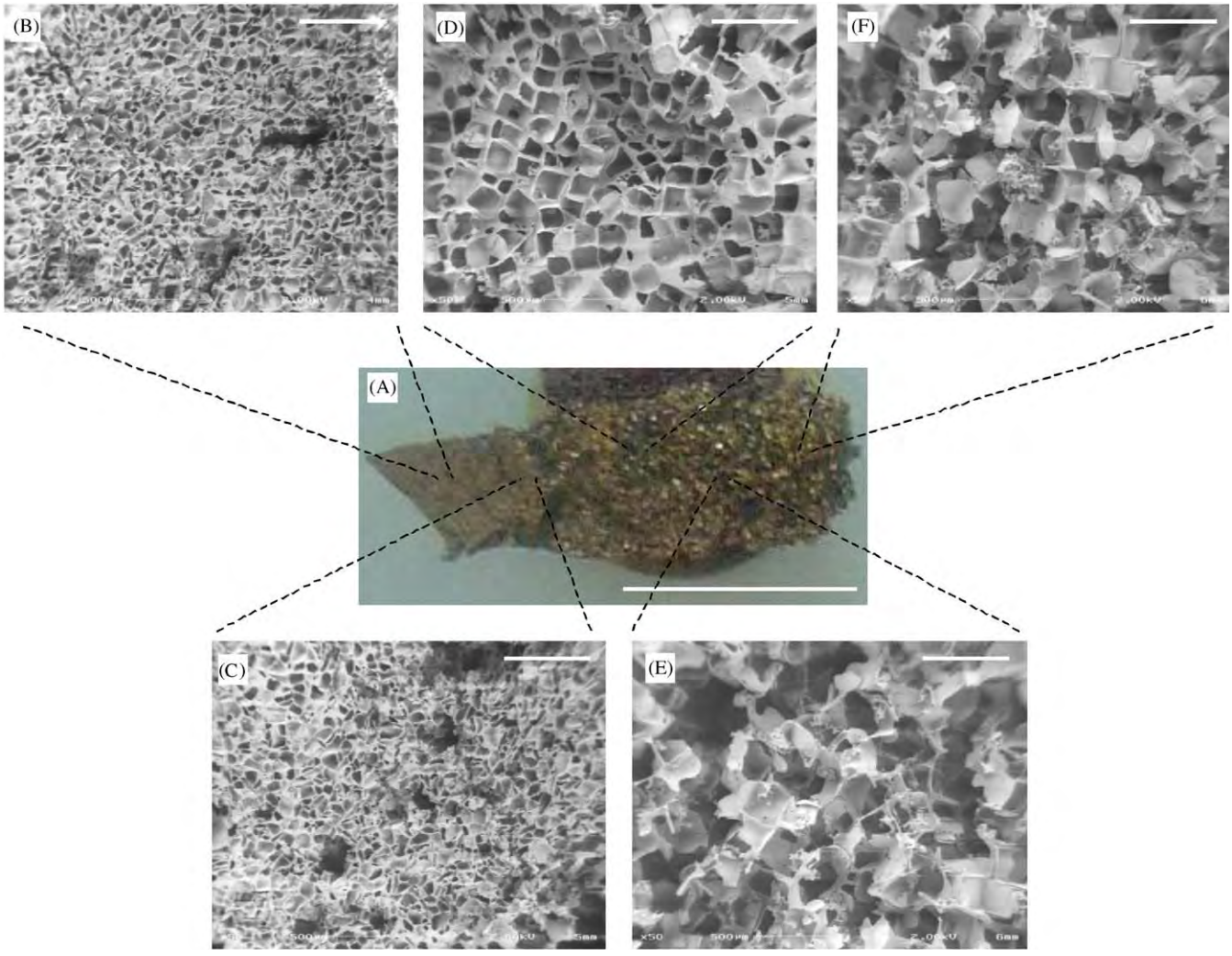

Fig. 1. Pore size gradient across a sponge made of silk fibroin. Pore sizes are 76.3±16.2 μm (B), 100.7±18.2 μm (C), 182.0±30.0 μm (D), 221.3±40.6 μm (E), and 260.3±75.9 μm (F). Bar lengths are 10 mm (A) and 500 μm (B–F).

the pore space and n a constant that depends on the microstructure.

7. Discussion and future aspects

Porosity and pore size both at the macroscopic and the microscopic level, are important morphological properties of a biomaterial scaffold for bone regeneration. Exact void volumes and pore sizes cannot be suggested as a general guide for optimal bone-tissue outcomes, due to the wide range of bone features in vivo and the diversity of biomaterials, cells and cytokines use in vitro and in vivo. However, some critical remarks can be provided based on this review. High porosity and large pores enhance bone ingrowth and osseointegration of the implant after surgery. Although there are a few reports in literature showing no difference in the osteogenic outcome for scaffolds with different porosities, there are no reports indicating a beneficial effect for implants with low porosity. Other factors, such as the rate of degradation of the scaffold for example, should be taken into account when porosity is assessed. Scaffolds fabricated from biomaterials with a high degradation rate should not have high porosities ($>90\%$), since rapid depletion of the biomaterial will compromise the mechanical and structural integrity before substitution by newly formed bone. In contrast, scaffolds fabricated from biomaterials with low degradation rates and robust mechanical properties can be highly porous, because the higher pore surface area interacting with the host tissue can accelerate degradation due to macrophages via oxidation and/or hydrolysis. In vitro lower porosity enhances osteogenesis due to cell aggregation and suppressed proliferation.

The minimum recommended pore size for a scaffold is 100 μm based on the early work of Hulbert et al. [34], but subsequent studies have shown better osteogenesis for implants with pores >300 μm [107–109]. Relatively larger pores favor direct osteogenesis, since they allow vascularization and high oxygenation, while smaller pores result in osteochondral ossification, although the type of bone ingrowth depends on the biomaterial and the geometry of the pores. There is, however, an upper limit in porosity and pore size set by constraints associated with mechanical properties. An increase in the void volume results in a reduction in mechanical strength of the scaffold, which can be critical for regeneration in load-bearing bones. The extent to which pore size can be increased while maintaining mechanical requirements is dependent on many factors including the nature of the biomaterial and the processing conditions

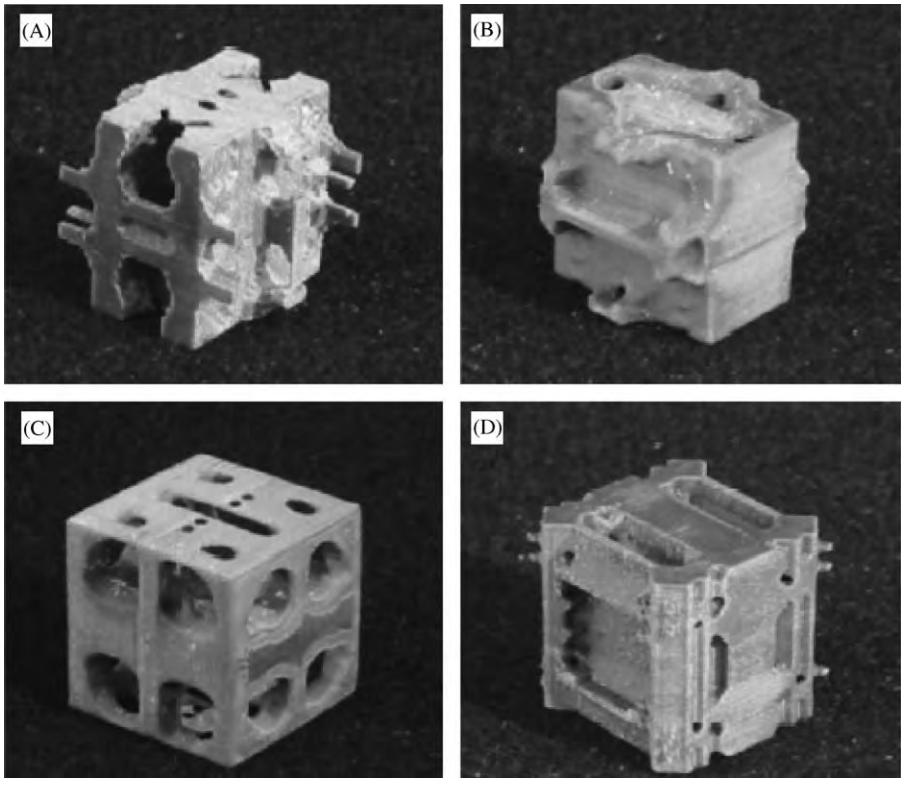

Fig. 2. Prototypes fabricated with 3D Ink Jet Printing with different porosities (61% (A), 49% (B), 48% (C) and 35% (D)) that match Minipig (a commonly used Temporomandibular Joint reconstruction animal model) mandibular condyle bone stiffness. Size 20 mm × 20 mm × 20 mm. Reprinted with permission from [124].

used in its fabrication into 3D scaffolds. An upper limit is also set from the dimensions of the pores of the specific bone-tissue repaired.

The differences of bone tissues in morphological (pore size and porosity) and mechanical properties, as well as gradient features of adsorbed cytokines, set challenges for fabricating biomaterial scaffolds that can meet the requirements set by the specific site of application. As a step forward in addressing this challenge, using salt-leaching we have been able to fabricate a pore size gradient across a slab made of silk fibroin (Fig. 1). Salt-leaching combined with solid-state polymerization has been used to create a porosity gradient in polyglycolide scaffolds both in the macroporous ($>100\,\mu m$) as well as in the microscopic ($<1\,\mu m$) scale [123]. Additionally, cylindrical polyglycolide scaffolds were formed with a microporous surface and macroporous interior to mimic the cortical surface and cancellous interior of natural bone [123]. Other researchers have proposed a computational algorithm, based on topology optimization, that paired different porosities with scaffold geometries for certain mechanical properties [124]. Prototypes of the designed scaffold architectures can be fabricated with techniques, such as solid-free form fabrication techniques (Fig. 2) [124]. The versatility provided by this technique will allow the fabrication of implants with different porosities, pore sizes and mechanical properties that can mimic the complex architecture of bone-specific sites to optimize bone tissue regeneration. In addition, fabricating scaffolds with gradients in porosity and pore sizes that will allow on one side of the scaffold high vascularization and direct osteogenesis, while promoting osteochondral ossification on the other, is appealing in terms of reproducing multiple tissues and tissue interfaces on the same biomaterial scaffold. When this control of design features is considered in concert with the growing understanding of cell biology and cytokine signaling, new opportunities for biomaterials designs for bone-related repair can be anticipated to flourish in the future.

Acknowledgements

We thank the NIH (DE13405-04 and EB003110-02) for support of this work. We also thank Ung-jin Kim and Hyong-Joon Jin for assistance with the micrograph of the gradient scaffold.

References

[1] Groeneveld EH, van den Bergh JP, Holzmann P, ten Bruggenkate CM, Tuinzing DB, Burger EH. Mineralization processes in demineralized bone matrix grafts in human maxillary sinus floor elevations. J Biomed Mater Res 1999;48(4):393–402.

[2] Marks Jr SC, Odgren PR. Structure and development of the skeleton. In: Bilezikian JP, Raisz LG, Rodan GA, editors. Principles of bone biology. 2nd ed. San Diego: Academic Press; 2002. p. 3–15.

[3] Kaplan FS, Hayes WC, Keaveny TM, Boskey A, Einhorn TA, Iannotti JP. Form and function of bone. In: Simon SR, editor. Orthopaedic basic science. Rosemont: American Academy of Orthopaedic Surgeons; 1994. p. 128–84.

[4] Keaveny TM, Morgan EF, Niebur GL, Yeh OC. Biomechanics of trabecular bone. Annu Rev Biomed Eng 2001;3:307–33.

[5] Cooper DM, Matyas JR, Katzenberg MA, Hallgrimsson B. Comparison of microcomputed tomographic and microradiographic measurements of cortical bone porosity. Calcif Tissue Int 2004.

[6] Follet H, Boivin G, Rumelhart C, Meunier PJ. The degree of mineralization is a determinant of bone strength: a study on human calcanei. Bone 2004;783–9.

[7] Bilezikian JP, Raisz LG, Rodan GA. Principles of bone biology. 2nd ed. San Diego: Academic Press; 2002.

[8] Currey JD. Tensile yield in compact bone is determined by strain, post-yield behaviour by mineral content. J Biomech 2004;549–56.

[9] Gogolewski S. Bioresorbable polymers in trauma and bone surgery. Injury 2000;31(Suppl. 4):28–32.

[10] Roy TD, Simon JL, Ricci JL, Rekow ED, Thompson VP, Parsons JR. Performance of degradable composite bone repair products made via three-dimensional fabrication techniques. J Biomed Mater Res A 2003;66(2):283–91.

[11] Rokkanen P, Bostman O, Vainionpaa S, Makela EA, Hirvensalo E, Partio EK, et al. Absorbable devices in the fixation of fractures. J Trauma 1996;40(Suppl. 3):S123–7.

[12] Coombes AG, Meikle MC. Resorbable synthetic polymers as replacements for bone graft. Clin Mater 1994;17(1):35–67.

[13] Disegi JA, Eschbach L. Stainless steel in bone surgery. Injury 2000;31(Suppl. 4):2–6.

[14] Meaney DF. Mechanical properties of implantable biomaterials. Clin Podiatr Med Surg 1995;12(3):363–84.

[15] Park HK, Dujovny M, Agner C, Diaz FG. Biomechanical properties of calvarium prosthesis. Neurol Res 2001;23(2–3):267–76.

[16] Pohler OE. Unalloyed titanium for implants in bone surgery. Injury 2000;31(Suppl. 4):7–13.

[17] Rah DK. Art of replacing craniofacial bone defects. Yonsei Med J 2000;41(6):756–65.

[18] Berven S, Tay BK, Kleinstueck FS, Bradford DS. Clinical applications of bone graft substitutes in spine surgery: consideration of mineralized and demineralized preparations and growth factor supplementation. Eur Spine J 2001;10(Suppl. 2):S169–77.

[19] Dard M, Sewing A, Meyer J, Verrier S, Roessler S, Scharnweber D. Tools for tissue engineering of mineralized oral structures. Clin Oral Investig 2000;4(2):126–9.

[20] Hollinger JO, Seyfer AE. Bioactive factors and bio synthetic materials in bone grafting. Clin Plast Surg 1994;21(3):415–8.

[21] Kirker-Head CA. Recombinant bone morphogenetic proteins: novel substances for enhancing bone healing. Vet Surg 1995;24(5):408–19.

[22] Lee SJ. Cytokine delivery and tissue engineering. Yonsei Med J 2000;41(6):704–19.

[23] Orban JM, Marra KG, Hollinger JO. Composition options for tissue-engineered bone. Tissue Eng 2002;8(4):529–39.

[24] Tabata Y. Tissue regeneration based on growth factor release. Tissue Eng 2003;9(Suppl. 1):S5–S15.

[25] Zellin G, Hedner E, Linde A. Bone regeneration by a combination of osteopromotive membranes with different BMP preparations: a review. Connect Tissue Res 1996;35(1–4):279–84.

[26] Cancedda R, Mastrogiacomo M, Bianchi G, Derubeis A, Muraglia A, Quarto R. Bone marrow stromal cells and their use in regenerating bone. Novartis Found Symp 2003;249: 133–43 (discussion 143–7, 170–4, 239–41).
[27] Warren SM, Nacamuli RK, Song HM, Longaker MT. Tissue-engineered bone using mesenchymal stem cells and a biodegradable scaffold. J Craniofac Surg 2004;15(1):34–7.
[28] Ohgushi H, Miyake J, Tateishi T. Mesenchymal stem cells and bioceramics: strategies to regenerate the skeleton. Novartis Found Symp 2003;249:118–27 (discussion 127–32, 170–4, 239–41).
[29] Ringe J, Kaps C, Burmester GR, Sittinger M. Stem cells for regenerative medicine: advances in the engineering of tissues and organs. Naturwissenschaften 2002;89(8):338–51.
[30] Noel D, Djouad F, Jorgense C. Regenerative medicine through mesenchymal stem cells for bone and cartilage repair. Curr Opin Investig Drugs 2002;3(7):1000–4.
[31] Leon y Leon CA. New perspectives in mercury porosimetry. Adv Colloid Interface Sci 1998;76–77:341–72.
[32] Kuboki Y, Takita H, Kobayashi D, Tsuruga E, Inoue M, Murata M, et al. BMP-induced osteogenesis on the surface of hydroxyapatite with geometrically feasible and nonfeasible structures: topology of osteogenesis. J Biomed Mater Res 1998;39(2):190–9.
[33] Story BJ, Wagner WR, Gaisser DM, Cook SD, Rust-Dawicki AM. In vivo performance of a modified CSTi dental implant coating. Int J Oral Maxillofac Implants 1998;13(6):749–57.
[34] Hulbert SF, Young FA, Mathews RS, Klawitter JJ, Talbert CD, Stelling FH. Potential of ceramic materials as permanently implantable skeletal prostheses. J Biomed Mater Res 1970; 4(3):433–56.
[35] Itala AI, Ylanen HO, Ekholm C, Karlsson KH, Aro HT. Pore diameter of more than 100 micron is not requisite for bone ingrowth in rabbits. J Biomed Mater Res 2001;58(6):679–83.
[36] Svehla M, Morberg P, Zicat B, Bruce W, Sonnabend D, Walsh WR. Morphometric and mechanical evaluation of titanium implant integration: comparison of five surface structures. J Biomed Mater Res 2000;15–22.
[37] Harvey EJ, Bobyn JD, Tanzer M, Stackpool GJ, Krygier JJ, Hacking SA. Effect of flexibility of the femoral stem on bone-remodeling and fixation of the stem in a canine total hip arthroplasty model without cement. J Bone Joint Surg Am 1999;81(1):93–107.
[38] Chang YS, Gu HO, Kobayashi M, Oka M. Influence of various structure treatments on histological fixation of titanium implants. J Arthroplasty 1998;13(7):816–25.
[39] D'Lima DD, Lemperle SM, Chen PC, Holmes RE, Colwell Jr CW. Bone response to implant surface morphology. J Arthroplasty 1998;13(8):928–34.
[40] Sul YT, Johansson CB, Jeong Y, Wennerberg A, Albrektsson T. Resonance frequency and removal torque analysis of implants with turned and anodized surface oxides. Clin Oral Implants Res 2002;13(3):252–9.
[41] Sul YT, Johansson CB, Roser K, Albrektsson T. Qualitative and quantitative observations of bone tissue reactions to anodised implants. Biomaterials 2002;23(8):1809–17.
[42] Sul YT, Johansson CB, Petronis S, Krozer A, Jeong Y, Wennerberg A, et al. Characteristics of the surface oxides on turned and electrochemically oxidized pure titanium implants up to dielectric breakdown: the oxide thickness, micropore configurations, surface roughness, crystal structure and chemical composition. Biomaterials 2002;23(2):491–501.
[43] Steflik DE, Corpe RS, Young TR, Sisk AL, Parr GR. The biologic tissue responses to uncoated and coated implanted biomaterials. Adv Dent Res 1999;27–33.
[44] Yuan H, Kurashina K, de Bruijn JD, Li Y, de Groot K, Zhang X. A preliminary study on osteoinduction of two kinds of calcium phosphate ceramics. Biomaterials 1999;20(19): 1799–806.
[45] Simon JL, Roy TD, Parsons JR, Rekow ED, Thompson VP, Kemnitzer J, et al. Engineered cellular response to scaffold architecture in a rabbit trephine defect. J Biomed Mater Res A 2003;66(2):275–82.
[46] Hu Y, Grainger DW, Winn SR, Hollinger JO. Fabrication of poly(alpha-hydroxy acid) foam scaffolds using multiple solvent systems. J Biomed Mater Res 2002;59(3):563–72.
[47] Maspero FA, Ruffieux K, Muller B, Wintermantel E. Resorbable defect analog PLGA scaffolds using CO_2 as solvent: structural characterization. J Biomed Mater Res 2002;62(1): 89–98.
[48] Kim HW, Knowles JC, Kim HE. Hydroxyapatite/poly(epsilon-caprolactone) composite coatings on hydroxyapatite porous bone scaffold for drug delivery. Biomaterials 2004;25(7–8): 1279–87.
[49] Dong J, Kojima H, Uemura T, Kikuchi M, Tateishi T, Tanaka J. In vivo evaluation of a novel porous hydroxyapatite to sustain osteogenesis of transplanted bone marrow-derived osteoblastic cells. J Biomed Mater Res 2001;57(2):208–16.
[50] Botchwey EA, Pollack SR, Levine EM, Laurencin CT. Bone tissue engineering in a rotating bioreactor using a microcarrier matrix system. J Biomed Mater Res 2001;55(2):242–53.
[51] Chen G, Ushida T, Tateishi T. Poly(DL-lactic-*co*-glycolic acid) sponge hybridized with collagen microsponges and deposited apatite particulates. J Biomed Mater Res 2001;57(1): 8–14.
[52] Oh SH, Kang SG, Kim ES, Cho SH, Lee JH. Fabrication and characterization of hydrophilic poly(lactic-*co*-glycolic acid)/poly(vinyl alcohol) blend cell scaffolds by melt-molding particulate-leaching method. Biomaterials 2003;24(22):4011–21.
[53] El-Ghannam AR. Advanced bioceramic composite for bone tissue engineering: design principles and structure–bioactivity relationship. J Biomed Mater Res A 2004;69(3):490–501.
[54] Li P. Biomimetic nano-apatite coating capable of promoting bone ingrowth. J Biomed Mater Res A 2003;66(1):79–85.
[55] Lewandrowski KU, Hile DD, Thompson BM, Wise DL, Tomford WW, Trantolo DJ. Quantitative measures of osteoinductivity of a porous poly(propylene fumarate) bone graft extender. Tissue Eng 2003;9(1):85–93.
[56] Nazarov R, Jin HJ, Kaplan DL. Porous 3-D scaffolds from regenerated silk fibroin. Biomacromolecules 2004;5(3):718–26.
[57] Zhang R, Ma PX. Poly(alpha-hydroxyl acids)/hydroxyapatite porous composites for bone-tissue engineering. I. Preparation and morphology. J Biomed Mater Res 1999;44(4):446–55.
[58] Zhao F, Yin Y, Lu WW, Leong JC, Zhang W, Zhang J, et al. Preparation and histological evaluation of biomimetic three-dimensional hydroxyapatite/chitosan-gelatin network composite scaffolds. Biomaterials 2002;23(15):3227–34.
[59] Kim HD, Valentini RF. Retention and activity of BMP-2 in hyaluronic acid-based scaffolds in vitro. J Biomed Mater Res 2002;59(3):573–84.
[60] Nishiguchi S, Kato H, Neo M, Oka M, Kim HM, Kokubo T, et al. Alkali- and heat-treated porous titanium for orthopedic implants. J Biomed Mater Res 2001;54(2):198–208.
[61] Park SN, Park JC, Kim HO, Song MJ, Suh H. Characterization of porous collagen/hyaluronic acid scaffold modified by 1-ethyl-3-(3-dimethylaminopropyl)carbodiimide cross-linking. Biomaterials 2002;23(4):1205–12.
[62] Damien E, Hing K, Saeed S, Revell PA. A preliminary study on the enhancement of the osteointegration of a novel synthetic hydroxyapatite scaffold in vivo. J Biomed Mater Res A 2003; 66(2):241–6.
[63] Gong W, Abdelouas A, Lutze W. Porous bioactive glass and glass-ceramics made by reaction sintering under pressure. J Biomed Mater Res 2001;54(3):320–7.

[64] Rocha LB, Goissis G, Rossi MA. Biocompatibility of anionic collagen matrix as scaffold for bone healing. Biomaterials 2002;23(2):449–56.
[65] Yuan H, de Bruijn JD, Zhang X, van Blitterswijk CA, de Groot K. Bone induction by porous glass ceramic made from Bioglass (45S5). J Biomed Mater Res 2001;58(3):270–6.
[66] Barry JJ, Gidda HS, Scotchford CA, Howdle SM. Porous methacrylate scaffolds: supercritical fluid fabrication and in vitro chondrocyte responses. Biomaterials 2004;25(17):3559–68.
[67] Cartmell S, Huynh K, Lin A, Nagaraja S, Guldberg R. Quantitative microcomputed tomography analysis of mineralization within three-dimensional scaffolds in vitro. J Biomed Mater Res A 2004;69(1):97–104.
[68] Lin AS, Barrows TH, Cartmell SH, Guldberg RE. Microarchitectural and mechanical characterization of oriented porous polymer scaffolds. Biomaterials 2003;24(3):481–9.
[69] Lee YM, Seol YJ, Lim YT, Kim S, Han SB, Rhyu IC, et al. Tissue-engineered growth of bone by marrow cell transplantation using porous calcium metaphosphate matrices. J Biomed Mater Res 2001;54(2):216–23.
[70] Chen F, Mao T, Tao K, Chen S, Ding G, Gu X. Bone graft in the shape of human mandibular condyle reconstruction via seeding marrow-derived osteoblasts into porous coral in a nude mice model. J Oral Maxillofac Surg 2002;60(10):1155–9.
[71] Zhang C, Wang J, Feng H, Lu B, Song Z, Zhang X. Replacement of segmental bone defects using porous bioceramic cylinders: a biomechanical and X-ray diffraction study. J Biomed Mater Res 2001;54(3):407–11.
[72] LeGeros RZ. Properties of osteoconductive biomaterials: calcium phosphates. Clin Orthop 2002;395:81–98.
[73] Tarvainen T, Tunturi T, Rautavuori J, Tormala P, Patiala H, Rokkanen P. Shear strength of loaded porous-glassy-carbon/bone interface—an experimental study on rabbits. Ann Biomed Eng 1986;14(5):417–24.
[74] Xynos ID, Hukkanen MV, Batten JJ, Buttery LD, Hench LL, Polak JM. Bioglass 45S5 stimulates osteoblast turnover and enhances bone formation In vitro: implications and applications for bone tissue engineering. Calcif Tissue Int 2000;67(4):321–9.
[75] Sepulveda P, Jones JR, Hench LL. Bioactive sol–gel foams for tissue repair. J Biomed Mater Res 2002;59(2):340–8.
[76] Akin FA, Zreiqat H, Jordan S, Wijesundara MB, Hanley L. Preparation and analysis of macroporous TiO_2 films on Ti surfaces for bone-tissue implants. J Biomed Mater Res 2001;57(4):588–96.
[77] Pilliar RM. Overview of surface variability of metallic endosseous dental implants: textured and porous surface-structured designs. Implant Dent 1998;7(4):305–14.
[78] van den Dolder J, Farber E, Spauwen PH, Jansen JA. Bone tissue reconstruction using titanium fiber mesh combined with rat bone marrow stromal cells. Biomaterials 2003;24(10):1745–50.
[79] Sikavitsas VI, van den Dolder J, Bancroft GN, Jansen JA, Mikos AG. Influence of the in vitro culture period on the in vivo performance of cell/titanium bone tissue-engineered constructs using a rat cranial critical size defect model. J Biomed Mater Res A 2003;67(3):944–51.
[80] Vehof JW, Haus MT, de Ruijter AE, Spauwen PH, Jansen JA. Bone formation in transforming growth factor beta-I-loaded titanium fiber mesh implants. Clin Oral Implants Res 2002;13(1):94–102.
[81] Rubin JP, Yaremchuk MJ. Complications and toxicities of implantable biomaterials used in facial reconstructive and aesthetic surgery: a comprehensive review of the literature. Plast Reconstr Surg 1997;100(5):1336–53.
[82] van Luyn MJ, van Wachem PB, Damink LO, Dijkstra PJ, Feijen J, Nieuwenhuis P. Relations between in vitro cytotoxicity and crosslinked dermal sheep collagens. J Biomed Mater Res 1992;26(8):1091–110.
[83] Santin M, Motta A, Freddi G, Cannas M. In vitro evaluation of the inflammatory potential of the silk fibroin. J Biomed Mater Res 1999;382–9.
[84] Altman GH, Diaz F, Jakuba C, Calabro T, Horan RL, Chen J, et al. Silk-based biomaterials. Biomaterials 2003;401–16.
[85] Panilaitis B, Altman GH, Chen J, Jin HJ, Karageorgiou V, Kaplan DL. Macrophage responses to silk. Biomaterials 2003;24(18):3079–85.
[86] Gosline JM, Demont ME, Denny MW. The structure and properties of spider silk. Endeavour 1986;37–43.
[87] Meinel L, Karageorgiou V, Hofmann S, Fajardo R, Snyder B, Li C, et al. Engineering bone-like tissue in vitro using human bone marrow stem cells and silk scaffolds. J Biomed Mater Res 2004 (in press).
[88] Yang XB, Roach HI, Clarke NM, Howdle SM, Quirk R, Shakesheff KM, et al. Human osteoprogenitor growth and differentiation on synthetic biodegradable structures after surface modification. Bone 2001;29(6):523–31.
[89] Li WJ, Laurencin CT, Caterson EJ, Tuan RS, Ko FK. Electrospun nanofibrous structure: a novel scaffold for tissue engineering. J Biomed Mater Res 2002;60(4):613–21.
[90] Vehof JW, Fisher JP, Dean D, van der Waerden JP, Spauwen PH, Mikos AG, et al. Bone formation in transforming growth factor beta-1-coated porous poly(propylene fumarate) scaffolds. J Biomed Mater Res 2002;60(2):241–51.
[91] Taboas JM, Maddox RD, Krebsbach PH, Hollister SJ. Indirect solid free form fabrication of local and global porous, biomimetic and composite 3D polymer-ceramic scaffolds. Biomaterials 2003;24(1):181–94.
[92] Schaefer D, Martin I, Shastri P, Padera RF, Langer R, Freed LE, et al. In vitro generation of osteochondral composites. Biomaterials 2000;21(24):2599–606.
[93] Trantolo DJ, Sonis ST, Thompson BM, Wise DL, Lewandrowski KU, Hile DD. Evaluation of a porous, biodegradable biopolymer scaffold for mandibular reconstruction. Int J Oral Maxillofac Implants 2003;18(2):182–8.
[94] An YH, Woolf SK, Friedman RJ. Pre-clinical in vivo evaluation of orthopaedic bioabsorbable devices. Biomaterials 2000;21(24):2635–52.
[95] Lickorish D, Ramshaw JA, Werkmeister JA, Glattauer V, Howlett CR. Collagen-hydroxyapatite composite prepared by biomimetic process. J Biomed Mater Res A 2004;68(1):19–27.
[96] Tache A, Gan L, Deporter D, Pilliar RM. Effect of surface chemistry on the rate of osseointegration of sintered porous-surfaced Ti-6Al-4V implants. Int J Oral Maxillofac Implants 2004;19–29.
[97] Vehof JW, Spauwen PH, Jansen JA. Bone formation in calcium-phosphate-coated titanium mesh. Biomaterials 2000;21(19):2003–9.
[98] Zhang X, Ayers RA, Thorne K, Moore JJ, Schowengerdt F. Combustion synthesis of porous materials for bone replacement. Biomed Sci Instrum 2001;37:463–8.
[99] Akay G, Birch MA, Bokhari MA. Microcellular polyHIPE polymer supports osteoblast growth and bone formation in vitro. 2004.
[100] Itoh M, Shimazu A, Hirata I, Yoshida Y, Shintani H, Okazaki M. Characterization of CO_3Ap-collagen sponges using X-ray high-resolution microtomography. Biomaterials 2004;25(13):2577–83.
[101] Takahashi Y, Tabata Y. Effect of the fiber diameter and porosity of non-woven PET fabrics on the osteogenic differentiation of mesenchymal stem cells. J Biomater Sci Polym Ed 2004;15(1):41–57.
[102] Lewandrowski KU, Gresser JD, Bondre S, Silva AE, Wise DL, Trantolo DJ. Developing porosity of poly(propylene

glycol-*co*-fumaric acid) bone graft substitutes and the effect on osteointegration: a preliminary histology study in rats. J Biomater Sci Polym Ed 2000;11(8):879–89.
[103] Chu TM, Orton DG, Hollister SJ, Feinberg SE, Halloran JW. Mechanical and in vivo performance of hydroxyapatite implants with controlled architectures. Biomaterials 2002;23(5):1283–93.
[104] Kruyt MC, de Bruijn JD, Wilson CE, Oner FC, van Blitterswijk CA, Verbout AJ, et al. Viable osteogenic cells are obligatory for tissue-engineered ectopic bone formation in goats. Tissue Eng 2003;9(2):327–36.
[105] Kujala S, Ryhanen J, Danilov A, Tuukkanen J. Effect of porosity on the osteointegration and bone ingrowth of a weight-bearing nickel–titanium bone graft substitute. Biomaterials 2003;24(25):4691–7.
[106] Fisher JP, Vehof JW, Dean D, van der Waerden JP, Holland TA, Mikos AG, et al. Soft and hard tissue response to photocrosslinked poly(propylene fumarate) scaffolds in a rabbit model. J Biomed Mater Res 2002;59(3):547–56.
[107] Kuboki Y, Jin Q, Takita H. Geometry of carriers controlling phenotypic expression in BMP-induced osteogenesis and chondrogenesis. J Bone Joint Surg Am 2001;83A(Suppl. 1(Pt 2)): S105–15.
[108] Tsuruga E, Takita H, Itoh H, Wakisaka Y, Kuboki Y. Pore size of porous hydroxyapatite as the cell-substratum controls BMP-induced osteogenesis. J Biochem (Tokyo) 1997;121(2):317–24.
[109] Gotz HE, Muller M, Emmel A, Holzwarth U, Erben RG, Stangl R. Effect of surface finish on the osseointegration of laser-treated titanium alloy implants. Biomaterials 2004;25(18):4057–64.
[110] Liu LS, Thompson AY, Heidaran MA, Poser JW, Spiro RC. An osteoconductive collagen/hyaluronate matrix for bone regeneration. Biomaterials 1999;20(12):1097–108.
[111] Ayers RA, Simske SJ, Bateman TA, Petkus A, Sachdeva RL, Gyunter VE. Effect of nitinol implant porosity on cranial bone ingrowth and apposition after 6 weeks. J Biomed Mater Res 1999;45(1):42–7.
[112] Jin QM, Takita H, Kohgo T, Atsumi K, Itoh H, Kuboki Y. Effects of geometry of hydroxyapatite as a cell substratum in BMP-induced ectopic bone formation. J Biomed Mater Res 2000;51(3):491–9.
[113] Kuboki Y, Jin Q, Kikuchi M, Mamood J, Takita H. Geometry of artificial ECM: sizes of pores controlling phenotype expression in BMP-induced osteogenesis and chondrogenesis. Connect Tissue Res 2002;43(2–3):529–34.
[114] Zhang Y, Zhang M. Three-dimensional macroporous calcium phosphate bioceramics with nested chitosan sponges for load-bearing bone implants. J Biomed Mater Res 2002;61(1):1–8.
[115] Barralet JE, Grover L, Gaunt T, Wright AJ, Gibson IR. Preparation of macroporous calcium phosphate cement tissue engineering scaffold. Biomaterials 2002;23(15):3063–72.
[116] Borden M, El-Amin SF, Attawia M, Laurencin CT. Structural and human cellular assessment of a novel microsphere-based tissue engineered scaffold for bone repair. Biomaterials 2003;24(4):597–609.
[117] Burdick JA, Frankel D, Dernell WS, Anseth KS. An initial investigation of photocurable three-dimensional lactic acid based scaffolds in a critical-sized cranial defect. Biomaterials 2003;24(9):1613–20.
[118] Burdick JA, Padera RF, Huang JV, Anseth KS. An investigation of the cytotoxicity and histocompatibility of in situ forming lactic acid based orthopedic biomaterials. J Biomed Mater Res 2002;63(5):484–91.
[119] Fisher JP, Holland TA, Dean D, Engel PS, Mikos AG. Synthesis and properties of photocross-linked poly(propylene fumarate) scaffolds. J Biomater Sci Polym Ed 2001;12(6): 673–87.
[120] Wolfe MS, Dean D, Chen JE, Fisher JP, Han S, Rimnac CM, et al. In vitro degradation and fracture toughness of multilayered porous poly(propylene fumarate)/beta-tricalcium phosphate scaffolds. J Biomed Mater Res 2002;61(1):159–64.
[121] Porter BD, Oldham JB, He SL, Zobitz ME, Payne RG, An KN, et al. Mechanical properties of a biodegradable bone regeneration scaffold. J Biomech Eng 2000;122(3):286–8.
[122] Zhang K, Wang Y, Hillmyer MA, Francis LF. Processing and properties of porous poly(L-lactide)/bioactive glass composites. Biomaterials 2004;25(13):2489–500.
[123] Schwarz K, Epple M. Hierarchically structured polyglycolide—a biomaterial mimicking natural bone. Macromol Rapid Commun 1998;19(12):613–7.
[124] Lin CY, Kikuchi N, Hollister SJ. A novel method for biomaterial scaffold internal architecture design to match bone elastic properties with desired porosity. J Biomech 2004; 37(5):623–36.
[125] Cullinane DM, Einhorn TA. Biomechanics of bone. In: Bilezikian JP, Raisz LG, Rodan GA, editors. Principles of bone biology. San Diego: Avademic Press; 2002. p. 17–32.
[126] Linde F, Hvid I. The effect of constraint on the mechanical behaviour of trabecular bone specimens. J Biomech 1989;22(5): 485–90.
[127] Rohlmann A, Zilch H, Bergmann G, Kolbel R. Material properties of femoral cancellous bone in axial loading. Part I: time independent properties. Arch Orthop Trauma Surg 1980;97(2):95–102.

Spine

SPINE Volume 40, Number 6, pp 399-404

EPIDEMIOLOGY

Implant Materials Generate Different Peri-implant Inflammatory Factors

Poly-ether-ether-ketone Promotes Fibrosis and Microtextured Titanium Promotes Osteogenic Factors

Rene Olivares-Navarrete, DDS, PhD,* Sharon L. Hyzy, MS,* Paul J. Slosar, MD,† Jennifer M. Schneider, MS,‡ Zvi Schwartz, DMD, PhD,*§ and Barbara D. Boyan, PhD*¶

Study Design. An *in vitro* study examining factors produced by human mesenchymal stem cells on spine implant materials.

Objective. The aim of this study was to examine whether the inflammatory microenvironment generated by cells on titanium-aluminum-vanadium (Ti-alloy, TiAlV) surfaces is affected by surface microtexture and whether it differs from that generated on poly-ether-ether-ketone (PEEK).

Summary of Background Data. Histologically, implants fabricated from PEEK have a fibrous connective tissue surface interface whereas Ti-alloy implants demonstrate close approximation with surrounding bone. Ti-alloy surfaces with complex micron/submicron scale roughness promote osteoblastic differentiation and foster a specific cellular environment that favors bone formation whereas PEEK favors fibrous tissue formation.

Methods. Human mesenchymal stem cells were cultured on tissue culture polystyrene, PEEK, smooth TiAlV, or macro-/micro-/nano-textured rough TiAlV (mmnTiAlV) disks. Osteoblastic differentiation and secreted inflammatory interleukins were assessed after 7 days. Fold changes in mRNAs for inflammation, necrosis, DNA damage, or apoptosis with respect to tissue culture polystyrene were measured by low-density polymerase chain reaction array. Data were analyzed by analysis of variance, followed by Bonferroni's correction of Student's *t*-test.

Results. Cells on PEEK upregulated mRNAs for chemokine ligand-2, interleukin (IL) 1β, IL6, IL8, and tumor necrosis factor. Cells grown on the mmnTiAlV had an 8-fold reduction in mRNAs for toll-like receptor-4. Cells grown on mmnTiAlV had reduced levels of proinflammatory interleukins. Cells on PEEK had higher mRNAs for factors strongly associated with cell death/apoptosis, whereas cells on mmnTiAlV exhibited reduced cytokine factor levels. All results were significant ($P < 0.05$).

Conclusion. These results suggest that fibrous tissue around PEEK implants may be due to several factors: reduced osteoblastic differentiation of progenitor cells and production of an inflammatory environment that favors cell death *via* apoptosis and necrosis. Ti alloy surfaces with complex macro/micro/nanoscale roughness promote osteoblastic differentiation and foster a specific cellular environment that favors bone formation.

Key words: mesenchymal stem cells, PEEK, Ti6Al4V, interbody spine cage, inflammatory mediators, implant surface, osteogenesis, fibrosis, mRNA array.

Level of Evidence: N/A

Spine 2015;40:399–404

From the *Department of Biomedical Engineering, Virginia Commonwealth University, Richmond, VA; †SpineCare Medical Group, San Francisco Spine Institute, San Francisco, CA; ‡Titan Spine, LLC, Mequon, WI; §Department of Periodontics, The University of Texas Health Science Center at San Antonio, San Antonio, TX; and ¶Wallace H. Coulter Department of Biomedical Engineering, Georgia Institute of Technology, Atlanta, GA.

Acknowledgment date: September 22, 2014. Revision date: December 16, 2014. Acceptance date: December 17, 2014.

The manuscript submitted does not contain information about medical device(s)/drug(s).

National Institute of Arthritis and Musculoskeletal and Skin Diseases of the National Institutes of Health under Award Number AR052102 funds were received to support this work.

Relevant financial activities outside the submitted work: board membership, consultancy, employment, grants, travel/accommodations/meeting expenses, royalties, stocks.

Address correspondence and reprint requests to Barbara D. Boyan, PhD, School of Engineering, Virginia Commonwealth University, 601 West Main St, Richmond, VA 23284; E-mail: bboyan@vcu.edu

DOI: 10.1097/BRS.0000000000000778

Materials such as titanium-aluminum-vanadium alloy (Ti-6Al-4V, TiAlV) and poly-ether-ether-ketone (PEEK) are commonly used in spinal interbody fusion surgical procedures. These 2 materials, while used for similar clinical applications, have substantially different surface characteristics, especially on a micron scale. Poly-ether-ether-ketone is popular because its modulus of 3 to 4 GPa[1,2] is close to that of native cortical bone, 14 to 18 GPa. In addition, PEEK is radiolucent, allowing surgeons to examine whether bone fills the intervertebral space. However, it is often encapsulated by fibrous tissue. The lack of bone integration can ultimately result in implant subsidence and nonunion.

Ti alloys have higher elastic moduli than bone but have yielded successful results clinically.[3,4] Studies in animal models show greater bone apposition to Ti and Ti alloy surfaces, particularly when the surfaces have a rough microtopography.[5–7]

In vitro studies indicate that microtextured Ti and Ti alloy surfaces promote osteoblast differentiation and production of factors that favor bone formation *in vivo*, whereas PEEK does not.[8–10]

After a material is implanted into the body, the immune system initiates an immune response sequence.[11] The inflammatory response to the biomaterial is mediated in large part by the local inflammatory microenvironment, which results in a cascade triggering migration of other cells to the vicinity. A high level of inflammation creates a longer resolution period. Fibroblasts initially produce extracellular matrix in an effort to support the damaged tissue; however, extended activation of macrophages and other immune cells leads to reduction in matrix remodeling and the fibrotic scar tissue that was formed in the support stage of wound healing, which remains.

The persistence of fibrosis around PEEK implants in contrast to peri-implant bone formation around Ti alloy suggests that PEEK may stimulate formation of microenvironment consisting of specific inflammatory cytokines that enhance fibrous tissue formation, whereas micron-scale–roughened Ti alloy surfaces reduce production of these factors. To test this hypothesis, we cultured human mesenchymal stem cells (MSCs) on disks consisting of machined PEEK, machined Ti6Al4V, and microtextured Ti6Al4V, and examined their production of factors associated with inflammation, apoptosis, and necrosis.

MATERIALS AND METHODS

Material Fabrication

Fifteen-millimeter diameter disks of PEEK, smooth TiAlV (sTiAlV), and macro-/micro-/nano-rough (mmnTiAlV) were provided by Titan Spine (Mequon, WI). Processing of these disks resulted in varying surface topographies with average roughness (S_a) for sTiAlV of 0.27 ± 0.01 μm or 2.74 ± 0.18 μm for mmnTiAlV. PEEK substrates were machined, resulting in a S_a of 0.43 ± 0.07 μm. Surface topography was visualized using scanning electron microscopy (SEM, Ultra 60 FEG-SEM; Carl Zeiss SMT Ltd., Cambridge, United Kingdom) recorded using a 5 kV accelerating voltage and 30-μm aperture. All disks were ultrasonically cleaned in ultrapure water (Millipore, Billerica, MA) and autoclave sterilized (Tuttnauer, Hauppauge, NY) before use in cell culture studies.[9]

Cell Culture

Human MSCs (Lonza Biosciences, Walkersville, MD) were seeded on PEEK, sTiAlV, or mmnTiAlV at an initial density of 10,000 cells/cm^2 and cultured in MSC growth media (MSCGM, Lonza Biosciences) at 5% CO_2 and 100% humidity. Cells cultured on tissue culture polystyrene (TCPS) served as an internal control.

Osteoblast Phenotype

When cells reached confluence on TCPS, the media were changed and cells were incubated for 24 hours. Cells were lysed in 0.05% Triton X-100 and homogenized using a sonic dismembrator. Alkaline phosphatase activity, an early marker of osteoblast differentiation that reaches a peak just before matrix mineralization, was assayed in lysates by measuring the release of *p*-nitrophenol from *p*-nitrophenyl phosphate at pH 10.2. Activity was normalized to total protein content (Thermo Fisher Pierce BCA Protein Assay, Rockford, IL) of the cell lysates. Secreted osteocalcin, a later marker of osteoblast differentiation important in modulating hydroxyapatite crystallization, was measured using a radioimmunoassay (Biomedical Technologies, Stoughton, MA) and normalized to DNA content (Quant-iT Assay Kit, Life Technologies, Carlsbad, CA) in the cell lysate.

Interleukin Protein Production

Cells were cultured as described previously and at confluence on TCPS, cells on all surfaces were incubated with fresh medium for 24 hours. Levels of secreted cytokines IL1β, IL6, IL8, and IL10 were assayed in the conditioned medium (R&D Systems DuoSet ELISA, Minneapolis, MN) and normalized to DNA in the cell lysate.

Polymerase Chain Reaction Array

Cells were cultured on TCPS, PEEK, sTiAlV, or mmnTiAlV substrates. Cells were incubated with fresh medium for 12 hours after reaching confluence on TCPS. RNA was harvested using a TRIzol (Life Technology) extraction method following manufacturer's protocol and was quantified (NanoDrop 1000, Thermo Scientific, Waltham, MA). RNA (500 ng) was amplified by reverse transcription (RT^2 First Strand Kit, Qiagen, Valencia, CA). mRNA was measured for 39 genes using PathwayFinder RT^2 Profiler PCR Array (polymerase chain reaction array; Qiagen) and fold change to TCPS was normalized to 3 housekeeping genes in the array using the Web-based PCR Array Data Analysis Software (Qiagen).

Statistical Analysis

PCR array experiments were performed on n = 3 samples per variable. Statistical differences were determined using Qiagen software, and changes greater than 2-fold was considered significant. All other experiments involved 6 independent cultures for each variable. Data from each experiment were analyzed separately by analysis of variance and significant differences between groups were determined using Bonferroni's modification of Student *t*-test in GraphPad Prism Version 5.04. *P* value of less than 0.05 was considered to be significant.

RESULTS

SEM imaging qualitatively demonstrated differences in surface structures. PEEK disks had relatively smooth surfaces and had only minor parallel grooves because of processing (Figure 1). Likewise, sTiAlV surfaces were mostly smooth, with superficial grooves from machining (Figure 1). Rough mmnTiAlV surfaces featured large pits and craters with superimposed micron- and submicron-scale features (Figure 1).

DNA content was significantly lower in cultures on PEEK and mmnTiAlV, but not different on sTiAlV, in comparison with TCPS (Figure 2A). Alkaline phosphatase activity

Figure 1. Scanning electron microscopy images of PEEK (left panel), sTiAlV (middle panel), and mmnTiAlV (right panel) surfaces obtained at 1k× magnification. PEEK indicates poly-ether-ether-ketone; sTiAlV, smooth titanium alloy; mmnTiAlV, micro-textured rough titanium alloy.

was the same in MSCs cultured on TCPS or PEEK (Figure 2B) and was significantly higher on TiAlV surfaces in comparison with both TCPS and PEEK. Levels were significantly higher on mmnTiAlV than activity on the sTiAlV surface. Likewise, osteocalcin production was increased only on the Ti alloy surfaces, with the effect being greater on mmnTiAlV (Figure 2C).

Production of proinflammatory interleukins IL1β, IL6, and IL8 by MSCs was highest on PEEK compared with all other materials (Figure 3A–C). Conversely, production was lowest on the mmnTiAlV surface and was even lower than on TCPS. These were consistent observations, regardless of the protein analyzed. Levels of anti-inflammatory IL10 were comparable in conditioned media of cultures grown on TCPS and the TiAlV surfaces (Figure 3D). Moreover, in cultures grown on the Ti alloy substrates, levels of IL10 were significantly greater than on PEEK.

The PCR array (Figure 4) demonstrated that cells cultured on mmnTiAlV exhibited the lowest levels of mRNAs for proinflammatory proteins (Figure 4A) and for proteins associated with necrosis (Figure 4B), DNA damage (Figure 4C), and apoptosis (Figure 4D). In contrast, fold changes in these mRNAs on PEEK were the highest in comparison with cells on TCPS.

DISCUSSION

Spine surgeons traditionally augment interbody fusion implants with bone graft or bone graft substitutes of varying biologic potency. It is, therefore, challenging to discern meaningful differences between Ti alloy and PEEK implant materials in a clinical study. An *in vitro* model can identify cellular response differences between materials without use of additives in the medium to promote osteogenesis.

Previous *in vitro* studies showed that osteoblast differentiation of human MSCs[12] and osteoblasts[13] is influenced by implant surface properties. When MSCs are cultured on PEEK, cells fail to exhibit known markers of bone formation such as increased alkaline phosphatase activity or osteocalcin production compared with cells cultured on TCPS. In contrast, MSCs cultured on rough Ti and Ti alloy do exhibit increased levels of these markers as well as production of proteins that favor osteoblast differentiation (BMP-2, BMP-4, VEGF), even in the absence of media supplements used to stimulate expression of an osteoblast phenotype.[12] These *in vitro* studies are supported by *in vivo* results examining peri-implant bone formation in sheep spine, where Ti alloy pedicle screws with micron scale and submicron scale roughness exhibited 2-fold increases in pullout strength.[14]

Histologically, Ti alloy implants demonstrate close apposition with surrounding bone; however, implants fabricated from PEEK develop a fibrous connective tissue interface.[1,14,15] Differences in the chemical and physical properties of an implant surface can directly affect immune cell response. Studies examining dendritic cell maturation show that it is sensitive to both chemistry and shape of a biomaterial,[16–18] including surface microstructure.[19] When immature dendritic cells were cultured on microtextured Ti surfaces compared with smooth surface Ti surfaces, the expression of a mature dendritic cell phenotype was reduced.

Our results suggest that differences in biological response to Ti alloy and PEEK may be due to differences in the inflammatory microenvironment generated by cells on the implant surface. Increase of proinflammatory cytokines, specifically high levels of IL1β, is associated with fibrous tissue formation,[20] and IL1β, IL6, and IL8 are increased in chronic inflammation. We observed the lowest levels of these inflammatory

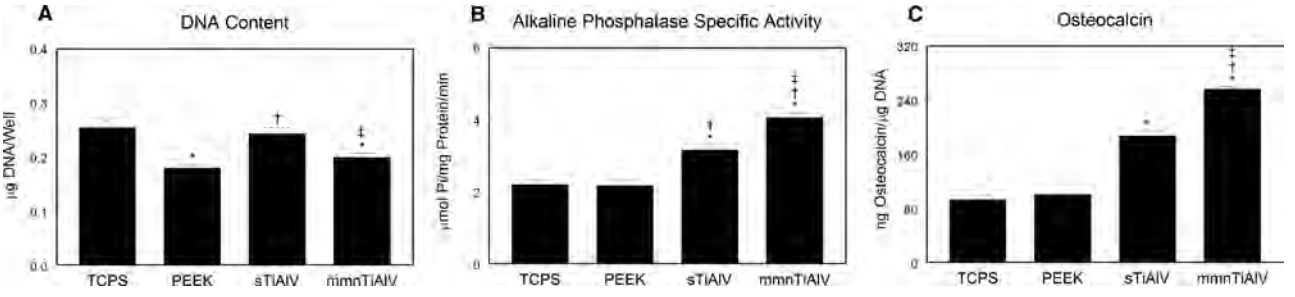

Figure 2. DNA content (**A**), alkaline phosphatase–specific activity (**B**), and osteocalcin production (**C**) in mesenchymal stem cells cultured on TCPS, PEEK, sTiAlV, or mmnTiAlV. *$P < 0.05$ versus TCPS; †$P < 0.05$ versus PEEK; ‡$P < 0.05$ versus sTiAlV. TCPS indicates tissue culture polystyrene; PEEK, poly-ether-ether-ketone; sTiAlV, smooth titanium-aluminum-vanadium alloy; mmnTiAlV, macro-/micro-/nano-textured rough TiAlV.

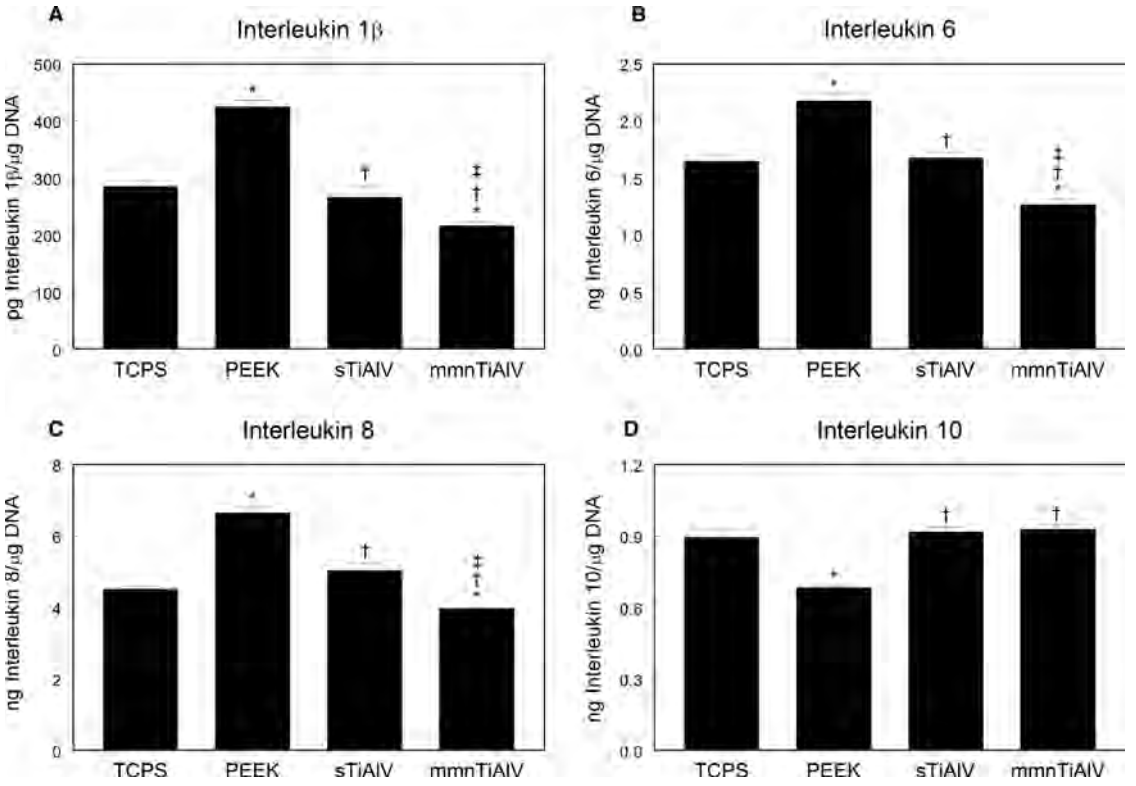

Figure 3. Levels of IL1β (**A**), IL6 (**B**), IL8 (**C**), and IL10 (**D**) in the conditioned media of mesenchymal stem cells cultured on TCPS, PEEK, sTiAlV, or mmnTiAlV. *$P < 0.05$ versus TCPS; †$P < 0.05$ versus PEEK; ‡$P < 0.05$ versus sTiAlV. TCPS indicates tissue culture polystyrene; PEEK, poly-ether-ether-ketone; sTiAlV, smooth titanium-aluminum-vanadium alloy; mmnTiAlV, macro-/micro-/nano-textured rough TiAlV.

factors in MSC cultures grown on mmnTiAlV. In contrast, the cultures grown on PEEK resulted in the highest levels, suggesting a profibrosis, inflammatory response.

The opposite was true with respect to the anti-inflammatory factor IL10. Reduced levels of this mediator favor a pro-inflammatory state, and PEEK was associated with reduced levels of IL10 compared with Ti. Taken together, our results showed that mmnTiAlV reduced the local inflammatory environment, decreasing the proinflammatory cytokines but also increasing the levels of the anti-inflammatory cytokine IL10.

Particularly interesting was the observation that expression of factors associated with DNA damage and necrosis was upregulated on PEEK but either unchanged or reduced on Ti alloy. Similarly, PEEK consistently upregulated factors for apoptosis whereas the mmnTiAlV reduced these factors more than smooth Ti. Our results suggest that cells grown on PEEK are exposed to cellular stress and increase expression of genes that lead to DNA damage, apoptosis, and necrosis. All results together demonstrate that cells grown on PEEK produce a proinflammatory environment, but it is not clear whether PEEK can induce apoptosis and necrosis by direct contact or as a result of the high proinflammatory environment.

The question remains as to whether our findings were due to PEEK's chemistry or to its surface structure. PEEK surface topography varies with processing, and rougher PEEK surfaces do support greater osteoblast differentiation of human osteoblasts than smooth surfaced PEEK.[21] Recent studies have shown that bone formation is improved around PEEK implants that have been blasted using biphasic calcium phosphate[22]; however, residual mineral may contribute to the outcome. PEEK that has been treated by oxygen plasma exhibits improved osseointegration,[23] supporting the hypothesis that surface topography is an important variable. *In vitro* studies also indicate that adipose-derived stem cells exhibit improved osteoblast differentiation when grown on PEEK treated by oxygen plasma, but the surface modifications lead to changes in contact angle and electrochemical properties in addition to altered nanostructure.[24] Another modification of the PEEK surface has been generated using a porogen filler, polymer extrusion, and removal of the filler.[25] Bone marrow stromal cells cultured on these surfaces exhibit osteoblast differentiation, but the contribution of surface chemistry is not known. Well-controlled experiments in which porosity on the PEEK surface is produced using various chemical methods show that small differences in resulting surface properties can alter osteoblast growth and differentiation as well as osseointegration.[26] Although these studies demonstrate the value of surface roughness in osteogenic effects of PEEK materials, few reports have directly compared responses to PEEK with responses to Ti6Al4V. Even those studies that have examined responses to PEEK and Ti6Al4V have not assessed effects on immune modulation.

Our study did not address the contribution of substrate stiffness to the outcomes measured. PEEK and Ti6Al4V have different moduli, both of which differ from that of the bone surface. Stiffness of a substrate does influence MSC differentiation, but it is very difficult to separate effects of stiffness

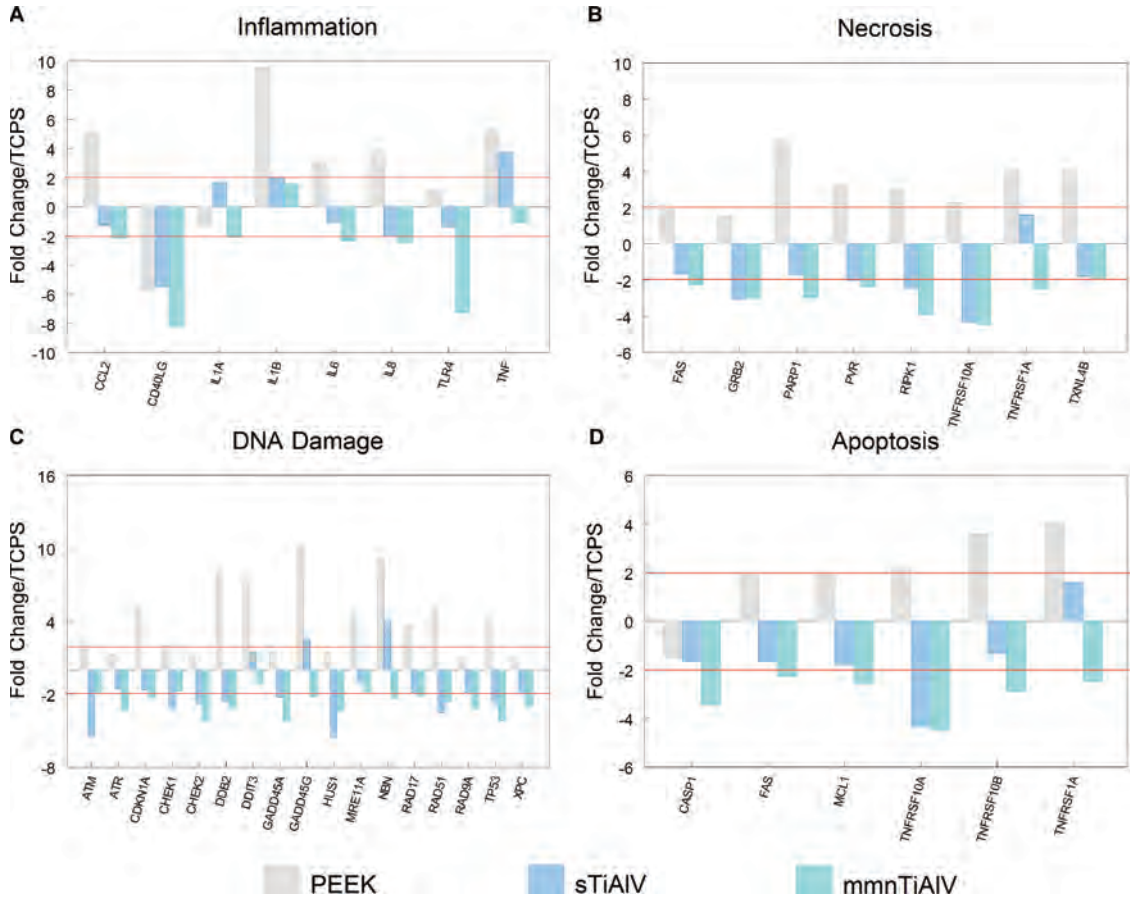

Figure 4. Analysis of inflammatory (**A**), necrotic (**B**), DNA damage (**C**), and apoptotic (**D**) factors by real-time qPCR array of mesenchymal stem cells cultured on PEEK, sTiAlV, or mmnTiAlV surfaces. Data are presented as fold change to TCPS (2-fold change indicated by solid horizontal line). TCPS, tissue culture polystyrene; PEEK, poly-ether-ether-ketone; sTiAlV, smooth titanium-aluminum-vanadium alloy; mmnTiAlV, macro-/micro-/nano-textured rough TiAlV.

from those of chemistry. We have attempted to investigate this very question using photopolymerized networks.[27] Our results indicated that chemistry was the primary regulator of osteoblast differentiation, and the effect of stiffness was secondary to the effect of surface chemistry. Although the greatest degree of osteoblast differentiation was on the stiffest polymers in 1 copolymer system, when grown on a different copolymer system, cells became more differentiated on the less stiff surface. When cells were grown on substrates with identical stiffness and surface topography but differing chemistry, chemistry proved to be a critical variable.[28,29] Thus, even if PEEK and Ti6Al4V could be fabricated to have comparable stiffness and surface microstructure, differences in biological response would be likely.

In conclusion, this study found that MSCs are compatible with the mmnTiAlV surface, and when cultured on it, reduce production of inflammatory mediators and enhance production of anti-inflammatory mediators compared with PEEK. Although we did not address fibrosis specifically, our results suggest that the fibrous tissue interface seen with PEEK implants may be due to increased inflammatory cytokines and decreased cell viability. In addition, the macro-/micro-/nano-scale–roughened Ti alloy surface is more effective than smooth Ti alloy in promoting an osteogenic environment with low inflammation and robust cell viability.

➢ Key Points

- ❑ MSCs differentiate into osteoblasts on micro-/nano-textured Ti alloy surfaces but not on PEEK surfaces.
- ❑ MSCs produce anti-inflammatory factors on micro-/nano-textured Ti alloy surfaces but not on PEEK surfaces.
- ❑ Factors produced by MSCs on PEEK surfaces may favor fibrosis whereas factors produced on Ti alloy surfaces favor osteogenesis.

Acknowledgment

Ti6Al4V and PEEK disks were provided as a gift to the Georgia Institute of Technology by Titan Spine LLC (Mequon, WI).

References

1. Kurtz SM, Devine JN. PEEK biomaterials in trauma, orthopedic, and spinal implants. *Biomaterials* 2007;28:4845–69.

2. Skinner HB. Composite technology for total hip arthroplasty. *Clin Orthop Relat Res* 1988;235:224–36.
3. Thome C, Krauss JK, Zevgaridis D. A prospective clinical comparison of rectangular titanium cages and iliac crest autografts in anterior cervical discectomy and fusion. *Neurosurg Rev* 2004;27:34–41.
4. Schmieder K, Wolzik-Grossmann M, Pechlivanis I, et al. Subsidence of the wing titanium cage after anterior cervical interbody fusion: 2-year follow-up study. *J Neurosurg Spine* 2006;4:447–53.
5. Stenport VF, Johansson CB. Evaluations of bone tissue integration to pure and alloyed titanium implants. *Clin Implant Dent Relat Res* 2008;10:191–9.
6. Linder L. Osseointegration of metallic implants. I. light microscopy in the rabbit. *Acta Orthop Scand* 1989;60:129–34.
7. De Leonardis D, Garg AK, Pecora GE. Osseointegration of rough acid-etched titanium implants: 5-year follow-up of 100 minimatic implants. *Int J Oral Maxillofac Implants* 1999;14:384–91.
8. Gittens RA, Olivares-Navarrete R, Schwartz Z, et al. Implant osseointegration and the role of microroughness and nanostructures: lessons for spine implants. *Acta Biomater* 2014;10:3363–71.
9. Olivares-Navarrete R, Hyzy SL, Gittens RA, et al. Rough titanium alloys regulate osteoblast production of angiogenic factors. *Spine J* 2013;13:1563–70.
10. Olivares-Navarrete R, Gittens RA, Schneider JM, et al. Osteoblasts exhibit a more differentiated phenotype and increased bone morphogenetic protein production on titanium alloy substrates than on poly-ether-ether-ketone. *Spine J* 2012;12:265–72.
11. Franz S, Rammelt S, Scharnweber D, et al. Immune responses to implants—a review of the implications for the design of immunomodulatory biomaterials. *Biomaterials* 2011;32:6692–709.
12. Olivares-Navarrete R, Hyzy SL, Hutton DL, et al. Direct and indirect effects of microstructured titanium substrates on the induction of mesenchymal stem cell differentiation towards the osteoblast lineage. *Biomaterials* 2010;31:2728–35.
13. Zhao G, Zinger O, Schwartz Z, et al. Osteoblast-like cells are sensitive to submicron-scale surface structure. *Clin Oral Implants Res* 2006;17:258–64.
14. Schwartz Z, Raz P, Zhao G, et al. Effect of micrometer-scale roughness of the surface of Ti6Al4V pedicle screws in vitro and in vivo. *J Bone Joint Surg Am* 2008;90:2485–98.
15. Webster TJ, Patel AA, Rahaman MN, et al. Anti-infective and osteointegration properties of silicon nitride, poly(ether ether ketone), and titanium implants. *Acta Biomater* 2012;8:4447–54.
16. Kou PM, Pallassana N, Bowden R, et al. Predicting biomaterial property-dendritic cell phenotype relationships from the multivariate analysis of responses to polymethacrylates. *Biomaterials* 2012;33:1699–713.
17. Kou PM, Babensee JE. Macrophage and dendritic cell phenotypic diversity in the context of biomaterials. *J Biomed Mater Res A* 2011;96:239–60.
18. Kou PM, Babensee JE. Validation of a high-throughput methodology to assess the effects of biomaterials on dendritic cell phenotype. *Acta Biomater* 2010;6:2621–30.
19. Kou PM, Schwartz Z, Boyan BD, et al. Dendritic cell responses to surface properties of clinical titanium surfaces. *Acta Biomater* 2011;7:1354–63.
20. Mahdavian Delavary B, van der Veer WM, van Egmond M, et al. Macrophages in skin injury and repair. *Immunobiology* 2011;216:753–62.
21. Sagomonyants KB, Jarman-Smith ML, Devine JN, et al. The in vitro response of human osteoblasts to polyetheretherketone (PEEK) substrates compared to commercially pure titanium. *Biomaterials* 2008;29:1563–72.
22. Daculsi G, Goyenvalle E, Aguado E. Improvement of bone ingrowth on PEEK surface implant. *Key Eng Mat* 2011;493–4:795–9.
23. Poulsson AH, Eglin D, Zeiter S, et al. Osseointegration of machined, injection moulded and oxygen plasma modified PEEK implants in a sheep model. *Biomaterials* 2014;35:3717–28.
24. Waser-Althaus J, Salamon A, Waser M, et al. Differentiation of human mesenchymal stem cells on plasma-treated polyetheretherketone. *J Mater Sci Mater Med* 2014;25:515–25.
25. Landy BC, Vangordon SB, McFetridge PS, et al. Mechanical and in vitro investigation of a porous PEEK foam for medical device implants. *J Appl Biomater Funct Mater* 2013;11:e35–44.
26. Zavalloni D, De Benedictis M, Pagnotta P, et al. New CoreValve Evolut 23 mm technology for treatment of degenerated bioprosthesis. *Heart Lung Circ* 2014;23:183–5.
27. Smith KE, Hyzy SL, Sunwoo M, et al. The dependence of MG63 osteoblast responses to (meth)acrylate-based networks on chemical structure and stiffness. *Biomaterials* 2010;31:6131–41.
28. Park JH, Wasilewski CE, Almodovar N, et al. The responses to surface wettability gradients induced by chitosan nanofilms on microtextured titanium mediated by specific integrin receptors. *Biomaterials* 2012;33:7386–93.
29. Park JH, Olivares-Navarrete R, Wasilewski CE, et al. Use of polyelectrolyte thin films to modulate osteoblast response to microstructured titanium surfaces. *Biomaterials* 2012;33:5267–77.

Published in final edited form as:
Spine J. 2013 November ; 13(11): . doi:10.1016/j.spinee.2013.03.047.

Rough Titanium Alloys Regulate Osteoblast Production of Angiogenic Factors

Rene Olivares-Navarrete, DDS, PhD[1], **Sharon L. Hyzy, BS**[1,4], **Rolando A. Gittens I., MS**[2], **Jennifer M. Schneider, MS**[3], **David Haithcock, BS**[1], **Peter Ullrich, MD**[5], **Paul J. Slosar, MD**[6], **Zvi Schwartz, DMD, PhD**[1,7], and **Barbara D. Boyan, PhD**[1]

[1]Wallace H. Coulter Department of Biomedical Engineering at Georgia Tech and Emory University, Georgia Institute of Technology, 315 Ferst Drive NW, Atlanta, GA, 30332

[2]School of Materials Science and Engineering, Georgia Institute of Technology, 711 Ferst Drive NW, Atlanta, GA, 30332

[3]Titan Spine, LLC, 6140 W. Executive Drive, Suite A, Mequon, WI, 53092

[4]School of Biology, Georgia Institute of Technology, 315 Ferst Drive NW, Atlanta, GA, 30332

[5]NeuroSpine Center of Wisconsin, 5320 West Michaels Drive, Appleton, WI, 54913

[6]San Francisco Spine Institute, 1199 Bush Street, San Francisco CA, 94109

[7]Department of Periodontics, University of Texas Health Science Center at San Antonio, 7703 Floyd Curl Drive, San Antonio, TX 78229

INTRODUCTION

An aging population has increased demand for orthopaedic implants to restore function. Lumbar and cervical interbody fusion surgery is a commonly used procedure for many types of spine pathology. Advantages to fusing the disc space anteriorly include the fact that the graft has compression loads applied to it (Wolff's Law), it has excellent vascularity, and it can hold large quantities of bone graft. Another advantage is that there is ready access to mesenchymal stem cells and osteoprogenitor cells, which help in the healing and osseointegration of the implant. While many factors contribute to the success of a spinal fusion procedure, including surgical technique, biologics or bone grafting materials, and the mechanical and structural properties of an interbody device, contributions of the implant material to inter-vertebral bone formation are not well known.

Currently, there are multiple material choices for an interbody implant. Of these, two of the most popular synthetic implant materials are titanium (typically titanium-aluminum-vanadium alloy [Ti6Al4V]) and poly-ether-ether-ketone (PEEK) (1–3). In addition to acting as a spacer between vertebrae, interbody implants provide surfaces that may have impacts on peri-implant bone formation. Studies examining bone formation adjacent to dental and total joint implant surfaces indicate that lack of bone apposition may lead to implant

Address for Correspondence: Barbara D. Boyan, Ph.D. Wallace H. Coulter Department of Biomedical Engineering, Georgia Institute of Technology, 315 Ferst Drive NW, Atlanta, Georgia 30332-0363, Phone: 404-385-4108, FAX: 404-894-2291, barbara.boyan@bme.gatech.edu.

micromotion and loosening with clinical failure (6, 7). Whereas implants fabricated from Ti6Al4V result in good bone-to-implant contact and are osseointegrated into the surrounding bone (8–10), PEEK does not integrate well with the surrounding bone, and instead may form a fibrous connective interface (3–5).

Development of a fusion mass is required for spine fusion and one role of an interbody device is to support osteogenesis across the interbody space. Bone graft materials and biologics facilitate this process by providing a surface and bioactive factors that promote migration of osteoblast progenitor cells and osteoblast differentiation. Macroscale properties, such as implant geometry are important with respect to vascular ingrowth but implant topography at the microscale is important for osteoblastic differentiation, osteoid synthesis and mineralization. *In vivo* success of titanium alloy implants may be due in part to a stimulatory effect of the device surface on osteoblastic differentiation. *In vitro* studies show that this effect is greater in osteoblasts cultured on titanium alloy with a micron-scale rough surface texture in comparison to smooth or machined titanium alloy (11, 12). *In vivo* observations support these in vitro results. Grit-blasted titanium alloy pedicle screws showed a 100% increase in pull-out force in sheep spines when compared with smooth screws (12).

Surface texture is also an important factor in normal bone formation. During healing and remodeling of bone, osteoblasts mature and mineralize their extracellular matrix in areas of the bone that have been pre-conditioned by osteoclasts. The action of the osteoclasts creates micron- and submicron-scale roughness (13). Most importantly, cells on rough surfaces produce increased levels of factors that increase osteogenesis in comparison to cells on smooth surfaces; these factors include transforming growth factor beta-1 (TGF-β1) and bone morphogenetic proteins (BMPs) (14, 15). This suggests that surface texture is an important factor in bone formation.

Bone formation is a result of several processes that work in concert to achieve net new bone. Osteoclast number and/or activity need to decrease in order to achieve less bone remodeling than new bone formation. When osteoblasts grow on microtextured titanium surfaces, they increase production of local factors that reduce osteoclastic bone remodeling in comparison with osteoblasts grown on smooth surfaces (16). These factors include osteoprotegerin (OPG), a decoy receptor for receptor activator for nuclear factor κB (RANK) ligand, which modulates osteoclast activity. It is not known if either titanium alloy or PEEK elicits a similar outcome.

Angiogenesis, new blood vessel formation stemming from existing vasculature, is important in bone formation, fracture healing, bone regeneration, and osseointegration (17–19). Angiogenic factors must create the vascularity needed to support bone creation. Angiogenesis is promoted by several growth factors including vascular endothelial growth factor-A (VEGF-A), fibroblast growth factor-2 (FGF-2), and angiopoietin-1 (Ang-1) (20–22). Studies examining the role of surface micro-architecture on osteoblast production of these factors showed that cells cultured on rough micro-textured titanium substrates produce higher levels of VEGF-A and FGF-2 (23). The results of these studies demonstrate that chemistry and microtexture of surfaces affect cell response, bringing into question how biomaterials used in interbody fusion, PEEK and titanium alloy, differ.

Osteoblasts interact with proteins adsorbed on implant surfaces through integrins, heterodimeric transmembrane receptors that bind specific extracellular matrix components. As cells adopt a more differentiated phenotype, complex interactions between cells and extracellular matrix occur, strengthening cell adhesion and possibly leading to improved biomaterial osseointegration (24, 25). While less differentiated osteoblasts express the integrin pair α5β1, the more differentiated cells on titanium and titanium alloy express α2β1,

which recognizes collagen (26–28). Several studies show that levels of integrin subunits α2 and β1 increase on rough titanium surfaces compared to smooth titanium and are required for enhanced osteoblast maturation on these surfaces (26–28). It is not known if osteoblasts on PEEK behave in a similar manner.

The aim of this study was to compare osteogenic and angiogenic factor production by human osteoblast-like cells cultured on smooth or microtextured (rough) titanium alloy substrates with cells cultured on PEEK, factors that regulate the cells via autocrine and paracrine pathways and contribute to peri-implant bone formation (16, 29, 30), and correlate these results to expression of specific integrin extracellular matrix receptors. To determine this, we assessed whether cells on these surfaces presented a mature osteoblast phenotype and whether secretion of local factors and angiogenic factors were affected by the chemistry and topography of the substrate. In addition, we investigated the types of integrins expressed by the cells as a first step in understanding why osteoblasts respond differentially to these two materials used in interbody fusions.

METHODS

Disk Preparation

Surgical grade titanium alloy (Ti6Al4V) and poly-ether-ether-ketone (PEEK) disks were provided by Titan Spine, LLC (Mequon, WI). Titanium alloy disks (15mm diameter) were machined, yielding a smooth surface texture (sTiAlV). Alternatively, the machined titanium alloy disks were etched with a proprietary process to create titanium alloy disks with a rough microtexture (rTiAlV). PEEK substrates were machined. All disks were ultrasonically cleaned, sonicated in ultrapure water (Millipore, Billerica, MA), and sterilized by autoclave (Tuttnauer, Hauppauge, NY) for 20 minutes at 121°C and 15 PSI b efore use in cell culture studies.

Disk Characterization

Scanning electron microscopy (SEM) and laser confocal microscopy (LCM) were used to characterize the surface topographies of the titanium alloy and PEEK disks. In addition, the chemistry of the surface was determined using energy dispersive X-ray spectroscopy (EDX) and sessile-drop contact angle. The detailed description of the methods used and the results have been published previously (31). Briefly, the PEEK disks had a machined surface finish with parallel grooves due to processing and no other distinctive features; sTiAlV disks also had a machined surface finish with shallower grooves than were seen on PEEK surfaces; and rTiAlV disks were characterized by 100–300 μm craters with superimposed micron-scale features. The roughness of each surface was determined by LCM [$S_a = 0.09 \pm 0.01$ μm for sTiAlV; $S_a = 0.43 \pm 0.07$ μm for PEEK; and $S_a = 1.81 \pm 0.51$ μm for rTiAlV]. EDX measurements confirmed that PEEK and the titanium alloy substrates had different chemistries. As expected, PEEK samples were composed of C and O. Both sTiAlV and rTiAlV were composed of Ti, Al, and V with no significant compositional differences between the two. Surface wettability assessed by contact angle measurements showed that all three substrates presented similar contact angles.

Cell Culture

Human MG63 cells (American Type Culture Collection, Manassas, VA) were used as a model for these studies. They have been well studied in cell response to titanium (32) and results correlate well with results obtained from *in vitro* studies using normal human osteoblasts, fetal and adult rat calvarial osteoblasts, and neonatal mouse calvarial osteoblasts (33–37) as well as with *in vivo* osseointegration of dental and orthopaedic implants (11, 12, 25). Cells were cultured at an initial density of 10,000 cells/cm^2 on tissue culture

polystyrene (TCPS, the surface of the cell culture plate wells), PEEK, sTiAlV, and rTiAlV. Medium (Dulbecco's modification of Eagle's medium [cellgro®, MediaTech, Manassas, VA] containing 10% fetal bovine serum [Hyclone, Thermo Scientific, Pittsburg, PA], and 1% penicillin-streptomycin [Gibco, Invitrogen, Carlsbad, CA]) was changed 24 hours after plating and then every 48 hours thereafter. When cultures reached confluence on TCPS, the cells on all surfaces were treated for an additional 24 hours with fresh medium. To ensure that cells were removed completely from the surfaces, the cells were released with two sequential 10-minute incubations in 0.25% trypsin-EDTA (Invitrogen) at 37°C and counted (Z2 Counter, Beckm an Coulter, Fullerton, CA).

The cell culture model was validated by assessing cell number, alkaline phosphatase specific activity of isolated cells and levels of osteocalcin in the conditioned medium as reported previously (31). Briefly, in comparison to growth on TCPS, cell number was reduced on the test substrates (TCPS>PEEK>sTiAlV>rTiAlV). Alkaline phosphatase specific activity was increased on the titanium alloy surfaces compared to TCPS and PEEK (TCPS=PEEK<sTiAlV<rTiAlV). Similarly, osteocalcin was elevated on the titanium alloy substrates in comparison to TCPS and PEEK, but there was no additional effect of roughness (TCPS=PEEK<sTiAlV, rTiAlV).

Analysis of Secreted Factors

Conditioned media were collected and assayed for secreted proteins and factors as described previously (33). OPG, VEGF-A, FGF-2, and Ang-1 were assayed using commercially available enzyme-linked immunosorbent assays (R&D Systems, Minneapolis, MN) following manufacturer's instructions. Active TGF-β1 was measured prior to acidification of the conditioned media using a commercially available ELISA (R&D Systems). Total TGF-β1 was measured after acidifying the media and latent TGF-β1 was defined as total TGF-β1 minus active TGF-β1. Results of immunoassays were normalized to total cell number.

Integrin Expression

Changes in integrin mRNA expression were measured using real-time PCR. When MG63 cells reached confluence on TCPS, all cultures were incubated for an additional 12 hours with fresh medium. RNA was isolated using TRIzol® (Invitrogen) and quantified using a Nanodrop spectrophotometer (Thermo Scientific, Waltham, MA). 250 ng of RNA was reverse transcribed to cDNA templates using High Capacity Reverse Transcription cDNA kit (Applied Biosystems, Carlsbad, CA). Gene specific primers and *Power* Sybr® Green Master Mix (Applied Biosystems) were used to quantify mRNA expression using the StepOnePlus Real-time PCR System (Applied Biosystems). Starting mRNA quantities were quantified using a standard curve of mRNA created from known dilutions of MG63 cells cultured on TCPS and related to threshold cycle values. Genes are presented as normalized to glyceraldehyde 3-phosphate dehydrogenase (GAPDH, F:5′-GCTCTCCAGAACATCATCC-3′; R:5′-TGCTTCACCACCTTCTTG-3′). Primers for integrin α1 (ITGA1, F:5′-CACTCGTAAATGCCAAGAAAAG-3′; R:5′-TAGAACCCAACACAAAGATGC-3′); integrin α2 (ITGA2, F:5′-ACTGTTCAAGGAGGAGAC-3′; R:5′-GGTCAAAGGCTTGTTTAGG-3′); integrin α5 (ITGA5, F:5′-ATCTGTGTGCCTGACCTG-3′; R:5′-AAGTTCCCTGGGTGTCTG-3′); integrin αv (ITGAV, F:5′-GTTGCTACTGGCTGTTTTGG-3′; R:5′-CTGCTCCCTTTCTTGTTCTTC-3′); integrin β1 (ITGB1, F:5′-ATTACTCAGATCCAACCAC-3′; R:5′-TCCTCCTCATTTCATTCATC-3′); and integrin β3 (ITGB3, F:5′-AATGCCACCTGCCTCAAC-3′; R:5′-GCTCACCGTGTCTCCAATC-3′) were designed using Beacon Designer™ (Premier Biosoft, Palo Alto, CA) and synthesized by Eurofins MWG Operon (Huntsville, AL).

Statistical Analysis

For each experiment, there were six independent cultures per type of surface. Experiments were repeated to ensure validity of the results. Data presented are from one representative experiment. Data were analyzed by ANOVA; when statistical differences were detected, Student's *t*-test was used with post hoc correction for multiple comparisons using Tukey's method. $P<0.05$ was considered significant.

RESULTS

Effects on Factors Modulating Osteoclast Activity

OPG production was sensitive to surface properties. Levels were increased in cultures grown on PEEK and smooth titanium alloy (sTiAlV) compared to TCPS ($p<0.05$). However, when cells were grown on rough titanium alloy (rTiAlV), production increased by 100% in comparison to TCPS and PEEK and by 30% in comparison to sTiAlV (Fig. 1A, $p<0.05$). Active TGF-β1 was more than 100% higher on titanium alloy surfaces compared to either TCPS or PEEK (Fig. 1B, $p<0.05$). Latent TGF-β1 was higher on sTiAlV than PEEK and further increased in cells on rTiAlV (Fig. 1C, $p<0.05$).

Angiogenic Factor Production

All experimental surfaces supported higher levels of VEGF than cells cultured on TCPS (Fig. 2A). However, cells on sTiAlV produced higher levels of VEGF than cells on PEEK, and rTiAlV enhanced this effect ($p<0.05$). Culture on TCPS and PEEK produced similar levels of FGF-2, but levels were 75% higher on sTiAlV and 100% higher on rTiAlV than on PEEK (Fig. 2B, $p<0.05$). Levels of Ang-1 decreased on PEEK in comparison to TCPS, but culture on titanium alloy, both smooth and rough, increased Ang-1 50% over cells on TCPS (Fig. 2C, $p<0.05$). The results show that cells cultured on titanium alloy produce higher levels of angiogenic factors than cells on PEEK, but the effect on VEGF and FGF-2 was enhanced on rough titanium alloy substrates.

Integrin Expression

Culture on sTiAlV and rTiAlV substrates stimulated higher expression of ITGA1 mRNA (Table 1), ITGA2 (Fig. 3B), ITGAV (Table 1), and ITGB1 (Fig. 3D) than on TCPS or PEEK ($p<0.05$). Moreover, ITGA2 expression was greater on rTiAlV than on sTiAlV (Fig. 3B, $p<0.05$). Expression of ITGA5 was higher on PEEK than on TCPS, reduced on titanium alloy surfaces in comparison to TCPS, and further reduced on rTiAlV was further reduced in comparison to sTiAlV (Table 1, $p<0.05$). Expression of ITGB3 was lower on PEEK than on TCPS, sTiAlV, or rTiAlV (Table 1, $p<0.05$).

DISCUSSION

Studies using both commercially pure titanium and titanium alloys (i.e., Ti6Al4V) have demonstrated *in vitro* that increased surface roughness enhances osteoblast maturation and production of local factors associated with osteogenesis and *in vivo* that the same topographies increase bone-to-implant contact and torque removal forces (12, 23, 38). We previously showed that osteoblasts on rough titanium substrates produce angiogenic factors (23). The present study indicates that osteoblasts also produced significantly higher VEGF-A and FGF-2 levels on smooth and roughened titanium alloy than on PEEK, an effect significantly more robust on rough titanium alloy. These results suggest that peri-implant osteoblasts may create an environment that modulates angiogenesis around the implant and in the adjacent tissue, indicating that the chemistry of the implant plays an important role in

determining the nature of the angiogenic milieu. Interestingly, cells grown on PEEK surfaces did not stimulate production of angiogenic factors.

The importance of angiogenesis in bone homeostasis is well appreciated. Vasculature is required for delivery of nutrients and removal of wastes, and provides a source of multipotent cells for tissue regeneration and remodeling (39). The factors measured in this study play distinct but cooperative roles in the process. VEGF-A is produced by diverse cells, including osteoblasts, and is one of the most important initiators of the signaling cascade during neovascularization in endothelial cells (40). FGF-2, a soluble factor with autocrine and paracrine functions, induces proliferation and migration of endothelial cells and is considered a key factor in angiogenesis (41). Ang-1 is known to control late stages of blood vessel formation, such as stabilization of the endothelial sprout and endothelial interaction with pericytes (42). Our results suggest that failure of osseointegration observed with PEEK implants is associated with reduced ability of cells on the implant surface to generate an environment rich in these factors.

Our results suggest that angiogenic factor production is associated with osteoblast maturation state. As we have noted previously, MG63 cells exhibit a more differentiated phenotype on rough titanium alloy, characterized by reduced cell number and increased osteocalcin production (31). This suggests that osteoblast differentiation is sensitive to general micron-scale elements. PEEK surfaces differ both chemically and physically from titanium alloy, so it is difficult to ascribe a specific parameter or feature of the surface to the lack of an angiogenic response. Cellular responses studies of PEEK have been limited to cell attachment and proliferation, but we previously showed that MG63 cells and normal human osteoblasts on PEEK do not exhibit increased alkaline phosphatase or osteocalcin production typical of differentiated osteoblast (31). Moreover, studies have attempted to modify PEEK using coatings of hydroxyapatite (43), titanium (44), or diamond-like carbon (45) to improve cellular response, supporting our findings that PEEK does not induce an osteogenic response.

In this experimental in vitro study, MG63 cells grown on roughened titanium alloy increased levels of active and latent TGF-β1 and OPG in their media, both of which are associated with bone formation. Osteoblasts produce TGF-β1 in latent form and store it in the extracellular matrix. In its active form, TGF-β1 stimulates osteoblast differentiation and matrix synthesis (46) while inhibiting osteoclast activity (47). OPG is produced by osteoblasts as a decoy receptor for receptor activator of nuclear factor κB (RANK) ligand, thereby reducing osteoblast-dependent osteoclast activation (48). Together these factors result in net new bone formation. This microenvironment may enhance bone formation while regulating bone remodeling in areas adjacent to the implant.

We previously showed that osteoblast differentiation and production of VEGF-A and FGF-2 on microtextured titanium are mediated by α2β1 integrin signaling (23). Here we show that mRNAs for integrins α1, α2, αv, and β1 were upregulated in cells grown on titanium alloy surfaces. Interestingly, ITGA2 and ITGB1 expression was higher on roughened titanium alloy surfaces than smooth surfaces, as was noted in cells grown on titanium (26). MG63 cells were grown on PEEK express similar integrin subunits as seen on TCPS, specifically α5, which is associated with cell attachment and proliferation but not with differentiation (27). These results may explain why PEEK failed to induce osteoblast maturation or yield an osteogenic environment.

CONCLUSIONS

This experimental study demonstrates that roughened titanium alloy stimulates an angiogenic and osteogenic environment with factors important in bone formation and remodeling. This osteogenic environment may enhance bone formation, implant stability, and fusion. Clinically, these findings point to the possibility that surface texture and material composition of spinal interbody implants can be manipulated to maximize the endogenous production of bone growth and angiogenic factors.

Acknowledgments

Sources of Funding:

This research was supported by US PHS grant NIH AR052102. Titan Spine, LLC provided the Ti6Al4V and PEEK substrates as a gift.

References

1. Toth JM, Wang M, Estes BT, Scifert JL, Seim HB 3rd, Turner AS. Polyetheretherketone as a biomaterial for spinal applications. Biomaterials. 2006; 27(3):324–34.16115677. [PubMed: 16115677]
2. Bruner HJ, Guan Y, Yoganandan N, Pintar FA, Maiman DJ, Slivka MA. Biomechanics of polyaryletherketone rod composites and titanium rods for posterior lumbosacral instrumentation. Presented at the 2010 Joint Spine Section Meeting. Laboratory investigation. J Neurosurg Spine. 2010; 13(6):766–72.21121756. [PubMed: 21121756]
3. Kurtz SM, Devine JN. PEEK biomaterials in trauma, orthopedic, and spinal implants. Biomaterials. 2007; 28(32):4845–69.17686513. [PubMed: 17686513]
4. Santos ER, Goss DG, Morcom RK, Fraser RD. Radiologic assessment of interbody fusion using carbon fiber cages. Spine (Phila Pa 1976). 2003; 28(10):997–1001.12768137. [PubMed: 12768137]
5. Anjarwalla NK, Morcom RK, Fraser RD. Supplementary stabilization with anterior lumbar intervertebral fusion--a radiologic review. Spine (Phila Pa 1976). 2006; 31(11):1281–7.16688045. [PubMed: 16688045]
6. Bauer TW, Schils J. The pathology of total joint arthroplasty. II. Mechanisms of implant failure. Skeletal Radiol. 1999; 28(9):483–97.10525792. [PubMed: 10525792]
7. Brunski JB. In vivo bone response to biomechanical loading at the bone/dental-implant interface. Adv Dent Res. 1999; 13:99–119.11276755. [PubMed: 11276755]
8. Stenport VF, Johansson CB. Evaluations of bone tissue integration to pure and alloyed titanium implants. Clin Implant Dent Relat Res. 2008; 10(3):191–9.18241219. [PubMed: 18241219]
9. De Leonardis D, Garg AK, Pecora GE. Osseointegration of rough acid-etched titanium implants: 5-year follow-up of 100 minimatic implants. Int J Oral Maxillofac Implants. 1999; 14(3):384–91.10379112. [PubMed: 10379112]
10. Linder L. Osseointegration of metallic implants. I. Light microscopy in the rabbit. Acta Orthop Scand. 1989; 60(2):129–34.2658464. [PubMed: 2658464]
11. Lincks J, Boyan BD, Blanchard CR, Lohmann CH, Liu Y, Cochran DL, et al. Response of MG63 osteoblast-like cells to titanium and titanium alloy is dependent on surface roughness and composition. Biomaterials. 1998; 19(23):2219–32.9884063. [PubMed: 9884063]
12. Schwartz Z, Raz P, Zhao G, Barak Y, Tauber M, Yao H, et al. Effect of micrometer-scale roughness of the surface of Ti6Al4V pedicle screws in vitro and in vivo. J Bone Joint Surg Am. 2008; 90(11):2485–98.18978418. [PubMed: 18978418]
13. Boyan BD, Schwartz Z, Lohmann CH, Sylvia VL, Cochran DL, Dean DD, et al. Pretreatment of bone with osteoclasts affects phenotypic expression of osteoblast-like cells. J Orthop Res. 2003; 21(4):638–47.12798063. [PubMed: 12798063]
14. Vlacic-Zischke J, Hamlet SM, Friis T, Tonetti MS, Ivanovski S. The influence of surface microroughness and hydrophilicity of titanium on the up-regulation of TGFbeta/BMP signalling in osteoblasts. Biomaterials. 2011; 32(3):665–71.20933273. [PubMed: 20933273]

15. Kieswetter K, Schwartz Z, Hummert TW, Cochran DL, Simpson J, Dean DD, et al. Surface roughness modulates the local production of growth factors and cytokines by osteoblast-like MG-63 cells. J Biomed Mater Res. 1996; 32(1):55–63.8864873. [PubMed: 8864873]
16. Schwartz Z, Olivares-Navarrete R, Wieland M, Cochran DL, Boyan BD. Mechanisms regulating increased production of osteoprotegerin by osteoblasts cultured on microstructured titanium surfaces. Biomaterials. 2009; 30(20):3390–6.19395022. [PubMed: 19395022]
17. Geris L, Gerisch A, Sloten JV, Weiner R, Oosterwyck HV. Angiogenesis in bone fracture healing: a bioregulatory model. J Theor Biol. 2008; 251(1):137–58.18155732. [PubMed: 18155732]
18. Duvall CL, Taylor WR, Weiss D, Wojtowicz AM, Guldberg RE. Impaired angiogenesis, early callus formation, and late stage remodeling in fracture healing of osteopontin-deficient mice. J Bone Miner Res. 2007; 22(2):286–97.17087627. [PubMed: 17087627]
19. Abshagen K, Schrodi I, Gerber T, Vollmar B. In vivo analysis of biocompatibility and vascularization of the synthetic bone grafting substitute NanoBone. J Biomed Mater Res A. 2009; 91(2):557–66.18985779. [PubMed: 18985779]
20. Schweigerer L, Neufeld G, Friedman J, Abraham JA, Fiddes JC, Gospodarowicz D. Capillary endothelial cells express basic fibroblast growth factor, a mitogen that promotes their own growth. Nature. 1987; 325(6101):257–9.2433585. [PubMed: 2433585]
21. Connolly DT, Heuvelman DM, Nelson R, Olander JV, Eppley BL, Delfino JJ, et al. Tumor vascular permeability factor stimulates endothelial cell growth and angiogenesis. J Clin Invest. 1989; 84(5):1470–8.2478587. [PubMed: 2478587]
22. Mehta VB, Besner GE. HB-EGF promotes angiogenesis in endothelial cells via PI3-kinase and MAPK signaling pathways. Growth Factors. 2007; 25(4):253–63.18092233. [PubMed: 18092233]
23. Raines AL, Olivares-Navarrete R, Wieland M, Cochran DL, Schwartz Z, Boyan BD. Regulation of angiogenesis during osseointegration by titanium surface microstructure and energy. Biomaterials. 2010; 31(18):4909–17.20356623. [PubMed: 20356623]
24. Anselme K, Bigerelle M. Topography effects of pure titanium substrates on human osteoblast long-term adhesion. Acta Biomater. 2005; 1(2):211–22.16701798. [PubMed: 16701798]
25. Anselme K, Bigerelle M, Noel B, Dufresne E, Judas D, Iost A, et al. Qualitative and quantitative study of human osteoblast adhesion on materials with various surface roughnesses. J Biomed Mater Res. 2000; 49(2):155–66.10571901. [PubMed: 10571901]
26. Olivares-Navarrete R, Raz P, Zhao G, Chen J, Wieland M, Cochran DL, et al. Integrin alpha2beta1 plays a critical role in osteoblast response to micron-scale surface structure and surface energy of titanium substrates. Proc Natl Acad Sci U S A. 2008; 105(41):15767–72.18843104. [PubMed: 18843104]
27. Raz P, Lohmann CH, Turner J, Wang L, Poythress N, Blanchard C, et al. 1alpha,25(OH)2D3 regulation of integrin expression is substrate dependent. J Biomed Mater Res A. 2004; 71(2):217–25.15386491. [PubMed: 15386491]
28. Siebers MC, ter Brugge PJ, Walboomers XF, Jansen JA. Integrins as linker proteins between osteoblasts and bone replacing materials. A critical review. Biomaterials. 2005; 26(2):137–46.15207460. [PubMed: 15207460]
29. Boyan BD, Lohmann CH, Sisk M, Liu Y, Sylvia VL, Cochran DL, et al. Both cyclooxygenase-1 and cyclooxygenase-2 mediate osteoblast response to titanium surface roughness. J Biomed Mater Res. 2001; 55(3):350–9.11255188. [PubMed: 11255188]
30. Bessho K, Carnes DL, Cavin R, Chen HY, Ong JL. BMP stimulation of bone response adjacent to titanium implants in vivo. Clin Oral Implants Res. 1999; 10(3):212–8.10522181. [PubMed: 10522181]
31. Olivares-Navarrete R, Gittens IRA, Schneider JM, Hyzy SL, Haithcock DA, Ullrich P, et al. Osteoblasts Exhibit a More Differentiated Phenotype and Increased BMP Production on Titanium Alloy Substrates than on PEEK. The Spine Journal: official journal of the North American Spine Society. 2012 In press.
32. Schwartz Z, Nasazky E, Boyan BD. Surface microtopography regulates osteointegration: the role of implant surface microtopography in osteointegration. Alpha Omegan. 2005; 98(2):9–19.16122142. [PubMed: 16122142]

33. Olivares-Navarrete R, Hyzy SL, Chaudhri RA, Zhao G, Boyan BD, Schwartz Z. Sex dependent regulation of osteoblast response to implant surface properties by systemic hormones. Biol Sex Differ. 2010; 1(1):4.21208469. [PubMed: 21208469]
34. Lohmann CH, Tandy EM, Sylvia VL, Hell-Vocke AK, Cochran DL, Dean DD, et al. Response of normal female human osteoblasts (NHOst) to 17beta-estradiol is modulated by implant surface morphology. J Biomed Mater Res. 2002; 62(2):204–13.12209940. [PubMed: 12209940]
35. Schneider GB, Perinpanayagam H, Clegg M, Zaharias R, Seabold D, Keller J, et al. Implant surface roughness affects osteoblast gene expression. J Dent Res. 2003; 82(5):372–6.12709504. [PubMed: 12709504]
36. Dekker RJ, van Blitterswijk CA, Hofland I, Engelberts PJ, Li J, de Bruijn JD. Studying the effect of different macrostructures on in vitro cell behaviour and in vivo bone formation using a tissue engineering approach. Novartis Found Symp. 2003; 249:148–67. discussion 67–9, 70–4, 239–41.12708655. [PubMed: 12708655]
37. Martin JY, Schwartz Z, Hummert TW, Schraub DM, Simpson J, Lankford J Jr, et al. Effect of titanium surface roughness on proliferation, differentiation, and protein synthesis of human osteoblast-like cells (MG63). J Biomed Mater Res. 1995; 29(3):389–401.7542245. [PubMed: 7542245]
38. Cochran DL, Nummikoski PV, Higginbottom FL, Hermann JS, Makins SR, Buser D. Evaluation of an endosseous titanium implant with a sandblasted and acid-etched surface in the canine mandible: Radiographic results. Clin Oral Implants Res. 1996; 7(3):240–52. ISI:A1996VU66800007. [PubMed: 9151588]
39. Heino TJ, Hentunen TA. Differentiation of osteoblasts and osteocytes from mesenchymal stem cells. Curr Stem Cell Res Ther. 2008; 3(2):131–45.18473879. [PubMed: 18473879]
40. Eilken HM, Adams RH. Dynamics of endothelial cell behavior in sprouting angiogenesis. Curr Opin Cell Biol. 2010; 22(5):617–25.20817428. [PubMed: 20817428]
41. Chen CH, Poucher SM, Lu J, Henry PD. Fibroblast growth factor 2: from laboratory evidence to clinical application. Curr Vasc Pharmacol. 2004; 2(1):33–43.15320831. [PubMed: 15320831]
42. Saharinen P, Bry M, Alitalo K. How do angiopoietins Tie in with vascular endothelial growth factors? Curr Opin Hematol. 2010; 17(3):198–205.20375888. [PubMed: 20375888]
43. Tan KH, Chua CK, Leong KF, Naing MW, Cheah CM. Fabrication and characterization of three-dimensional poly(ether- ether- ketone)/-hydroxyapatite biocomposite scaffolds using laser sintering. Proc Inst Mech Eng H. 2005; 219(3):183–94.15934394. [PubMed: 15934394]
44. Han CM, Lee EJ, Kim HE, Koh YH, Kim KN, Ha Y, et al. The electron beam deposition of titanium on polyetheretherketone (PEEK) and the resulting enhanced biological properties. Biomaterials. 2010; 31(13):3465–70.20153890. [PubMed: 20153890]
45. Wang H, Xu M, Zhang W, Kwok DT, Jiang J, Wu Z, et al. Mechanical and biological characteristics of diamond-like carbon coated poly aryl-ether-ether-ketone. Biomaterials. 2010; 31(32):8181–7.20692699. [PubMed: 20692699]
46. Bonewald LF, Dallas SL. Role of active and latent transforming growth factor beta in bone formation. J Cell Biochem. 1994; 55(3):350–7.7962167. [PubMed: 7962167]
47. Janssens K, ten Dijke P, Janssens S, Van Hul W. Transforming growth factor-beta1 to the bone. Endocrine Reviews. 2005; 26(6):743–74.15901668. [PubMed: 15901668]
48. Kobayashi Y, Udagawa N, Takahashi N. Action of RANKL and OPG for osteoclastogenesis. Crit Rev Eukaryot Gene Expr. 2009; 19(1):61–72.19191757. [PubMed: 19191757]

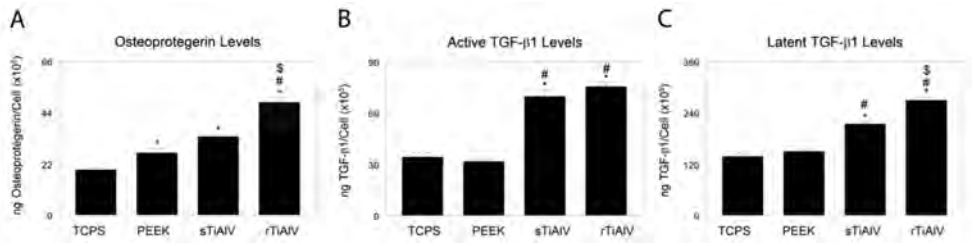

Figure 1.

Secreted osteoprotegerin (A), active TGF-β1 (B), and latent TGF-β1 (C) were measured in the conditioned media of cells cultured on TCPS, PEEK, smooth titanium alloy (sTiAlV), or rough titanium alloy (rTiAlV). Levels were normalized to total cell number. *p<0.05, versus TCPS; #p<0.05, versus PEEK; $p<0.05, versus sTiAlV. TCPS, tissue culture polystyrene; PEEK, poly-ether-ether-ketone; sTiAlV, smooth Ti6Al4V; rTiAlV, roughened Ti6Al4V.

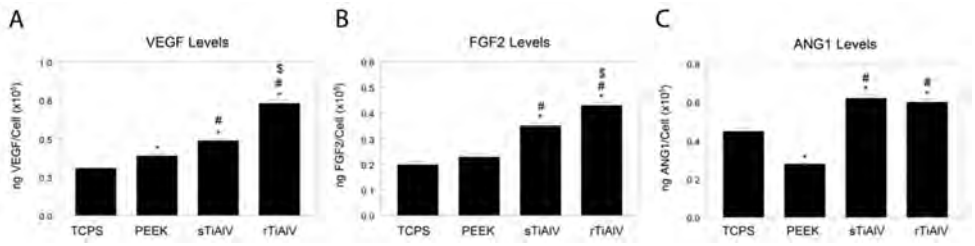

Figure 2.

Secreted VEGF-A (A), FGF-2 (B), and angiopoietin-1 (ANG1, C) were measured in the conditioned media of cells cultured on TCPS, PEEK, smooth titanium alloy (sTiAlV), or rough titanium alloy (rTiAlV). Levels were normalized to total cell number. *$p<0.05$, versus TCPS; #$p<0.05$, versus PEEK; \$$p<0.05$, versus sTiAlV. TCPS, tissue culture polystyrene; PEEK, poly-ether-ether-ketone; sTiAlV, smooth Ti6Al4V; rTiAlV, roughened Ti6Al4V.

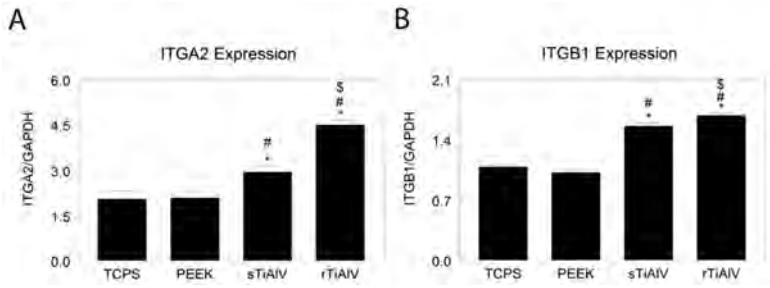

Figure 3.

Expression of messenger RNA for ITGA2 (A) and ITGB1 (B) were measured by real-time qPCR of cells cultured on TCPS, PEEK, smooth titanium alloy (sTiAlV), or rough titanium alloy (rTiAlV). Expression is normalized to GAPDH. *p<0.05, versus TCPS; #p<0.05, versus PEEK; $p<0.05, versus sTiAlV. TCPS, tissue culture polystyrene; BMP, bone morphogenetic protein; qPCR, quantitative polymerase chain reaction; GAPDH, glyceraldehyde 3-phosphate dehydrogenase; PEEK, poly-ether-ether-ketone; sTiAlV, smooth Ti6Al4V; rTiAlV, roughened Ti6Al4V.

Table 1

Expression of mRNA for ITGA1, ITGA5, ITGAV, and ITGB3. Human MG63 osteoblast-like cells were harvested 12 hours after confluence on TCPS. Expression of mRNA for ITGA1, ITGA5, ITGAV, and ITGB3 were measured by real-time quantitative PCR of cells cultured on TCPS, PEEK, smooth titanium alloy (sTiAlV), or rough titanium alloy (rTiAlV). Expression is normalized to GAPDH.

Surface	Gene Expression (Mean ± SEM)			
	ITGA1	ITGA5	ITGAV	ITGB3
TCPS	0.935±0.057	1.403±0.026	1.008±0.030	1.211±0.040
PEEK	0.875±0.128	1.686±0.022*	0.829±0.020	0.862±0.102*
sTiAlV	1.407±0.114*,#	1.115±0.023*,#	1.402±0.079*,#	1.301±0.091#
rTiAlV	1.577±0.108*,#	0.892±0.023*,#,$	1.569±0.037*,#	1.161±0.059

*p<0.05, v. TCPS;

#p<0.05, v. PEEK;

$p<0.05, v. sTiAlV.

In vivo performance of selective electron beam-melted Ti-6Al-4V structures

Sabine Ponader,[1]* Cornelius von Wilmowsky,[1]* Martin Widenmayer,[1] Rainer Lutz,[1] Peter Heinl,[2] Carolin Körner,[2] Robert F. Singer,[2] Emeka Nkenke,[1] Friedrich W. Neukam,[1] Karl A. Schlegel[1]
[1]*Department of Oral and Maxillofacial Surgery, University of Erlangen-Nuremberg, Erlangen, Germany*
[2]*Department of Materials Science, Institute of Science and Technology of Metals, University of Erlangen-Nuremberg, Erlangen, Germany*

Received 25 January 2008; revised 18 July 2008; accepted 26 August 2008
Published online 22 January 2009 in Wiley InterScience (www.interscience.wiley.com). DOI: 10.1002/jbm.a.32337

Abstract: Highly porous titanium structures are widely used for maxillofacial and orthopedic surgery because of their excellent mechanical properties similar to those of human bone and their facilitation of bone ingrowth. In contrast to common methods, the generation of porous titanium products by selective electron beam melting (SEBM), an additive manufacturing technology, overcomes difficulties concerning the extreme chemical affinity of liquid titanium to atmospheric gases which consequently leads to strongly reduced ductility of the metal. The purpose of this study was to assess the suitability of a smooth compact and a porous Ti-6Al-4V structure directly produced by the SEBM process as scaffolds for bone formation. SEBM-processed titanium implants were placed into defects in the frontal skull of 15 domestic pigs. To evaluate the direct contact between bone and implant surfaces and to assess the ingrowth of osseous tissue into the porous structure, microradiographs and histomorphometric analyses were performed 14, 30, and 60 days after surgery. Bone ingrowth increased significantly during the period of this study. After 14 days the most outer regions of the implants were already filled with newly formed bone tissue (around 14%). After 30 days the bone volume inside the implants reached almost 30% and after 60 days abundant bone formation inside the implants attained 46%. During the study only scarce bone–implant contact was found around all implants, which did not exceed 9% around compact specimens and 6% around porous specimens after 60 days. This work demonstrates that highly porous titanium implants with excellent interconnectivity manufactured using the SEBM method are suitable scaffolds for bone ingrowth. This technique is a good candidate for orthopedic and maxillofacial applications. © 2009 Wiley Periodicals, Inc. J Biomed Mater Res 92A: 56–62, 2010

Key words: titanium alloys; porous structures; selective electron beam melting (SEBM); bone ingrowth; bone regeneration

INTRODUCTION

Titanium and its alloys are widely used in the areas of maxillofacial and orthopedic surgery because of their excellent biocompatibility[1,2] and good mechanical properties.[3] The fixation of compact Ti-based implants remains a problem, because the mismatch of implant stiffness to that of autologous bone leads to stress shielding followed by implant loosening.[4] Porous structures show promising effects of adaptation of mechanical properties of the implant to those of human bone.[5] Additionally, a cellular structure permits the bone to grow into the implant leading to a better fixation.[6] Over the years a variety of fabrication methods have been developed which result in porous structures, such as gas injection into the metal melt or plasma spraying resulting in closed-cell structures, whereas open-cell structures can be generated, for example, by sintering metal powders/fibers, the space holder method, or rapid prototyping.[4] In turn, the manufacturing of porous titanium products is associated with some difficulties, most notably the extreme chemical affinity of liquid titanium to atmospheric gases such as oxygen, hydrogen, and nitrogen, which eventually leads to strongly reduced ductility.[7] Selective electron beam melting (SEBM), a new additive manufacturing technology, shows high capability for the fabrication of complex shaped and porous titanium architectures with varied densities and prevents the absorption of atmospheric gases because the processing is carried out under vacuum atmosphere, result-

*These authors contributed equally to this work.

Correspondence to: S. Ponader; e-mail: sabine.ponader@uk-erlangen.de

Contract grant sponsor: DFG GZ; contract grant number: NE 339/5-1

ing in structures with adjustable mechanical properties.[8] The structures are generated layer-by-layer by selective melting of discrete powder layers directly from 3D model data using an electron beam.

MATERIALS AND METHODS

Specimen preparation

Compact and porous titanium cylinders (8 mm long, 4 mm diameter) were prepared by SEBM of a commercially available Ti-6Al-4V powder (particle size: 45–100 μm) using EBM S12 system (Arcam AB, Mölndal, Sweden).

The basic principle for the manufacturing of compact components and porous structures by SEBM is similar. The generation process takes place layer-by-layer. Then, an electron beam scans a homogeneously applied layer of metal powder in parallel lines and creates one cross-section of the component by fusing the powder particles. Subsequently, the created layer is lowered by the thickness of one layer (here: 100 μm), a new powder layer is applied, and the process is repeated until the whole component has been built. The process is performed under vacuum atmosphere (10^{-4} to 10^{-5} mbar). The geometrical information of the component is derived from a computer-aided design (CAD) model.

For compact components, the offset between the scanned lines is smaller than the spot size of the electron beam and the molten lines overlap. One method for producing porous structures by SEBM is the increase of the line offset so that the molten lines do no longer overlap. By alternating the scanning direction of the electron beam by 90° after a certain number of layers, a three-dimensional lattice structure is created. The architecture of the structure is determined by the process parameters, whereas the outer shape is defined by the CAD model. More detailed information about the manufacturing of porous titanium structures by SEBM are given by Heinl et al.[8]

The lattice structure examined in the present study was produced with an energy input per unit length of the electron beam of 0.55 J/mm, a line offset of 1.0 mm and the scanning direction was altered with 90° every eight layers.

After the manufacturing process the compact as well as the porous cylinders were blasted with Ti-6Al-4V powder to remove adherent slightly sintered powder. To get a smooth surface (R_a = 0.08 μm) the as-produced compact cylinders were polished with SiC paper up to 2400 grit in the final step. All samples were sonicated for 30 min in EtOH (70%) and distilled water and steam sterilized at 121°C for 30 min. The appearance of the compact sample with smooth surface (Ti-1) and the porous sample (Ti-2) is depicted in Figure 1.

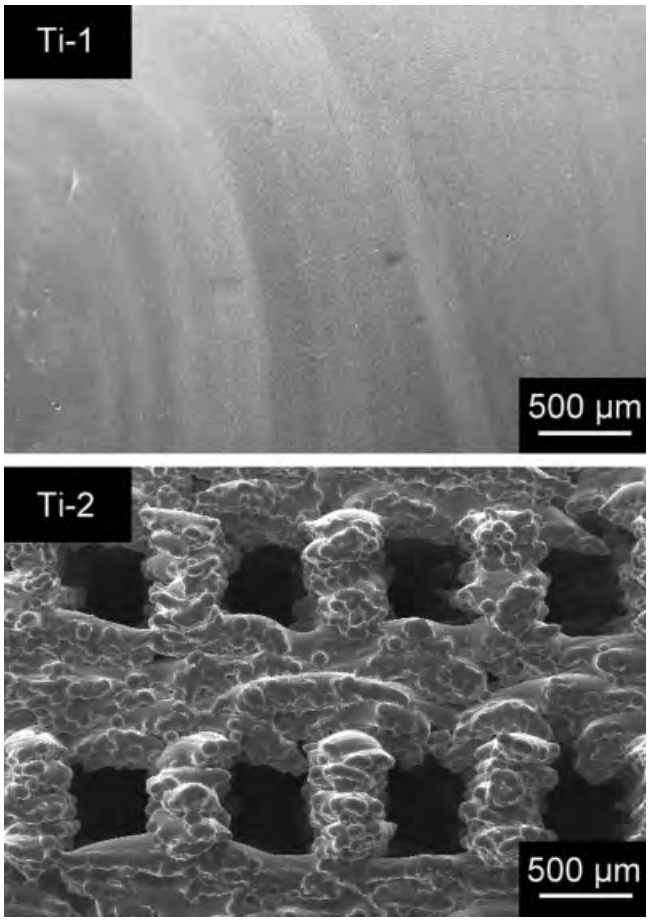

Figure 1. SEM micrograph of smooth compact (Ti-1) and microrough porous (Ti-2) titanium implants, manufactured using selective electron beam melting (SEBM).

Animals and surgical procedures

With regard to bone healing and remodeling, the pig is considered to be a suitable animal species for implant biomaterial research.[9] Fifteen adult female domestic pigs (18 months old, 120 ± 20 kg) were included in this study. Housing and feeding were according to standard animal-care protocols. The study has been approved by the Animal Research Committee for animal research of the government of Midfrankonia, Ansbach, Germany (approval no. 54-2531.31-7/06). All surgical procedures were performed under general anesthesia. Streptomycin (0.5 g/kg and day; Grünenthal GmbH, Stolberg, Germany) was applied intramuscularly 1 h preoperatively and 2 days postoperatively. An incision was first made to the skin and the periosteum of the front skull to create access to the neurocranium. The implant sites were prepared with slow drilling and copious irrigation using a trephine burr (4 mm diameter, 8 mm length; Straumann, GmbH, Freiburg, Germany) and filled with the samples. Finally the periosteum and skin over the defects were sutured in two layers (Vicryls 3.0, Vicryls 1.0; Ethicon GmbH & Co. KG, Norderstedt, Germany).

Removal and sample preparation

The animals were sacrificed 14, 30, and 60 days (five animals at each point) postoperatively using an intramuscular injection of azaperone (1 mg/kg) and midazolam (1 mg/kg) in the neck and euthanized by an intravascular injection of 20% pentobarbital solution until cardiac arrest occurred. The skull caps of the sacrificed animals were removed and immediately frozen at −80°C. The exact

implants position was evaluated by X-ray unit (Faxitron Cabinet X-ray Systems, IL) prior to further processing. The implants and surrounding bone were separated using a standard cutting system (Exakt Apparatebau GmbH, Norderstedt, Germany). All implants, along with the surrounding bone, were fixed in 1.4% paraformaldehyde at 4°C for 48 h and dehydrated in a graded alcohol series at room temperature in a dehydration unit (Shandon Citadel 1000; Shandon GmbH, Frankfurt, Germany). For the preparation of thin sections, all samples were embedded in methylmethacrylate (Technovit® 9100; Heraeus Kulzer GmbH, Wehrheim, Germany) which is suitable for the cutting-grinding technique according to Donath and Breuner.[10]

Microradiography and histology

To produce microradiographs, the resin-embedded sections were reduced to 120 μm using a grinding machine (Exakt Apparatebau GmbH, Norderstedt, Germany). Subsequently, the samples were irradiated in the cabinet X-ray system (Faxitron X-ray, IL) unit using 13 kV tube voltage and 0.3 mA for 2.5 min. The developed radiographs (Kodak, Stuttgart, Germany) were scanned into tiff format (Epson Perfection 4990 Photo; Seiko Epson, Nagano, Japan).

For histomorphometric observations, all specimens were reduced to 20–30 μm and stained with toluidine blue O. Each sample was examined under a light microscope (Axioskop; Zeiss, Jena, Germany) and a digital photo was taken (Axiocam; Zeiss).

The percentage of direct contact between mineralized bone and the implant surface (bone–implant contact, BIC) was determined by using the image analyzing tool Bioquant Osteo software V7.10.10 (Nashville, TN, USA).

For quantifying osseous tissue ingrowth into the porous specimens, they were classified into three regions: a most outer one (region 1), a middle one (region 2), and an inner one (region 3) (Fig. 2). The amount of newly formed bone inside the defect was measured in the pores of the porous implants by using the image analyzing tool Bioquant Osteo software V7.10.10 and expressed as a percentage (total pore volume equals 100%). Pristine bone (untouched during surgical procedures) around the implants was measured and used as a control value.

Statistics

Multiple measurements per individual, localization, and day were aggregated prior to analysis. For the analyses of all data the software program SPSS (version 15.0 for Windows) was used. Differences among groups and days were established with t test analyses by an independent sample comparison. Values of $p \leq 0.05$ were considered to be statistically significant and are indicated by an asterisk (*).

RESULTS

Characteristics of the porous structure

The mechanical and structural properties of the investigated porous structure are presented in Table I. These properties were evaluated in a previous study by Heinl et al.[11] The mechanical properties were determined by compression testing with loading direction parallel and perpendicular to the building direction of the porous structure. The structural properties were evaluated by microcomputer tomography.

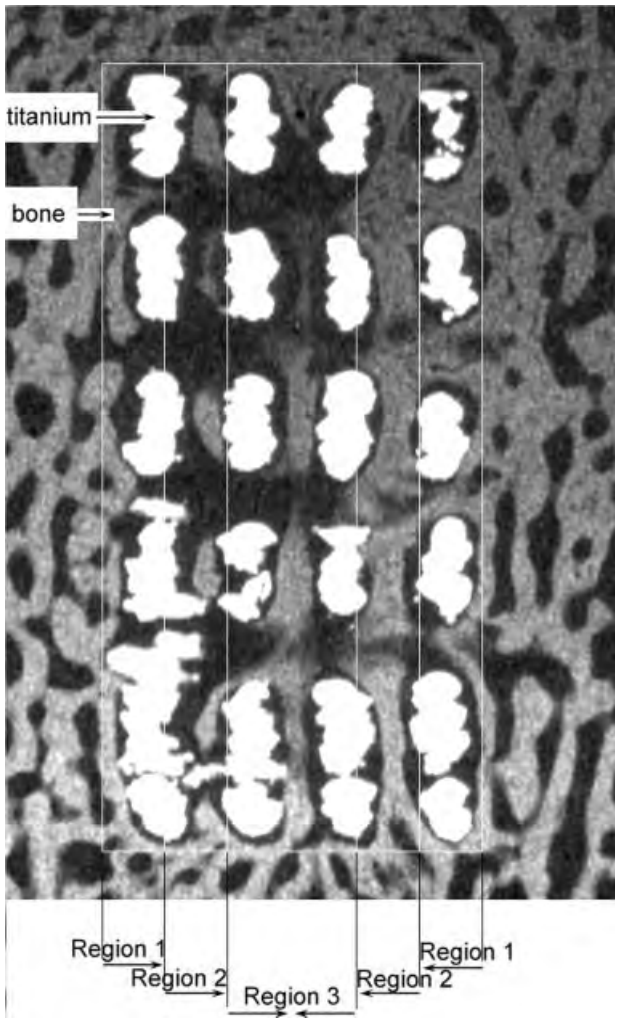

Figure 2. Scheme of quantitative evaluation of bone ingrowth. Samples are classified into three regions: a most outer one (region 1), a middle one (region 2), and an inner one (region 3). The amount of newly formed bone volume was measured in the pores of the titanium implants and expressed as a percentage (total pore volume equals 100%).

Bone regeneration and bony ingrowth

Wound healing was characterized by an ongoing trabecular bone formation around all implants leading to the complete closure of the defects after 60 days. Microradiographs show the bony regeneration around the implants and abundant tissue ingrowth into the porous Ti-2 structure (Fig. 3). After 14 days

TABLE I
Mechanical and Structural Properties of the Investigated Porous Ti-6Al-V4 Structure

Material	Loading Direction	E (GPa)	$\sigma_{y,0.2}$ (MPa)	σ_{max} (MPa)	Mean Pore Size (mm)	Porosity (%)
Porous Ti-6Al-4V structure	Parallel	12.9 (±0.9)	107.5 (±3.6)	148.4 (±3.5)	0.45	61.3
	Perpendicular	3.9 (±2.1)	49.6 (±20.6)	127.1 (±29.2)		

The mechanical properties were determined in compression with loading direction parallel and perpendicular to the building direction of the specimens; E is the elastic modulus, $\sigma_{y,0.2}$ is the yield strength, σ_{max} is the maximum strength, and values in parentheses are the standard deviations. The structural properties were derived from microcomputer tomography.

only minor bone ingrowth into the outer region could be observed. After 30 days a noticeable growth of osseous tissue could be discovered in the outer as well as the central regions. After 60 days the implants were filled completely with bony tissue.

The quantification of mineralized osseous ingrowth into the porous implants is illustrated in Figure 4. The percentage of bone volume over tissue volume inside the pores steadily increased throughout the study period regarding as well the depth of bone ingrowth into the implants as the bone density of newly formed tissue. After 14 days the value reached 14.44% ± 6.78% in the most outer region (region 1), 2.01% ± 1.16% in region 2, and 0.22% ± 0.13% in region 3. After 30 days the bone volume reached 29.46% ± 2.59% in region 1, 9.7% ± 5.72% in region 2, and 2.19% ± 2.19% in region 3. After 60 days of healing the bone volume attained 46.31% ± 3.42% in region 1, 27.77% ± 4.63% in region 2, and 28.55% ± 5.77% in region 3, respectively. The values of bone density rose significantly from day 14 to 60 (region 1: $p = 0.024$; region 2: $p = 0.008$; region 3: $p = 0.016$). Furthermore, significant higher values were shown in region 1 ($p = 0.009$) and region 3 ($p = 0.014$) on day 60 when compared with day 30. On days 30 and 60 the bone density of region 1 was significantly higher compared with region 2 (day 30: $p = 0.033$; day 60: $p = 0.02$) and region 3 (day 30: $p < 0.001$; day 60: $p = 0.047$). The density of newly formed bone tissue did not totally reach the density

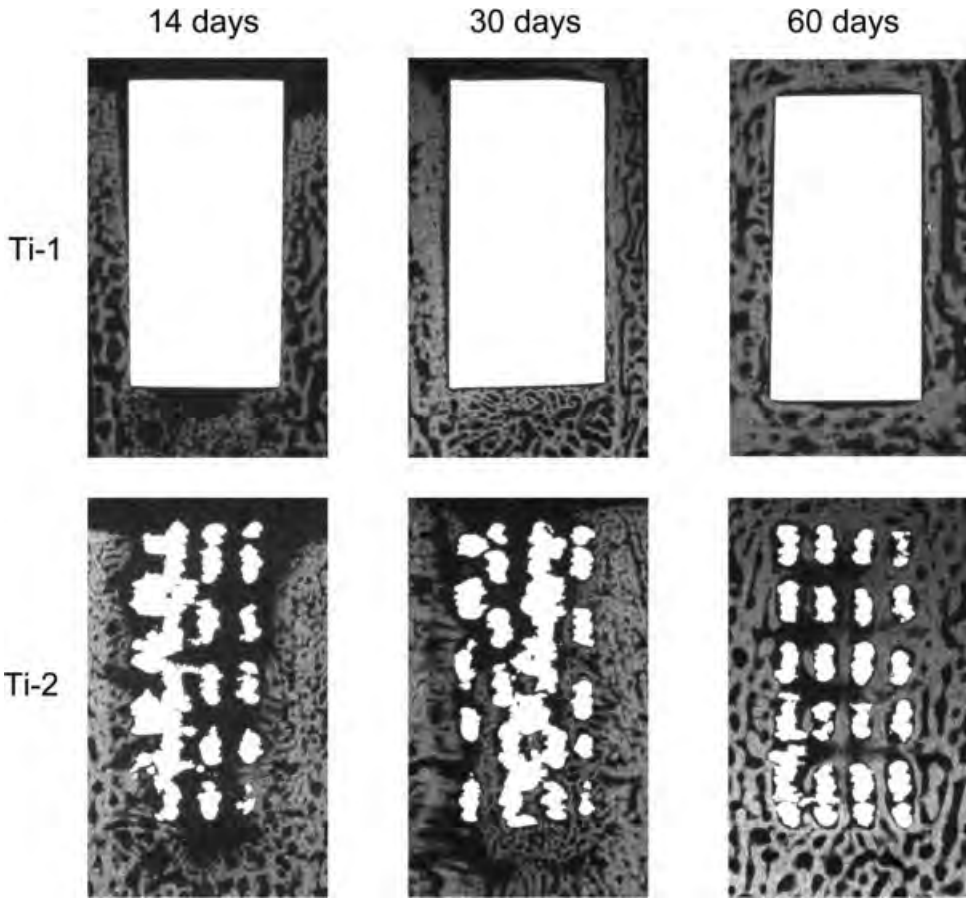

Figure 3. Microradiographs of compact smooth (Ti-1) and porous titanium implants (Ti-2).

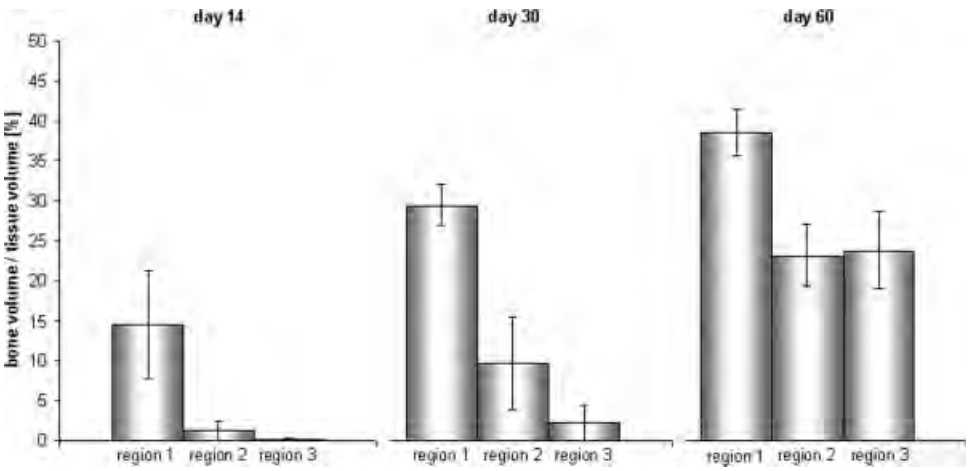

Figure 4. Quantitative evaluation of bone volume inside the outer region (region 1), the middle region (region 2), and the inner region (region 3) of the implants.

of pristine bone tissue around the implants. However, after 60 days of healing the comparison of bone volumes in region 1 (46.31% ± 3.42%) and outside the defects (59.98% ± 1.63%) revealed no longer significant differences ($p = 0.089$).

Consistent with the microradiographic findings, intense trabecular bone regeneration around all implants and strong bone ingrowth into Ti-2 specimens were detected in the toluidine blue O staining (Fig. 5).

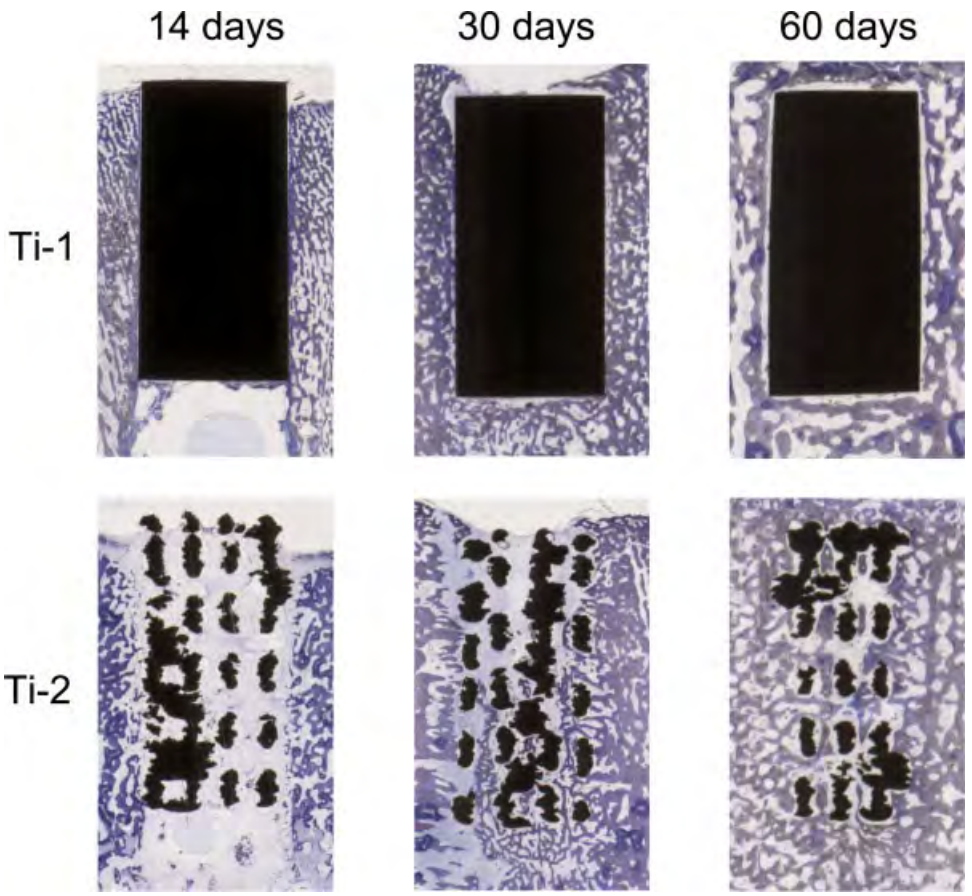

Figure 5. Toluidine blue O staining of compact smooth (Ti-1) and porous titanium implants (Ti-2). [Color figure can be viewed in the online issue, which is available at www.interscience.wiley.com.]

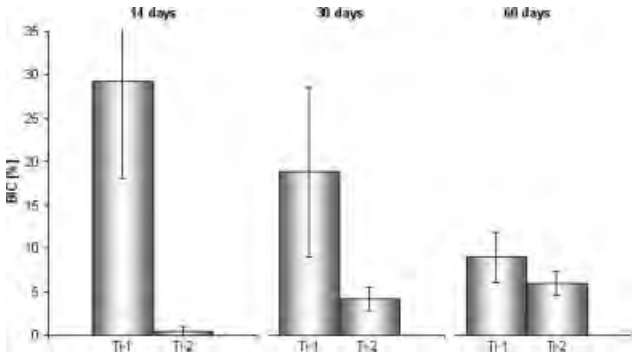

Figure 6. Bone–implant contact. Ti-1: smooth compact sample; Ti-2: porous sample.

Bone–implant contact

The histological analysis revealed only scarce BIC. Fibrous tissue has been observed between bone tissue and implant. Figure 6 shows the quantitative evaluation of the percentage of direct contact between mineralized bone and the implant surface at different points. For the compact samples the BIC decreased constantly during the study from 29.27% ± 11.23% on day 14 to 18.78% ± 9.74% on day 30 and 8.98% ± 2.89% on day 60. In contrast, the BIC around porous samples increased continually and attained 0.47% ± 0.47% on day 14, 4.14% ± 4.14% on day 30, and 5.96% ± 1.36% on day 60. Compared with day 14 they reached significance on day 30 ($p = 0.031$) and day 60 ($p = 0.007$). The difference of the BIC around the compact compared with that around the porous structure did not reach significance (day 14: $p = 0.062$; day 30: $p = 0.271$; day 60: $p = 0.105$). A high variability of BIC among the specimens within one group was found.

DISCUSSION

In this study, the bone regeneration as well as the ingrowth of osseous tissue into porous SEBM-processed Ti-6Al-4V scaffolds in domestic pig calvaria bone were evaluated and, therefore, the suitability of such scaffolds as bone substitutes was assessed.

Recently, SEBM Ti-6Al-4V scaffolds turned out to be not cytotoxic to human fetal osteoblasts and their accelerating effect on proliferation and differentiation of osteoblastic cells could be shown.[12] The present study demonstrates that observed achievement of osteoblasts behavior *in vitro* does not result in an effective osseointegration of the scaffolds within the first 60 days but an effective tissue ingrowth into porous SEBM structures can be performed at least.

Generally, implants inserted with a press-fit are very stable at the time of surgery. However, a few days after surgery, BIC decreases because of immediate resorption of the necrotic bone adjacent to the material surface resulting in reduced mechanical stability of the implant.[13,14] It is also a well-known phenomenon that micromovements of the implant prevent bone formation leading to floppy fixation by fibrous tissue.[15] This effect was observed around compact SEBM specimens, where the BIC decreased constantly leading to a loose anchorage of the implant surrounded by a fibrous tissue layer until day 60. By contrast, the BIC around porous SEBM scaffolds increased, even if the achieved BIC of around 5% after 60 days is significantly less compared with other studies. For example, titanium implants inserted into sheep tibiae with and without autologous bone grafts led to a BIC of 29.54% ± 9.00% for grafted implants and 26.76% ± 5.00% for the controls after 2 months.[16] In another study, commercially pure titanium microimplants with machined and sandblasted acid-etched surfaces were inserted into human maxillae. After a healing period of 2 months the mean BIC was 20.66% ± 14.54% for the machined surfaces and 40.08% ± 9.89% for the sandblasted acid-etched surfaces.[17] Another reason for the low BIC ratio around porous SEBM structures could be the inhibiting effect of space between implant and bone. If such gaps are larger than 1 mm, they significantly affect the attachment of cells and bone ingrowth.[4]

Titanium exhibits one of the greatest resistance to corrosion compared with other metals or alloys used in surgery.[18] Nevertheless, titanium implant corrosion turned out to have a noteworthy effect on the BIC *in vivo*. Recently, Olmedo et al. found a close contact between lamellar bone and an irregular metal surface with uneven and indented edges only in areas with no pitting corrosion of the titanium surface.[19] They detected corrosion products migrating in the surrounding peri-implant tissues. Metal debris of the SEBM-processed implant surfaces released into the tissues as a result of manufacturing defects, corrosion, surface contamination, or mechanical damage during the implantation may hinder the osseous tissue to approach the implant surface and to build up a close BIC. Among the specimens within one group a high variability of the BIC was observed. This variability is based on the inhomogeneity of the specimens.

In various studies the bone ingrowth into porous titanium implants was intensely examined. Li et al. studied porous titanium implants (pore size between 160 and 680 μm; porosity between 39% ± 1.3% and 68% ± 2.5%) fabricated using 3D fiber deposition and inserted these implants into goats.[20] After 12 weeks they found a bone ingrowth between 5 and 10%. Another recent study showed a quite higher bone ingrowth into porous rapid prototyped titanium scaffolds with pore sizes of 800 μm (porosity: 59.73% ± 5.2%) and 1200 μm (porosity: 59.08% ±

2.4%). After 8 weeks, bone ingrowth was 14.2% ± 3.2% for the 800-μm pore structure and 10.3% ± 2.8% for the 1200-μm pore structure.[21] Considering these results, the found ratio of bone ingrowth into porous SEBM implants of 40% after 60 days can be considered as very effective. For maximized bone ingrowth the literature discusses implant porosities around 45–60% and average pore sizes between 100 and 300 μm, whereas relative larger pores promote direct osteogenesis, since they allow vascularization and oxygenation.[22] According to Heinl et al., the applied SEBM-processed specimens fulfill these requirements, as their porosity is 61.3%, the averaged pore size is 450 μm, and the porous structures are interconnected in all dimensions.[11] This is considered as the most important requirement for bone ingrowth.[23] Furthermore, it could be shown by Heinl et al. that the mechanical properties of the implants correspond to those of human bone.[11] Thus the scaffolds provide adequate architecture and mechanical properties in order to optimize ingrowth of surrounding bone tissue, which could be shown by the present histological findings. Bony ingrowth proceeded steadily during the period of this study regarding as well the depth of bone ingrowth into the implants as the bone density of newly formed tissue, respectively. After 60 days of healing the bone structure in the most outer region of the implants was already comparable with that of pristine bone, as the density of newly formed bone tissue almost reached the level of pristine bone tissue around the implants.

CONCLUSIONS

In this study it could be demonstrated that 3D Ti-6Al-4V implants with a porous architecture directly manufactured using SEBM can be completely infiltrated by osseous tissue within 60 days. To improve the BIC performance of SEBM scaffolds, a bioactive surface could be designed to induce a specific biological activity, which can lead to strong bonding to bone. We conclude that porous SEBM specimens exhibit suitable scaffolds for bone regeneration.

The authors thank Ms. Heidemarie Heider for her valuable help and additional advice regarding histological methods.

References

1. Long M, Rack HJ. Titanium alloys in total joint replacement–a materials science perspective. Biomaterials 1998;19:1621–1639.
2. Yamamoto A, Honma R, Sumita M. Cytotoxicity evaluation of 43 metal salts using murine fibroblasts and osteoblastic cells. J Biomed Mater Res 1998;39:331–340.
3. Niinomi M. Mechanical properties of biomedical titanium alloys. Mat Sci Eng A 1998;243:231–236.
4. Ryan G, Pandit A, Apatsidis DP. Fabrication methods of porous metals for use in orthopaedic applications. Biomaterials 2006;27:2651–2670.
5. Li JP, Li SH, Van Blitterswijk CA, de Groot K. A novel porous Ti6Al4V: Characterization and cell attachment. J Biomed Mater Res A 2005;73:223–233.
6. Kienapfel H, Sprey C, Wilke A, Griss P. Implant fixation by bone ingrowth. J Arthroplasty 1999;14:355–368.
7. Dunand DC. Processing of Titanium foams. Adv Eng Mater 2004;6:369–376.
8. Heinl P, Rottmair A, Körner C, Singer RF. Cellular Titanium by selective electron beam melting. Adv Eng Mater 2007;9:360–364.
9. Pearce AI, Richards RG, Milz S, Schneider E, Pearce SG. Animal models for implant biomaterial research in bone: A review. Eur Cell Mater 2007;13:1–10.
10. Donath K, Breuner G. A method for the study of undecalcified bones and teeth with attached soft tissues. The Sage-Schliff (sawing and grinding) technique. J Oral Pathol 1982;11:318–326.
11. Heinl P, Müller L, Körner C, Singer RF, Müller FA. Cellular Ti-6Al-4V structures with interconnected macro porosity for bone implants fabricated by selective electron beam melting. Acta Biomater 2008;4:1536–1544.
12. Ponader S, Vairaktaris E, Heinl P, Wilmowsky CV, Rottmair A, Korner C, Singer RF, Holst S, Schlegel KA, Neukam FW, Nkenke E. Effects of topographical surface modifications of electron beam melted Ti-6Al-4V titanium on human fetal osteoblasts. J Biomed Mater Res A 2008;84:1111–1119.
13. Dhert WJ, Thomsen P, Blomgren AK, Esposito M, Ericson LE, Verbout AJ. Integration of press-fit implants in cortical bone: A study on interface kinetics. J Biomed Mater Res 1998;41:574–583.
14. Simmons CA, Valiquette N, Pilliar RM. Osseointegration of sintered porous-surfaced and plasma spray-coated implants: An animal model study of early postimplantation healing response and mechanical stability. J Biomed Mater Res 1999;47:127–138.
15. Soballe K, Hansen ES, H BR, Jorgensen PH, Bunger C. Tissue ingrowth into titanium and hydroxyapatite-coated implants during stable and unstable mechanical conditions. J Orthop Res 1992;10:285–299.
16. De Riu G, De Riu N, Spano G, Pizzigallo A, Petrone G, Tullio A. Histology and stability study of cortical bone graft influence on titanium implants. Oral Surg Oral Med Oral Pathol Oral Radiol Endod 2007;103:e1–e7.
17. Grassi S, Piattelli A, Ferrari DS, Figueiredo LC, Feres M, Iezzi G, Shibli JA. Histologic evaluation of human bone integration on machined and sandblasted acid-etched titanium surfaces in type IV bone. J Oral Implantol 2007;33:8–12.
18. Sharma M, Kumar AV, Singh N. Electrochemical corrosion behaviour of dental/implant alloys in saline medium. J Mater Sci Mater Med 2008;19:2647–2653.
19. Olmedo DG, Duffo G, Cabrini RL, Guglielmotti MB. Local effect of titanium implant corrosion: An experimental study in rats. Int J Oral Maxillofac Surg 2008;37:1032–1038.
20. Li JP, Habibovic P, van den Doel M, Wilson CE, de Wijn JR, van Blitterswijk CA, de Groot K. Bone ingrowth in porous titanium implants produced by 3D fiber deposition. Biomaterials 2007;28:2810–2820.
21. Lopez-Heredia MA, Goyenvalle E, Aguado E, Pilet P, Leroux C, Dorget M, Weiss P, Layrolle P. Bone growth in rapid prototyped porous titanium implants. J Biomed Mater Res A 2008;85:664–673.
22. Karageorgiou V, Kaplan D. Porosity of 3D biomaterial scaffolds and osteogenesis. Biomaterials 2005;26:5474–5491.
23. Hutmacher DW. Scaffolds in tissue engineering bone and cartilage. Biomaterials 2000;21:2529–2543.

Available online at www.sciencedirect.com
ScienceDirect
Biomaterials 28 (2007) 2810–2820
Biomaterials
www.elsevier.com/locate/biomaterials

Bone ingrowth in porous titanium implants produced by 3D fiber deposition

Jia Ping Li[a,b,e,*], Pamela Habibovic[a], Mirella van den Doel[c], Clayton E. Wilson[b], Joost R. de Wijn[a], Clemens A. van Blitterswijk[a], Klaas de Groot[a,d]

[a]*Department of Tissue Regeneration, Institute for Biomedical Technology, University of Twente, The Netherlands*
[b]*Porogen, B.V, The Netherlands*
[c]*Cellcotec, B.V, The Netherlands*
[d]*CAM Implants, B.V, The Netherlands*
[e]*School of Mechanical Engineering and Automation, BeiHang University, China*

Received 8 December 2006; accepted 16 February 2007

Abstract

3D fiber deposition is a technique that allows the development of metallic scaffolds with accurately controlled pore size, porosity and interconnecting pore size, which in turn permits a more precise investigation of the effect of structural properties on the in vivo behavior of biomaterials.

This study analyzed the in vivo performance of titanium alloy scaffolds fabricated using 3D fiber deposition. The titanium alloy scaffolds with different structural properties, such as pore size, porosity and interconnecting pore size were implanted on the decorticated transverse processes of the posterior lumbar spine of 10 goats. Prior to implantation, implant structure and permeability were characterized. To monitor the bone formation over time, fluorochrome markers were administered at 3, 6 and 9 weeks and the animals were sacrificed at 12 weeks after implantation. Bone formation in the scaffolds was investigated by histology and histomorphometry of non-decalcified sections using traditional light- and epifluorescent microscopy. In vivo results showed that increase of porosity and pore size, and thus increase of permeability of titanium alloy implants positively influenced their osteoconductive properties.

Keywords: Osteoconduction; Porous Ti6Al4V; Scaffold; 3D fiber deposition

1. Introduction

At present, most widely used clinical therapies for bone replacement and regeneration employ autologous and allogeneic bone grafts. It is well known that autologous bone graft is considered to be the golden standard in spinal fusions, i.e. for achieving a bony bridge between transverse processes. However, treatments with both autografts and allografts exhibit a number of limitations. The harvest of the autologous graft requires an additional invasive surgical procedure that may lead to donor site morbidity, chronic post-operative pain, hypersensitivity and infection [1–5]. Another important drawback of the use of autograft is the limited availability. Unlike autologous bone, allogeneic grafts are widely available and do not require an additional surgery on the patient. However, allogeneic bone has to undergo processing techniques such as lyophilization, irradiation or freeze-drying to remove all immunogenic proteins in order to avoid any risk of immunogenic reaction [6]. In turn, these processing techniques have a negative effect on osteoinductive and osteoconductive potential of the allograft [7], which consequently decreases its biological performance as compared to autografts [8].

Therefore, the use of synthetic biomaterials for orthopedic reconstructive surgery as a means of replacing autografts and allografts is of increasing interest and the

*Corresponding author. Institute for Biomedical Technology, Department of Tissue Regeneration. University of Twente, The Netherlands. Tel.: +31 30 2295289; fax: +31 30 2280255.
E-mail address: j.li@tnw.utwente.nl (J.P. Li).

0142-9612/$ - see front matter © 2007 Elsevier Ltd. All rights reserved.
doi:10.1016/j.biomaterials.2007.02.020

large number of scientific reports confirm this trend. Calcium-phosphate-based biomaterials, such as ceramics and cements and polymeric biomaterials are attractive as they can be produced in such a way that they mimic the mineral composition and/or the porous structure of bone. However, although ceramics show excellent corrosion resistance and good bioactive properties, porous ceramic structures, as they are available today, are limited to non-load-bearing applications, due to their intrinsic brittleness. Likewise, porous polymeric systems are deemed to be ductile with insufficient rigidity and inability to sustain the mechanical forces present in bone replacement surgery.

Metals have so far shown the greatest potential to be the basis of implants for long-term load-bearing orthopedic applications, owing to their excellent mechanical strength and resilience when compared to alternative biomaterials, such as polymers and ceramics. Particularly, titanium and its alloys have been widely used in orthopedic and dental devices because of their excellent mechanical properties and biocompatibility [9].

Several factors have shown their influence on bone ingrowth into porous implants, such as porous structure (pore size, pore shape, porosity and interconnecting pore size) of the implant, duration of implantation, biocompatibility, implant stiffness, micromotion between the implant and adjacent bone etc. [10–22]. The architecture of a porous implant has been suggested to have a great effect on implant integration by newly grown bone [23,24]. However, up to now, porous structures of most metallic implants are not very well controlled due to their production techniques, involving porogens and replication methods [25,26]. These techniques mostly result in porous structures with a certain pore size range, rather than structures with an accurately defined pore size.

Recently, rapid prototyping, such as fused deposition modeling and 3D printing, has been employed to fabricate 3D scaffolds with accurately designed structure [27,28], which allowed investigation of architectural influences on tissue regeneration. However, these studies focused on porous scaffolds made of ceramics and polymers [12,29,30], while very little is known about porous titanium scaffolds with precisely controlled pore structure.

Because there is hardly consensus regarding the optimal pore size for effective bone ingrowth, researchers have created scaffolds with pore sizes between 150–300 μm and 500–710 μm to promote bone formation [31]. A minimum pore size of 100–150 μm is generally considered acceptable for bone ingrowth [20,32–35].

3D porous Ti6Al4V scaffolds were successfully fabricated in our group by a rapid prototyping technology, named 3D fiber (3DF) deposition [36]. 3DF deposition, being a layer-by-layer manufacturing technique, can be used to manufacture prototypes in which each layer may have a different fiber diameter, thickness, fiber space and fiber orientation. This technique, therefore, provides a possibility to develop scaffolds with well-controlled pore size, porosity and interconnecting pore size. The advantage of scaffolds produced by 3DF is that they permit parametric analyses to be conducted, which is essential in investigations of how scaffolds perform as a function of their physical characteristics.

In the present study, implants with different pore size, porosity and interconnecting pore size were fabricated by 3DF technique. Influence of the structural characteristics on the bone ingrowth was screened by using the well-established multi-channel cage model [37–40] that was adapted to use on the transverse process of the goat lumbar spine.

2. Materials and methods

2.1. Implants

Five different porous TI6Al4V scaffolds made by 3DF deposition were used in this study. The preparation procedure of these scaffolds was described earlier [2]. In short, Ti6Al4V slurry (80 wt% of Ti6Al4V powder with a mean particle diameter of 45 μm (AP&C Inc., Canada) in 0.5% aqueous water methylcellulose solution), is forced through the syringe nozzle by using a 3D-bioplotter machine (Envisiontec, GmbH, Germany). The slurry is plotted on a stage as a fiber, which rapidly solidifies by drying, and the scaffold is fabricated by layering a pattern of fibers. After deposition, the obtained Ti6Al4V scaffolds were dried for 24 h at RT, and sintered under high vacuum at 1200 °C for 2 h. By varying spacing and fiber lay-down pattern, 5 different Ti alloy scaffolds (low porosity (3DFL), middle porosity (3DF), high porosity (3DFH), double-layered (3DFDL) and gradient porosity (3DFG)) were produced as is specified in Table 1.

2.2. Cage

A cage design and its fabrication were described previously [40]. In brief, polyacetal cages were designed for fixation to the transverse process of the goat lumbar spine. Each cage consisted of two sidewalls, two end pieces, four stainless steel machine screws for cage assembly and two self-tapping bone screws to attach the cage to the transverse process. Three scaffolds ($4 \times 7 \times 8\,mm^3$) were plugged into a cage and separated by thin

Table 1
3D fiber deposition conditions for different implants

Implant	Fiber spacing (μm)	Lay down angle	Layer thickness (μm)
3DFL	200	0/45	320
3DF	500	0/45	320
3DFH	800	0/45	320
3DFDL	500	0/0/45/45	320
3DFG	800→200(bottom to top)	0/90	320

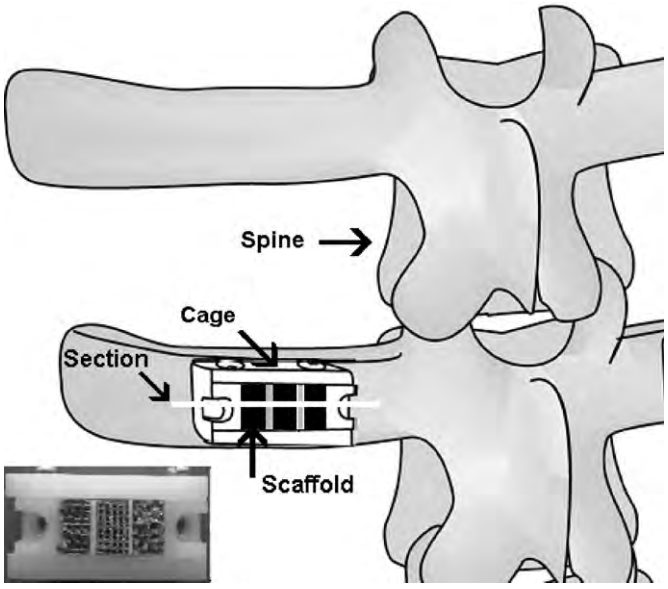

Fig. 1. Schematic drawing of the implantation on the goat's transverse process. The lower left is a cage with three implants.

Teflon plates ($0.5 \times 7 \times 8\,mm^3$). These scaffolds were open to both the underlying bone and the overlying soft tissues, had cross sections of $4 \times 7.0\,mm^2$ and 8.0 mm in height (Fig. 1). The polyacetal components and the metal screws were sterilized by autoclave.

2.3. Implant characterization

Cubical implants ($4 \times 7 \times 8\,mm^3$) were machined by using a wire electric discharge machine, with demineralized water as medium. The structure of different implants was characterized by using an environmental scanning electron microscope (ESEM; XL30, ESEM-FEG, Philips, The Netherlands) in the secondary electron mode. The porosity of the material was determined by volume/weight method ($n = 10$) and the following calculation: 100%−[(weight of the porous implant/the weight of a dense implant with the same size) × 100%]. A permeability test was performed with a self-designed permeability-meter [41]. Briefly, a cylindrical sample was mounted in a tube connected to a wide diameter water reservoir, which was positioned at a certain constant height. The flow of water through the sample was measured in ml/s. Normalized for the dimensions of the sample, it provided measure of the sample's permeability. Two samples for each condition were tested.

2.4. Animal study

2.4.1. Experimental design

A total of 10 adult Dutch milk goats, which were 2–4 years of age with a body weight ranging from 64–75 kg, were used following the approval of the institutional animal care committee. Four spinal cages containing a total of twelve different Ti implants (three per cage), were implanted bilaterally on the transverse processes of the L4 and L5 vertebrae of each goat according to a randomized complete block design. To monitor the bone formation over time, fluorochrome markers were administered at 3, 6 and 9 weeks and the animals were sacrificed at 12 weeks after implantation. Bone formation into the porous titanium scaffolds was investigated by histology and histomorphometry of non-decalcified sections using epifluorescent and light microscopy. In this paper, scaffolds with different pore size, porosity and interconnecting pore size were studied. Other Ti scaffolds implanted in these animals will be discussed and published separately.

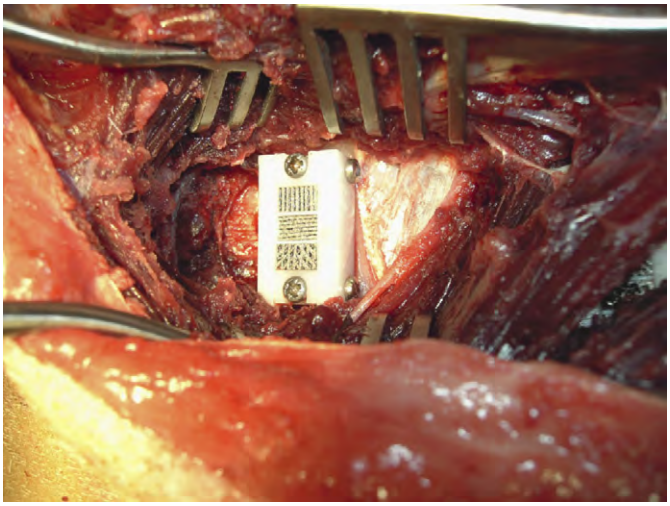

Fig. 2. Conduction cage placed on a transverse process of a goat lumbar spine.

2.4.2. Implantation procedure

The goats were housed at Central Animal Laboratory Institute (GDL), Utrecht, The Netherlands, at least 4 weeks prior to surgery.

Before the surgical procedure, a dose of 0.1 mL in 5 mL of physiologic saline solution (× 1 mL/25 kg body weight) of Domosedan (Pfizer Animal Health BV, Capelle a/d Ijssel, The Netherlands) was administered by intravenous injection. The surgical procedure itself was performed under general inhalation anesthesia of the animals. Thiopental (Nesdonal, ±400 mg/70 kg of body weight, on indication, Rhone Merieux, Amstelveen, The Netherlands) was injected intravenously, and anesthesia was maintained with a gas mixture of nitrous oxide, oxygen and Halothane (ICI-Farma, Rotterdam, The Netherlands).

Prior to the surgical procedure, four spinal cages for each animal were aseptically assembled with the 12 titanium scaffolds conditions arranged according to a randomized complete block design.

The surgical procedure was described previously [40]. After shaving and disinfecting the thoracolumbar region, a central skin incision, from approximately T8 to L1, was made to expose the muscle fascia. This incision supported implantation of both spinal implants and intramuscular implants, which are not discussed in the present manuscript. Bilateral muscle incisions were then made and retracted to expose both transverse processes of the L4 and L5 vertebrae. The processes were decorticated using an angled bone drill by dental driller. Care was taken to ensure an even decortication of a flat surface with an area sufficient for placement of a cage. One cage was placed on each transverse process and pilot holes were drilled under saline irrigation. Two stainless steel self-tapping screws were then inserted to firmly attach each cage. Light finger pressure was applied to the top of each cage just prior to muscle closure to ensure the scaffolds were in contact with the underlying bone (Fig. 2). The muscle fascia was closed with non-resorbable sutures and the skin was closed in two layers with resorbable sutures. Durogesic 25 (fentanyl transdermal CII patches; Janssen-Cilag EMEA, Beerse, Belgium) was administered for postoperative pain relief.

2.5. Fluorochrome labeling

Sequential fluorochrome markers were administered at 3, 6 and 9 weeks after implantation. Calcein Green (10 mg/kg intravenously, Sigma, The Netherlands) was administered at 3 weeks, Oxytetracyclin (Engemycine 32 mg/kg intramuscularly, Mycofarm, The Netherlands) at 6 weeks and Xylenol Orange (80 mg/kg intravenously, Sigma, The Netherlands) at 9 weeks after implantation. At 12 weeks, the animals were sacrificed by an overdose of pentobarbital (Euthasaat, Organon, The Netherlands) and the implants retrieved.

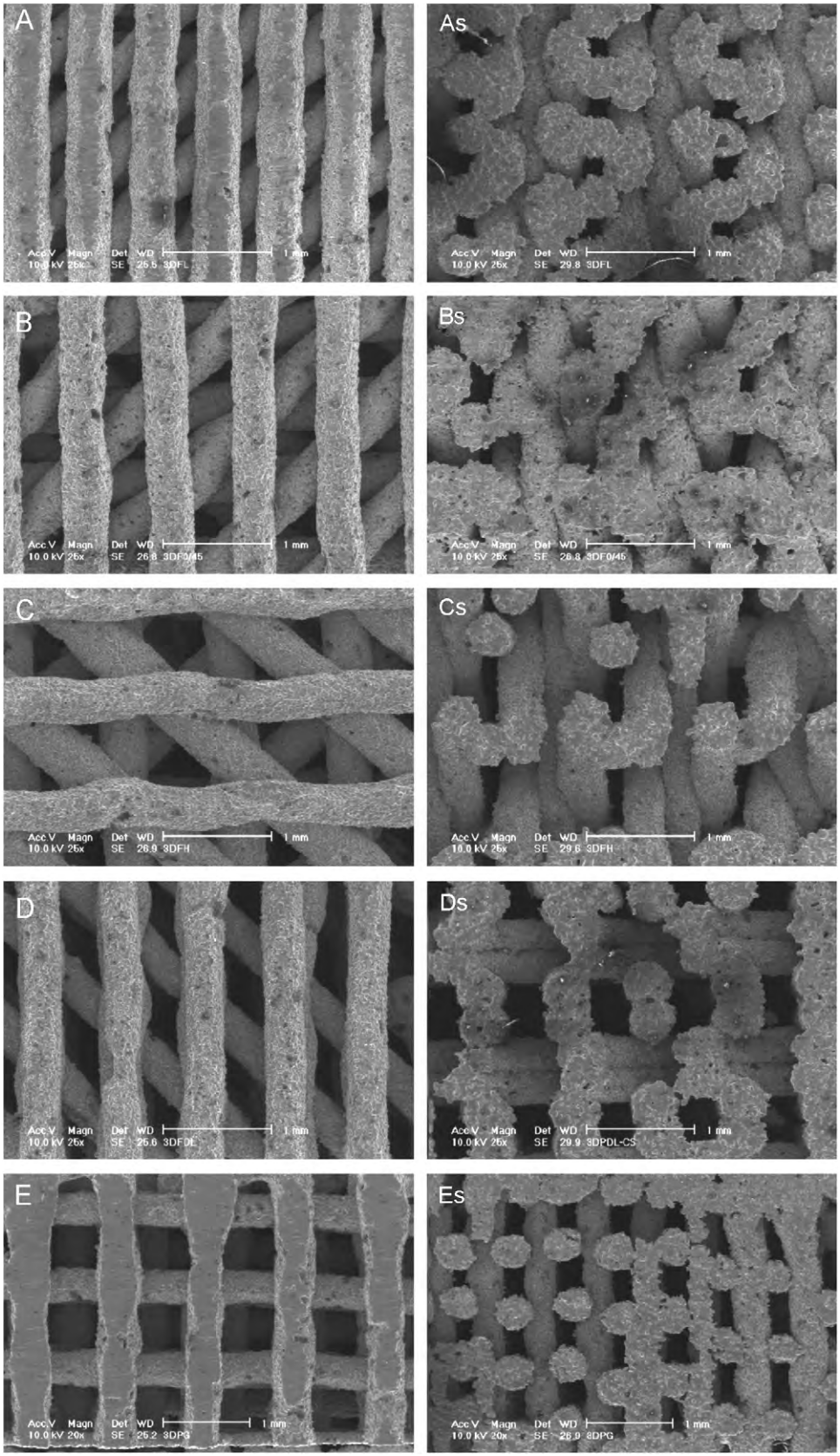

Fig. 3. ESEM photographs of Ti alloy scaffolds (magnification 25 ×): 3DFL top view (A) and side view (As), 3DF top view (B) and side view (Bs), 3DFH top view (C) and side view (Cs), 3DFDL top view (D) and side view (Ds) and 3DFG top view (E) and side view (Es). Refer to Table 1 for preparation conditions.

Table 2
Implant pore size, interconnecting pore size and porosity

Implant	Pore size under Z (um)	Interconnecting pore size (um)	Porosity
3DFL	160 ± 11	$\sim 160 \times 280$	39 ± 1.3
3DF	396 ± 16	$\sim 400 \times 280$	55 ± 1.1
3DFH	680 ± 36	$\sim 680 \times 280$	68 ± 2.5
3DFDL	400 ± 22	$\sim 400 \times 400$	56 ± 1.7
3DFG	160–660	$\sim 160 \times 280$–680×280	53 ± 3.5

2.6. Histological processing and histomorphometry

The explanted samples were fixated in a solution of 5% glutaraldehyde and 4% paraformaldehyde at 4 °C. They were then dehydrated by ethanol series (70%–100%) and transferred into a methylmethacrylate (MMA) solution that polymerized at 37 °C within 1 week. Three centrally located longitudinal 10–15 μm thick sections were cut from each sample using a sawing microtome (Leica, Germany). The second section remained unstained for epifluorescence microscopy and the other two sections were stained with 1% methylene blue and 0.3% basic fuchsin after etching with HCl/ethanol mixture for histology. High-resolution digital scans of the stained sections were made for histomorphometry using a photographic film scanner (Dimage Scan Elite 5400, Minolta, Japan). The general tissue response, bone formation and fluorochrome markers were evaluated using a light/fluorescence microscope (E600, Nikon, Japan) equipped with a quadruple filter block (XF57, dichroic mirror 400, 485, 558 and 640 nm, Omega Optics, The Netherlands). Prior to histomorphometry analysis, using Adobe Photoshop 6.0, bone and material were pseudocoloured, red and green, respectively. Image analysis was performed using a PC-based system with the KS400 software (version 3, Zeiss, Germany). Before measurements the system was geometrically calibrated with an image of a block of known dimensions. A custom macro program was developed to measure the bone area and contact between new bone and implant surface. These parameters were measured in both total implant area, and 25% of the implant area closest to host bone bed. Following parameters were investigated:

(1) *%b. ROI*: the percentage of bone area in total implant area [(bone area/total implant area) × 100%];
(2) *%b. pore total*: the percentage of bone area in total available pore space [(bone area/(total implant area−total scaffold area) × 100%];
(3) *%b. pore low*: the percentage of bone area in available pore space in the 25% of the scaffold closest to host bone bed;
(4) *%b. cont. total*: percentage of length of contact between bone and available scaffold surface in the total implant area: [(bone contact scaffold length/scaffold outline length) × 100%];

In addition, bone ingrowth depth was effectively measured at 3, 6 and 9 weeks by measuring the maximum height of each fluorochrome marker and at 12 weeks by measuring the maximum bone height on the stained sections.

2.7. Statistics

Statistical calculations were done with the SPSS (Chicago, IL) 11.5 software. Statistical analyses were performed on histomorphometrical results of bone area, bone contact and bone ingrowth depth by ANOVA for randomized complete block design with a post hoc Tukey's HSD ($p = 0.05$) to determine differences between scaffold conditions.

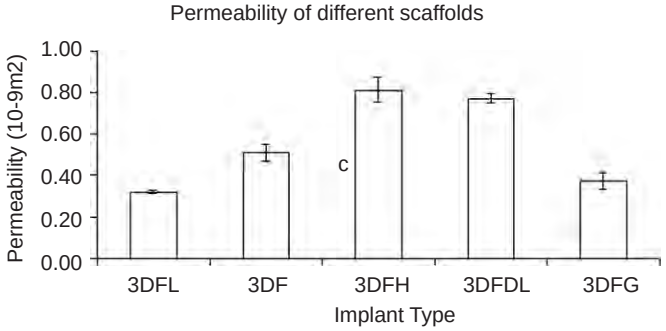

Fig. 4. Permeability results of different scaffolds.

3. Results

3.1. Implant characterization

The pore size and porous structure were analyzed by ESEM and porosity was calculated by the volume/weight method. The porous structures of different Ti alloy samples are shown in Fig. 3. It can be seen that the pores of the implants are completely interconnected. Table 2 gives a summary of pore sizes and porosities. The first three implant types, 3DFL, 3DF and 3DFH were produced by a similar lay down pattern of the fibers (0/45°) but with increasing spacing between fibers, which resulted in an identical structure but increasing pore size and porosity. The porosity of 3DFDL was similar to that of 3DF, however, because of double layering of the fibers, the distance between the layers of 3DFDL was larger as compared to 3DF resulting in a larger interconnecting pore size. 3DFG also had a similar porosity to that of 3DF and 3DFDL. The pore sizes of five implant types varied. Fig. 4 shows the results of the permeability test. All implants were found to be highly permeable. It can be seen that permeability increases with increasing pore size and interconnecting pore size.

3.2. In vivo results

One goat had to be euthanized before the end of the study due to complications not directly related to the performed surgery and was replaced by another goat. In total 10 goats were included in the study. There were no

surgical complications and all cages were firmly attached to the underlying transverse process at retrieval. No macroscopic or microscopic signs of infection were found. In total, 50 titanium implants were examined.

In all implants bone ingrowth started from the host bone bed towards the implant. New bone did not completely fill any of the scaffolds, so the final amount of bone in the scaffolds could be used for measuring the effect of various conditions to new bone formation.

Fluorescent microscopy of the sequential fluorochrome labels revealed the dynamics of bone formation in different implants (Fig. 5). In most implants, all three labels were present, suggesting start of bone formation before the third week of implantation. In some implants, however, the 3-weeks label could not be detected, indicating a delayed start of new bone formation. This delay was not directly related to a certain implant type, but more to individual animals.

Histological observations of stained sections revealed bone formation in different scaffolds. The newly formed bone was in close contact with the Ti alloy surface (Fig. 6). The results showed that in all implants a relatively low amount of bone was formed (about 2–4.5% of the total area of implants and about 5–10% of total available pore space was filled with new bone).

Fig. 7 represents histomorphometrical data of the bone area in the total region of interest after 12 weeks of implantation. As can be observed, the general trend is that the amount of bone increased with both increasing porosity and increasing pore size. 3DFL showed less bone than 3DF, while 3DFH had more bone as compared to 3DF. 3DFDL showed a similar amount of bone as 3DFH, while the amount of bone in 3DFG was between that of 3DFL and 3DF. Due to relatively high variations in the amount of formed bone between individual animals, and with the relatively low number of animals, significant differences were only observed between 3DFL and 3DFH ($p<0.01$) and between 3DFL and 3DFDL ($p<0.01$).

Concerning the bone formation in the available pore space inside the implants (Fig. 8a), a similar trend was

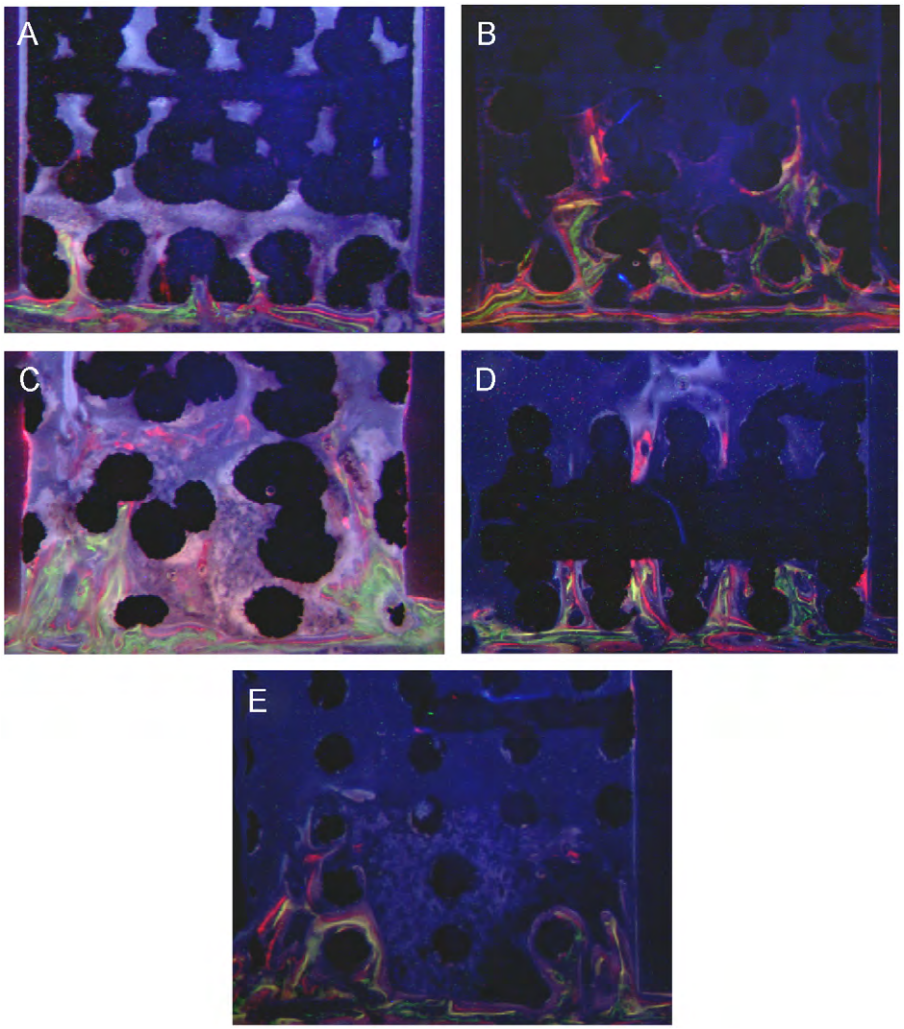

Fig. 5. Epifluorescent microscopy images of fluorochrome markers in 3DFL (A), 3DF (B), 3DFH (C), 3DFDL (D) and 3DFG (E). In all images the earliest label is green (3 weeks, calcein green), the middle label is yellow (6 weeks, oxytetracyclin) and the final label is orange (9 weeks, xylenol orange). The dark blue areas indicate scaffold.

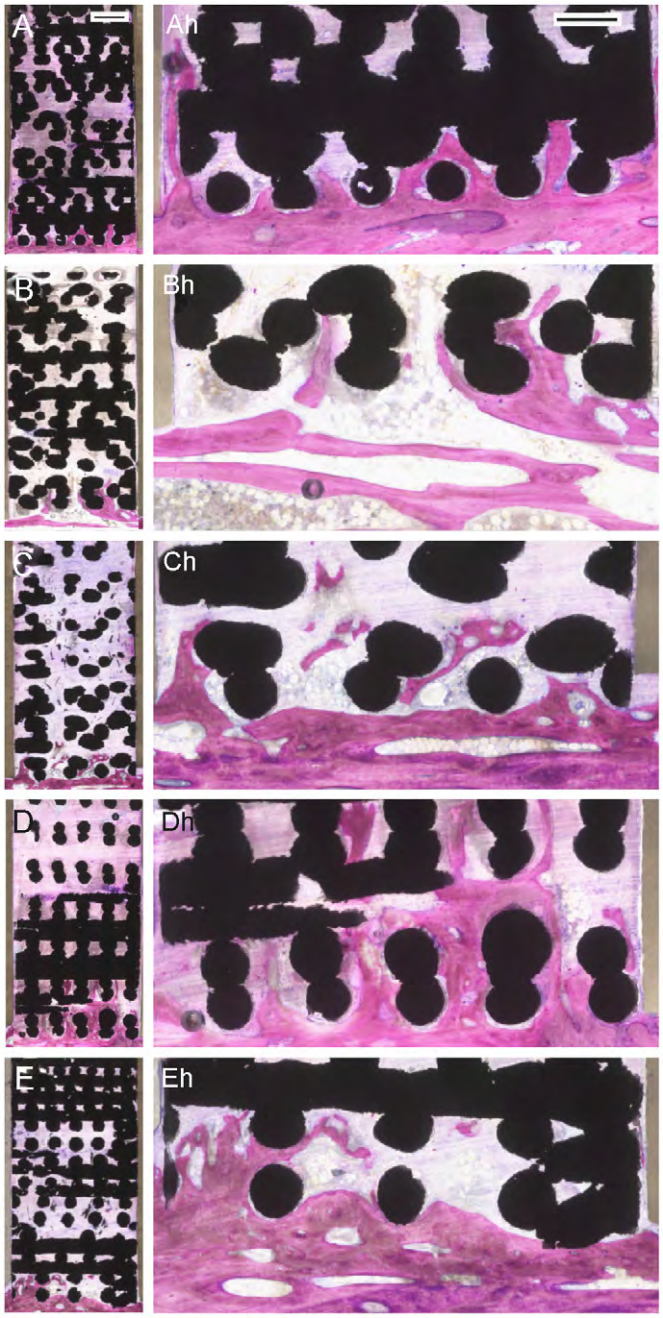

Fig. 6. Digital photographs of stained (methylene blue/basic fuchsine) histological sections. Bone is stained pink/red and Ti alloy black. The transverse process can be seen at the bottom of the implants and Teflon plates are visible between the implants. Implant in the image is A = 3DFL, B = 3DF, C = 3DFH, D = 3DFDL, E = 3DFG. Bar = 1 mm. The high magnification of interface between bone and implant is shown in Ah to Eh (correspond to 3DFL, 3DF, 3DFH, 3DFDL and 3DFG, respectively).

observed to the one in the total region of interest. Significant differences were found between 3DFL and 3DFDL ($p<0.01$) and between 3DFG and 3DFDL ($p = 0.035$).

Analysis of the area of new bone in the available pore space in the quarter of the implant closest to the host bone bed showed no significant differences between the five

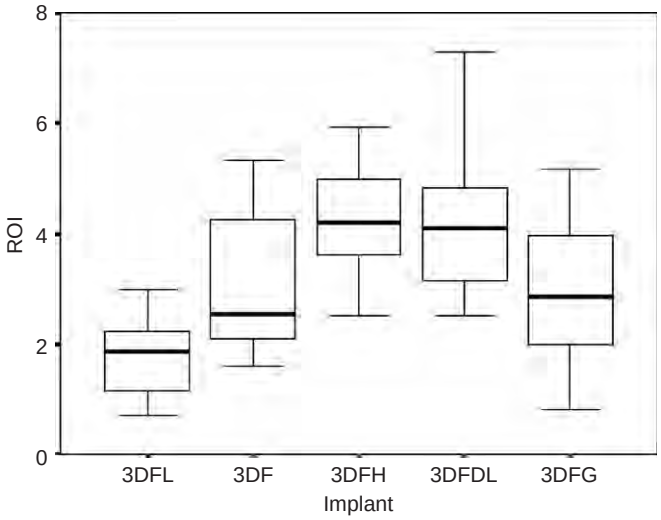

Fig. 7. Histomorphometrical results: boxplots (mean and interquartile values) of bone area in the total implant area (region of interest).

material types (Fig. 8b), indicating differences in the bone ingrowth depth inside the implants.

Boxplots with data of the depth of bone ingrowth after 3, 6, 9 and 12 weeks of implantation, based either on fluorochrome labels (for 3, 6 and 9 weeks) or histological analysis (12 weeks) are shown in Fig. 9. Bone growth in all implants progressively increased in the first 9 weeks, after which no significant increase was observed, indicating the start of a bone remodeling process. As expected, increasing porosity and pore size resulted in an increase of the depth of bone ingrowth. At 3, 6 and 9 weeks, 3DFDL showed the highest and 3DFL the lowest bone ingrowth. Significant difference was found at 9 weeks between the 3DFL and 3DFDL ($p = 0.001$). At 12 weeks, 3DFDL showed a lower value for bone depth than 3DFH, which might suggest a different phase of bone remodeling. Both 3DFH and 3DFDL showed significantly deeper bone ingrowth as compared to 3DFL ($p = 0.013$ and 0.031, respectively) at 12 weeks of implantation.

Measurements of contact between bone and implant surface showed similar results to the bone area measurements (data not shown).

4. Discussion

In this goat study, we investigated the in vivo behavior of a porous Ti6Al4V material, produced by 3DF deposition. As we did not find any signs of toxicity or deviating inflammation related to the implants, we can conclude that our novel material is biocompatible as bone graft substitute.

Characterization of the porous structure of the materials indicated that 3DF deposition allows fabrication of scaffolds with well-controlled porous structure. Fiber spacing between fibers, layer thickness between two layers as well as the angle of fiber deposition are parameters that can be used to control porosity, pore size and spatial

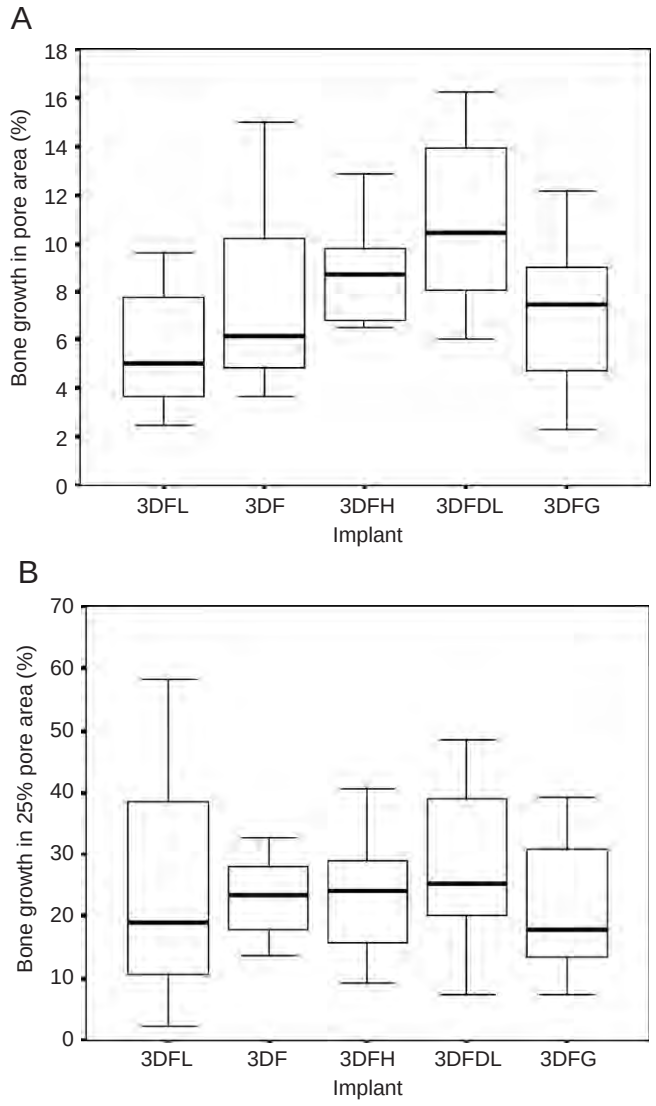

Fig. 8. Histomorphometrical results: boxplots (mean and interquartile values) of bone formation in available pore space in the total implant area (A) and in 25% of the implant closest to host bone bed (B).

arrangement. This control over architecture permits testing of the influences of specific geometrical parameters on biological performance of biomaterials, such as their osteoconductive properties.

New bone growth into porous metal implant depends on several factors, including pore size and porosity of the implant, interconnecting pore size, stability and degree of micromotion between the implant and bone, and presence of gaps between the implant and the bone surface [16,20,42]. In the present study, in order to minimize gapping and micromotion of the implant, care was taken to ensure an even decortication of the surface of transverse processes. Tight press was applied to the top of each cage to ensure that bottom of each implant was in contact with the underlying bone while two stainless steel self-tapping screws were then inserted to firmly attach each cage onto bone.

There are a vast number of studies in which the influence of porosity and pore size on the biological behavior of bone graft substitutes has been investigated; however, no consensus has been reached yet with regard to the optimum pore size. Recently, Holister et al. [29] examined pore size and geometry using HA scaffolds with well-controlled architecture. Their results demonstrated that overall bone ingrowth was not dependent on the pore sizes between 400 and 1200 μm. Also the shape of the pores, often defined by pore aspect ratio did not influence the bone growth. In contrast, many other studies [32–34,43,44] suggested that changes in pore size and shape can radically affect the success of bone development. The optimal pore size for bone ingrowth has been reported to be in the range of 150–600 μm. It should, however, be noted that this optimal pore size range was determined in studies with either porous-coated metallic implants or porous calcium-phosphate implants. Furthermore, scaffolds used in these studies did not have a well-controlled architecture. In the present study, in which fully porous metallic implants with precisely controlled pore size were used, the optimal pore size (range) may be different.

The pore sizes of implants evaluated in the present study were between the lower and the upper limit of this "optimal pore range" for porous materials. Data showed that scaffold with smallest pore size and lowest porosity had significantly less bone ingrowth. And further, the implant with the largest pore size and highest porosity conducted most new bone formation. There were statistical differences in the amount of newly formed bone between 3DFL and 3DFH. However, although the trend of positive effect of increasing porosity on bone growth was observed, no significant difference between 3DF and 3DFH was found. These data suggest that, for the implants investigated in the present study, bone conduction is definitely influenced by, but not highly sensitive to changes in porosity.

Apart from the pore size and porosity of the implant, interconnecting pore size of porous implant also affects osteoconductivity. In our study, the 3DF and 3DFDL implants had similar porosities, but their interconnecting pore sizes were different. 3DFDL showed better results for all measured parameters as compared to 3DF. Due to double layers, the amount of surface available for bone ingrowth inside 3DFDL was larger as compared to 3DF. The permeability test proved that 3DFDL had a higher permeability compared to 3DF. This high permeability is beneficial for cell attachment and tissue formation, allowing the cells to diffuse into the center of the scaffold and provide space for the ingrowth of tissue and subsequent vascularization [45,46]. These results are in agreement with many studies suggesting that good interconnecting fenestrations in porous implants are essential to provide the space for vascular tissue ingrowth followed by new bone formation [13,29,47].

It should be noted that the amount of formed bone as well as bone contact between bone and Ti alloy surface in this study were relatively low. As it is well known, Ti and

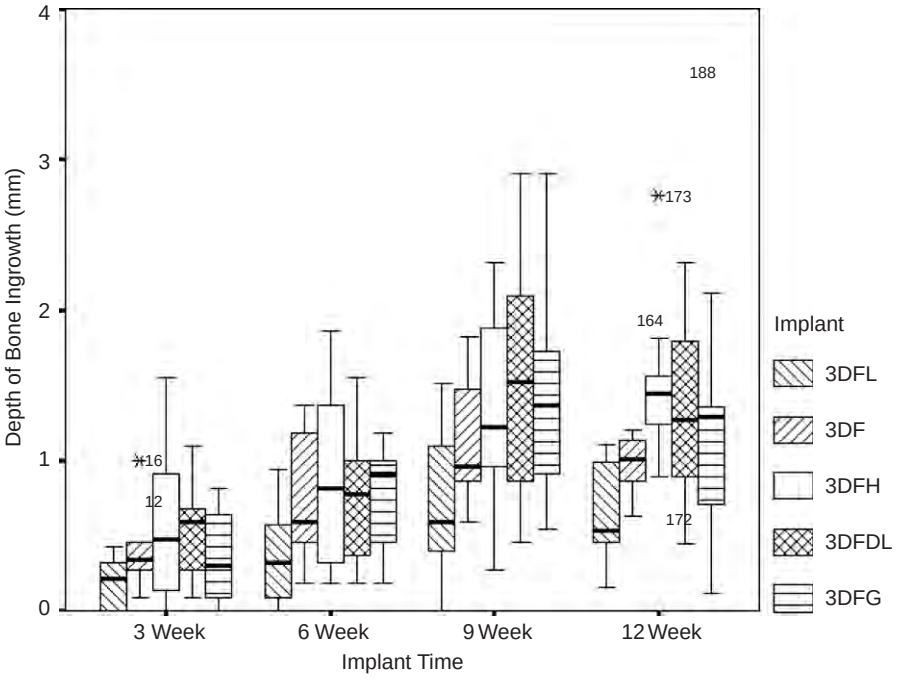

Fig. 9. Box plots of bone height at 3, 6 and 9 weeks, measured on fluorescent microscope images, and at 12 weeks, measured on stained histological sections. The symbol "○" indicates outlier and the symbol "∗" indicates an extreme outlier.

its alloys are bionert, but not bioactive materials. Therefore, in order to improve their biological performance it might be necessary to either combine them with other, more bioactive biomaterial types or to improve their bioactivity by surface modification. Coating Ti alloy surfaces with CaP ceramic and chemical and thermal treatments of the surface have been reported to be successful ways of increasing metal bioactivity [48,49].

Although increased porosity and pore size are obviously preferential for new bone growth facilitation in Ti alloy implants, it should be kept in mind that an other consequence of the porosity and pore size increase is reduction of the implant mechanical properties. Thus depending on the intended application, a balance between mechanical properties and the biological performance should be found. This is again simplified by the use of 3DF deposition technique.

It is interesting that bone growth in all implants progressively increased in the first 9 weeks, after which this increase leveled off. This behavior is related to the bone-healing mechanism. After a bone fracture occurs, formation of a hematoma, regeneration, and maturation by modeling and remodeling are generally recognized as the three stages of bone healing. At the early stage, there is a fast ingrowth of bone into the porous implant. After that, bone modeling and remodeling are restructured in response to stress and strain (Wolff's Law) [50]. In our study, no mechanical loading was applied on the implant, resulting in the start of resorption after 9 weeks of implantation.

Although not as realistic as a load-bearing model, the screening model of transverse process of goat lumbar spine as used in the present study is very useful for the initial characterization of new porous biomaterials. Using the appropriate instruments, a flat plane on which the implant is attached to bone can be made ensuring a uniform initial fit of all implants.

In this study, we have demonstrated the capability to control scaffold architecture variables of the metallic implants by using 3DF deposition technique. Design and fabrication of a bone graft substitute should find a balance between mechanical function and biological performance. The versatility and possibility provided by 3DF deposition technique allows the fabrication of implants with different porosities, pore sizes and thus different mechanical properties. In addition, bone structures at specific implantation sites can be mimicked in order to optimize bone tissue regeneration in the intended application.

5. Conclusion

Bone ingrowth into porous titanium alloy implants with varying pore size, porosity and interconnecting pore size, produced by 3D fiber deposition was evaluated in a goat lumbar spine model. Increase of porosity and pore size, and hence permeability of the 3D fiber deposition Ti6Al4V implants had a positive effect on the amount of new bone growth. 3D fiber deposition is a rapid prototyping technique that allows the development of porous implants with accurately controlled structural properties and therewith the investigation of the effect of structural parameters on the in vivo behavior of biomaterials.

Acknowledgments

Authors would like to thank Dr. Maarten Terlou from the Image Analysis Department of the University Utrecht for developing the software used for the histomorphometry and Dr. Kruyt for the kind help for spine image.

This study was financially supported by CAM Implants B.V., Leiden, The Netherlands.

References

[1] Brown KL, Cruess RL. Bone and cartilage transplantation in orthopaedic surgery. A review. J Bone Joint Surg Am 1982;64(2): 270–9.
[2] Damien CJ, Parsons JR. Bone graft and bone graft substitutes: a review of current technology and applications. J Appl Biomater 1991; 2(3):187–208.
[3] Lane JM, Tomin E, Bostrom MP. Biosynthetic bone grafting. Clin Orthop Relat Res 1999(Suppl 367):S107–17.
[4] Arrington ED, Smith WJ, Chambers HG, Bucknell AL, Davino NA. Complications of iliac crest bone graft harvesting. Clin Orthop Relat Res 1996(329):300–9.
[5] Mendicino RW, Leonheart E, Shromoff P. Techniques for harvesting autogenous bone graft of the lower extremity. J Foot Ankle Surg 1996;35(5):428–35.
[6] Brantigan JW, Cunningham BW, Warden K, McAfee PC, Steffee AD. Compression strength of donor bone for posterior lumbar interbody fusion. Spine 1993;18(9):1213–21.
[7] Lane JM, Sandhu HS. Current approaches to experimental bone grafting. Orthop Clin North Am 1987;18(2):213–25.
[8] Prolo DJ, Rodrigo JJ. Contemporary bone graft physiology and surgery. Clin Orthop Relat Res 1985(200):322–42.
[9] Long M, Rack HJ. Review titanium alloys in total joint replacement materials science perspective. Biomaterials 1998;19:1621–39.
[10] Nishikawa M, Myoui A, Ohgushi H, Ikeuchi M, Tamai N, Yoshikawa H. Bone tissue engineering using novel interconnected porous hydroxyapatite ceramics combined with marrow mesenchymal cells: quantitative and three-dimensional image analysis. Cell Transplant 2004;13(4):367–76.
[11] Kujala S, Ryhanen J, Danilov A, Tuukkanen J. Effect of porosity on the osteointegration and bone ingrowth of a weight-bearing nickel-titanium bone graft substitute. Biomaterials 2003;24(25):4691–7.
[12] Simon JL, Roy TD, Parsons JR, Rekow ED, Thompson VP, Kemnitzer J, et al. Engineered cellular response to scaffold architecture in a rabbit trephine defect. J Biomed Mater Res A 2003;66(2):275–82.
[13] Mastrogiacomo M, Scaglione S, Martinetti R, Dolcini L, Beltrame F, Cancedda R, et al. Role of scaffold internal structure on in vivo bone formation in macroporous calcium phosphate bioceramics. Biomaterials 2006;27(17):3230–7.
[14] Konttinen YT, Zhao D, Beklen A, Ma G, Takagi M, Kivela-Rajamaki M, et al. The microenvironment around total hip replacement prostheses. Clin Orthop Relat Res 2005(430):28–38.
[15] Whiteside LA, White SE, Engh CA, Head W. Mechanical evaluation of cadaver retrieval specimens of cementless bone-ingrown total hip arthroplasty femoral components. J Arthroplasty 1993;8(2):147–55.
[16] Cameron HU, Pilliar RM, MacNab I. The effect of movement on the bonding of porous metal to bone. J Biomed Mater Res 1973;7(4): 301–11.
[17] Deporter DA, Watson PA, Pilliar RM, Howley TP, Winslow J. A histological evaluation of a functional endosseous, porous-surfaced, titanium alloy dental implant system in the dog. J Dent Res 1988;67(9):1190–5.
[18] Du C, Meijer GJ, van de Valk C, Haan RE, Bezemer JM, Hesseling SC, et al. Bone growth in biomimetic apatite coated porous Polyactive 1000PEGT70PBT30 implants. Biomaterials 2002;23(23): 4649–56.
[19] Pilliar RM. Porous-surfaced metallic implants for orthopedic applications. J Biomed Mater Res 1987;21(Suppl A1):1–33.
[20] Pilliar RM. P/M processing of surgical implants: sintered porous surfaces for tissue-to-implant fixation. Int J Powder Metall 1998; 34(8):33–45.
[21] Simmons CA, Valiquette N, Pilliar RM. Osseointegration of sintered porous-surfaced and plasma spray-coated implants: an animal model study of early postimplantation healing response and mechanical stability. J Biomed Mater Res 1999;47(2):127–38.
[22] Clemow AJ, Weinstein AM, Klawitter JJ, Koeneman J, Anderson J. Interface mechanics of porous titanium implants. J Biomed Mater Res 1981;15(1):73–82.
[23] Chen PQ, Turner TM, Ronnigen H, Galante J, Urban R, Rostoker W. A canine cementless total hip prosthesis model. Clin Orthop 1983(176):24–33.
[24] Nasca RJ, Montgomery RD, Moeini SM, Lemons JE. Intervertebral spacer as an adjunct to anterior lumbar fusion. Part II. Six-month implantation in baboons. J Spinal Disord 1998;11(2):136–41.
[25] Matin B, Cornelia S, Bronkremer HP, Baur H. High-porosity titanium, stainless steel, and superalloy parts. Adv Eng Mater 2000; 2(4):196–9.
[26] Li JP, Li SH, Van Blitterswijk CA, De Groot K. A novel porous Ti6Al4V: characterization and cell attachment. J Biomed Mater Res 2005;73A:223–33.
[27] Woodfield TB, Van Blitterswijk CA, De Wijn J, Sims TJ, Hollander AP, Riesle J. Polymer scaffolds fabricated with pore-size gradients as a model for studying the zonal organization within tissue-engineered cartilage constructs. Tissue Eng 2005;11(9–10):1297–311.
[28] Tan KH, Chua CK, Leong KF, Naing MW, Cheah CM. Fabrication and characterization of three-dimensional poly(ether-ether-ketone)/-hydroxyapatite biocomposite scaffolds using laser sintering. Proc Inst Mech Eng [H] 2005;219(3):183–94.
[29] Hollister S, Lin C, Saito E, Schek R, Taboas J, Williams J, et al. Engineering craniofacial scaffolds. Orthod Craniofac Res 2005;8(3): 162–73.
[30] Hollister SJ. Porous scaffold design for tissue engineering. Nat Mater 2005;4(7):518–24.
[31] Ishaug-Riley SL, Crane-Kruger GM, Yaszemski MJ, Mikos AG. Three-dimensional culture of rat calvarial osteoblasts in porous biodegradable polymers. Biomaterials 1998;19(15):1405–12.
[32] Bobyn JD, Pilliar RM, Cameron HU, Weatherly GC. The optimum pore size for the fixation of porous-surfaced metal implants by the ingrowth of bone. Clin Orthop 1980(150):263–70.
[33] Bobyn JD, Hacking SA, Chan SP. Characterization of a new porous tantalum biomaterial for reconstructive orthopaedics. Anaheim, CA; 1999.
[34] Bobyn JD, Wilson GJ, MacGregor DC, Pilliar RM, Weatherly GC. Effect of pore size on the peel strength of attachment of fibrous tissue to porous-surfaced implants. J Biomed Mater Res 1982;16(5):571–84.
[35] Pilliar RM. Overview of surface variability of metallic endosseous dental implants: textured and porous surface-structured designs. Implant Dent 1998;7(4):305–14.
[36] Li JP, de Wijn JR, Van Blitterswijk CA, de Groot K. Porous Ti6Al4V scaffold directly fabricating by rapid prototyping: preparation and in vitro experiment. Biomaterials 2006;27(8):1223–35.
[37] Frenkel SR, Jaffe WL, Dimaano F, Iesaka K, Hua T. Bone response to a novel highly porous surface in a canine implantable chamber. J Biomed Mater Res B Appl Biomater 2004;71(2):387–91.
[38] Spivak JM, Ricci JL, Blumenthal NC, Alexander H. A new canine model to evaluate the biological response of intramedullary bone to implant materials and surfaces. J Biomed Mater Res 1990;24(9): 1121–49.
[39] Frenkel SR, Simon J, Alexander H, Dennis M, Ricci JL. Osseointegration on metallic implant surfaces: effects of microgeometry and growth factor treatment. J Biomed Mater Res 2002;63(6): 706–13.

[40] Wilson CE, Kruyt MC, de Bruijn JD, van Blitterswijk CA, Oner FC, Verbout AJ, et al. A new in vivo screening model for posterior spinal bone formation: comparison of ten calcium phosphate ceramic material treatments. Biomaterials 2006;27(3):302–14.
[41] Li SH, De Wijn JR, Li JP, Layrolle P. Biphasic calcium phosphate scaffold with high permeability/porosity ratio. Tissue Eng 2003;9(3): 535–48.
[42] Pilliar RM, Lee JM, Maniatopoulos C. Observations on the effect of movement on bone ingrowth into porous-surfaced implants. Clin Orthop 1986(208):108–13.
[43] Chang BS, Lee CK, Hong KS, Youn HJ, Ryu HS, Chung SS, et al. Osteoconduction at porous hydroxyapatite with various pore configurations. Biomaterials 2000;21(12):1291–8.
[44] Boyde A, Corsi A, Quarto R, Cancedda R, Bianco P. Osteoconduction in large macroporous hydroxyapatite ceramic implants: evidence for a complementary integration and disintegration mechanism. Bone 1999;24(6):579–89.
[45] Eckert M, Wittmann I, Rollinghoff M, Gessner A, Schnare M. Endotoxin-induced expression of murine bactericidal permeability/increasing protein is mediated exclusively by toll/IL-1 receptor domain-containing adaptor inducing IFN-beta-dependent pathways. J Immunol 2006;176(1):522–8.
[46] Kuo SM, Chang SJ, Chen TW, Kuan TC. Guided tissue regeneration for using a chitosan membrane: an experimental study in rats. J Biomed Mater Res A 2006;76(2):408–15.
[47] Shimko DA, Shimko VF, Sander EA, Dickson KF, Nauman EA. Effect of porosity on the fluid flow characteristics and mechanical properties of tantalum scaffolds. J Biomed Mater Res B Appl Biomater 2005;73(2):315–24.
[48] Spoerke ED, Murray NG, Li H, Brinson LC, Dunand DC, Stupp SI. A bioactive titanium foam scaffold for bone repair. Acta Biomater 2005;1(5):523–33.
[49] Habibovic P, Li J, Van Der Valk CM, Meijer G, Layrolle P, Van Blitterswijk CA, et al. Biological performance of uncoated and octacalcium phosphate-coated Ti6Al4V. Biomaterials 2005;26(1):23–36.
[50] Buckwalter JA, Glimcher MJ, Cooper RR, Recker R. Bone biology. II: Formation, form, modeling, remodeling, and regulation of cell function. Instr Course Lect 1996;45:387–99.